

High-throughput discovery of high-temperature conventional superconductors

Alice M. Shipley,^{*} Michael J. Hutcheon,[†] and Richard J. Needs
*Theory of Condensed Matter Group, Cavendish Laboratory,
J. J. Thomson Avenue, Cambridge CB3 0HE, United Kingdom*

Chris J. Pickard[‡]
*Department of Materials Science and Metallurgy,
27 Charles Babbage Rd, Cambridge CB3 0FS, United Kingdom and
Advanced Institute for Materials Research, Tohoku University,
2-1-1 Katahira, Aoba, Sendai, 980-8577, Japan*
(Dated: August 6, 2021)

We survey the landscape of binary hydrides across the entire periodic table from 10 to 500 GPa using a crystal structure prediction method. Building a critical temperature (T_c) model, with inputs arising from density of states calculations and Gaspari-Gyorffy theory, allows us to predict which energetically competitive candidates are most promising for high- T_c superconductivity. Implementing optimisations, which lead to an order of magnitude speed-up for electron-phonon calculations, then allows us to perform an unprecedented number of “high-throughput” calculations of T_c based on these predictions and to refine the model in an iterative manner. Converged electron-phonon calculations are performed for 121 of the best candidates from the final model. From these, we identify 36 above-100 K dynamically stable superconductors. To the best of our knowledge, superconductivity has not been previously studied in 27 of these. Of the 36, 18 exhibit superconductivity above 200 K, including structures of NaH₆ (248-279 K) and CaH₆ (216-253 K) at the relatively low pressure of 100 GPa.

I. INTRODUCTION

A number of dense metal hydrides have been shown to be conventional superconductors with high critical temperatures (T_c) [1–6]. However, electron-phonon calculations, used to determine the T_c of such materials from first principles, remain computationally expensive. It is not necessarily clear *before* performing these calculations which particular systems and structures might exhibit high-temperature superconductivity. Coupled with this, a huge variety of hydride stoichiometries and structures are either stable or metastable under pressure, even when the discussion is limited solely to binaries. This means that exhaustive theoretical investigation of this class of materials is a huge challenge. A combined searching and screening protocol could therefore provide a desirable and efficient way to discover new high- T_c superconductors.

In this work, we use a crystal structure prediction method to explore binary hydrides of elements from across the entire periodic table over a 10 to 500 GPa pressure range. Stable and metastable structures are screened using a model built to predict T_c from inputs including electronic density of states (DOS) ratios and electron-phonon coupling estimates from Gaspari-Gyorffy theory [7]. High-throughput electron-phonon calculations are then performed for a large number of structures, selected based on the predictions of this model. This provides more T_c results which can be

fed back into the training set, allowing us to improve the model iteratively. The results of this high-throughput model-training stage allow us to identify the most promising candidate systems at each pressure; more thorough structure searching is then carried out for each of these systems and fully converged electron-phonon calculations are performed for the best predicted candidates. A large number of high- T_c superconductors are efficiently identified, including many not reported in previous work.

II. METHODOLOGY

A. Initial structure searching

The structure searching calculations in this work were performed using *ab initio* random structure searching (AIRSS) [8, 9] and the plane-wave pseudopotential code CASTEP [10]. The Perdew-Burke-Ernzerhof (PBE) generalised gradient approximation [11], CASTEP QC5 pseudopotentials, a 340 eV plane-wave cut-off and a \mathbf{k} -point spacing of $2\pi \times 0.07 \text{ \AA}^{-1}$ were used. For the initial searches, sp-AIRSS [12] was utilised and structures with 8-48 symmetry operations were generated. This served the dual purpose of (1) reducing the computational cost of the searches and subsequent calculations during the training phase and (2) putting additional focus on high-symmetry structures (which may be metastable or stabilised at non-zero temperatures). Throughout this work, we aim to consider the broadest set of compositions possible. To this end, we construct a convex hull for binary hydrides of the form X_nH_m for every element X in the periodic table at 10, 100, 200, 300 and 500 GPa

^{*} ams277@cam.ac.uk; These authors contributed equally.

[†] mjh261@cam.ac.uk; These authors contributed equally.

[‡] cjp20@cam.ac.uk

in order to assess their stability. Structures on or near these static-lattice convex hulls were then selected for further investigation at the relevant pressure. In particular, in the training phase, stoichiometries within 80 meV/formula unit of the hull were selected (for each of these stoichiometries just the lowest energy structure was chosen). In order to discuss stability more clearly in this work, we introduce two quantities: E_{stoic} , the distance of the given stoichiometry from the static-lattice convex hull, and E_{struc} , the distance of the given structure from the lowest energy structure of the same stoichiometry. Here, for example, we are selecting structures with $E_{stoic} \leq 80$ meV/formula unit and $E_{struc} = 0$.

B. Electron-phonon coupling estimates

McMillan [13] showed that for strong-coupled superconductors the electron-phonon coupling constant, λ , can be expressed as

$$\lambda = \frac{N(E_F) \langle I^2 \rangle}{M \langle \omega^2 \rangle} \quad (1)$$

where $N(E_F)$ is the DOS at the Fermi level, $\langle I^2 \rangle$ is the Fermi surface averaged electron-phonon matrix element, M is the atomic mass, and $\langle \omega^2 \rangle$ is the average squared phonon frequency. The numerator in this expression can be relabelled as η , the so-called Hopfield parameter. In situations where the vibrational modes can be well-separated into those of different atomic character (as we typically see in binary hydrides) we can write

$$\lambda = \sum_j \lambda_j = \sum_j \frac{\eta_j}{M_j \langle \omega_j^2 \rangle} \quad (2)$$

where j is the atom type.

Hopfield established that, in a local phonon representation, electron-phonon interactions mainly consist of scatterings that change the electronic angular momentum l [14]; building on this observation, Gaspari-Gyorffy theory [7] then provides a way to approximate $\langle I^2 \rangle$ in Eq. 1. Beginning from a multiple-scattering Green's function formalism, adopting the rigid muffin-tin approximation [15] allows a number of approximations concerning the potential and wavefunction to be applied [16]. These approximations reduce the expression for the Hopfield parameter to a combination of electronic scattering phase shifts and (partial) electronic densities of states [16]. Recent work has emerged using Gaspari-Gyorffy theory for metal hydrides under high pressure [16, 17].

The final form of the rigid-ion Gaspari-Gyorffy formula is

$$\langle I^2 \rangle = \frac{E_F}{\pi^2 N^2(E_F)} \sum_l \frac{2(l+1) \sin^2(\delta_{l+1} - \delta_l) N_l(E_F) N_{l+1}(E_F)}{N_l^{(1)} N_{l+1}^{(1)}} \quad (3)$$

where $N_l^{(1)}$ is the free-scatterer DOS - the DOS at the Fermi level for a single muffin-tin potential in a zero-potential background - and δ_l are the scattering phase shifts.

The scattering phase shifts can be obtained by matching the logarithmic derivative for solutions inside and outside the muffin-tin at the muffin-tin radius, $r = R_{MT}$, as detailed in Ref. [18]. The free scatterer DOS can also be easily computed from properties of the radial wavefunction. From a self-consistent DOS calculation, partitioned by both atom and angular momentum l , we therefore have all the components needed to approximate $\langle I^2 \rangle$ for each atom type. These quantities can then be multiplied by $N(E_F)$ to give each η_j .

Gaspari-Gyorffy theory was implemented in the ELK code [19] in Ref. [20]; this modified version of the code is used in this work to calculate η_H and η_X . The traditional way to use these approximate Hopfield parameters (or ‘‘Gaspari-Gyorffy electron-phonon coupling estimates’’) is to calculate the average phonon frequency and use this to estimate λ via Eq. 1 (or, in our case, Eq. 2). This λ value can in turn be used to obtain T_c from the McMillan [13] or Allen-Dynes [21] equations. However, the phonon calculation required to obtain $\langle \omega^2 \rangle$ means that this approach would be too expensive to be useful in a high-throughput screening scenario. Therefore, in this work, we do not obtain direct estimates of λ or T_c from Gaspari-Gyorffy theory and instead use the η_j values themselves as descriptors in our T_c model.

C. Electron-phonon coupling calculations

At several stages during this work electron-phonon coupling calculations are performed using density functional perturbation theory (DFPT) in the QUANTUM ESPRESSO code [22, 23] and the results treated using Migdal-Eliashberg theory [24] to obtain T_c values from first principles. Within the theory, an electron in an occupied state $|n, \mathbf{k}\rangle$ is coupled to an unoccupied state $|m, \mathbf{k} + \mathbf{q}\rangle$ by a phonon with momentum \mathbf{q} and frequency $\omega_{\mathbf{q},\nu}$. At the temperatures of interest for superconductivity, we will have $\omega_{\mathbf{q},\nu} \sim k_b T \ll 1$ eV, so the initial and final electronic states will lie very close to the Fermi energy. However, on the finite \mathbf{k} -point grids used in DFT calculations, Kohn-Sham states will rarely lie this close to the Fermi level. To overcome this, we follow the method used in Ref. [25] and smear out the electronic energies using Gaussians with a characteristic smearing width σ , chosen according to the procedure outlined in Ref. [26].

Both the initial (\mathbf{k}) and final ($\mathbf{k} + \mathbf{q}$) states must be present in the \mathbf{k} -point grid. To ensure that this is the case, we take our \mathbf{k} -point grids to be fixed multiples of the \mathbf{q} -point grids, increasing the multiplicative factor until convergence is achieved (typically this results in \mathbf{k} -point grids larger than $30 \times 30 \times 30$). Coupling strengths are then interpolated onto a finer \mathbf{q} -point grid (8 times larger in each direction) to construct the Eliashberg func-

tion, $\alpha^2F(\omega)$. From $\alpha^2F(\omega)$, we obtain the superconducting critical temperature either by direct solution of the Eliashberg equations using the ELK code [19] or using the Allen-Dynes equation [21]. We compare these two methods in Sec. IV F.

Throughout this work, we profiled the electron-phonon coupling calculations in the QUANTUM ESPRESSO code and implemented optimizations [27]. In particular, through optimized symmetrization of the electron-phonon matrix elements and evaluation of Gaussian smearing, we reduced the time to calculate T_c for our $Fm\bar{3}m$ -LaH₁₀ test system by a factor of 8. Combined with the selective ability of our screening method, this near-order-of-magnitude speedup enables us to perform the present wide-ranging study.

III. T_c MODEL AND TRAINING PHASE

Our T_c model is a Gaussian Process Regression model, initially trained using a set of 160 structures and corresponding T_c values from the literature (collected from Refs. [20, 26, 28–71]). The model inputs are the Gaspari-Gyorffy electron-phonon coupling estimates for hydrogen and element X (η_H and η_X), the mass of atom X in atomic units (M_X), the total DOS at the Fermi energy ($N(E_F)$, normalised by cell volume), and the hydrogen DOS divided by the total DOS at the Fermi energy ($N_H(E_F)/N(E_F)$). Throughout this work, whether the structure originated from the literature or from our own searches, these inputs were computed using the modified version of ELK [19] from Ref. [20]. In cases where a literature structure was not given at the same pressure as T_c was reported, the structure was relaxed at the correct pressure using CASTEP [10]. Refs. [1–3, 72] and the data tables within were found to be helpful for identifying additional points to include in the original literature set.

The model was trained via optimisation of model parameters and hyperparameters in MATLAB [73] and was tested using nested cross-validation, with an inner loop used to optimise the parameters and an outer loop used to monitor the fit of the resulting model to unseen data. The correlation was evaluated in this way, repeated over several different random splittings of the data each time.

The overall process used in the training phase was iterative; structures at a given pressure were selected for further study based on the predictions of the model, with T_c values for the best predicted structures calculated explicitly using DFPT and fed back into the model’s training set for use in the next iteration (provided the structure was found to be dynamically stable). The model was then retrained and predictions were made for a set of search structures at the next pressure until all pressures had been considered. To make performing a large number of electron-phonon calculations feasible, a relatively sparse \mathbf{q} -point sampling was used in the training stage, chosen to reproduce the known result for $Fm\bar{3}m$ -LaH₁₀ [26, 74].

This corresponds to a \mathbf{q} -point spacing of $2\pi \times 0.15\text{\AA}^{-1}$ (a $2 \times 2 \times 2$ grid for $Fm\bar{3}m$ -LaH₁₀ at 200 GPa). In keeping with the initial literature training set, the Allen-Dynes equation was used to estimate T_c throughout the training phase.

Our method is summarised in Fig. 1. Fig. 2 shows the number of structures considered in total at each stage of the training process - given the relatively large cost of electron-phonon calculations (even in high-throughput operation), this figure highlights the importance of the stability filtering and model-based screening steps in our workflow. In total, 119 new DFPT data points were added to the training set in this work. Predictions for all previously-considered search structures were recalculated using the final model to ensure nothing of interest had been missed in earlier iterations. Most of the electron-phonon calculations performed in the training phase were for structures with a high predicted T_c according to our model, however, occasionally these calculations were performed for structures with mid-range or low T_c predictions in order to improve the behaviour of the model. The correlation of the predicted T_c values with the calculated T_c values across the training set decreased slightly on addition of more data (see Fig. 1). This is not surprising for two reasons: (1) as mentioned previously, the results we add to the training set are computed in a high-throughput manner and therefore will be somewhat under-converged compared to typical values found in the literature, and (2) the final training set contains a wider range of elements and pressures than the original literature-based training set.

During the training of our model, we were able to efficiently rediscover a number of binary hydrides (with relatively high T_c values) which had been reported previously, including the structures $Im\bar{3}m$ -H₃S [44, 45, 75], $Im\bar{3}m$ -LaH₆ [76], $I4/mmm$ -AcH₁₂ [28], $Im\bar{3}m$ -SeH₃ [46], $R\bar{3}m$ -SrH₆ [72], $R\bar{3}m$ -LiH₆ [77, 78], $Fm\bar{3}m$ -LaH₁₀ [26, 50, 74, 76, 79, 80], $Fm\bar{3}m$ -YH₁₀ [26, 76], $Im\bar{3}m$ -ScH₆ [57, 76, 81], $P6_3/mmc$ -ThH₉ [63], $R\bar{3}m$ -SrH₁₀ [82], $Pm\bar{3}m$ -SiH₃ [58], $C2/m$ -LaH₇ [50], $Im\bar{3}m$ -CaH₆ [35], $Im\bar{3}m$ -MgH₆ [83], $Fm\bar{3}m$ -ThH₁₀ [62, 63], and the stoichiometries KH₆ [49], LaH₈ [50, 79], BaH₁₂ [70], LaH₅ [50], AcH₁₀ [28], LiH₈ [77], LaH₁₁ [50], MgH₁₂ [84], YH₉ [76, 85] and ScH₁₂ [57]. Although found previously, only half of these 26 stoichiometries appeared in our original training set; the other half were re-predicted, highlighting the capabilities of our method. We also identified a number of other systems with the potential to exhibit high- T_c superconductivity. The most promising systems overall are studied further in Sec IV.

IV. FOCUSED SEARCHES AND FINAL RESULTS

From the T_c results obtained during training, the most promising candidate systems could be identified and studied in more depth. More focused structure searches

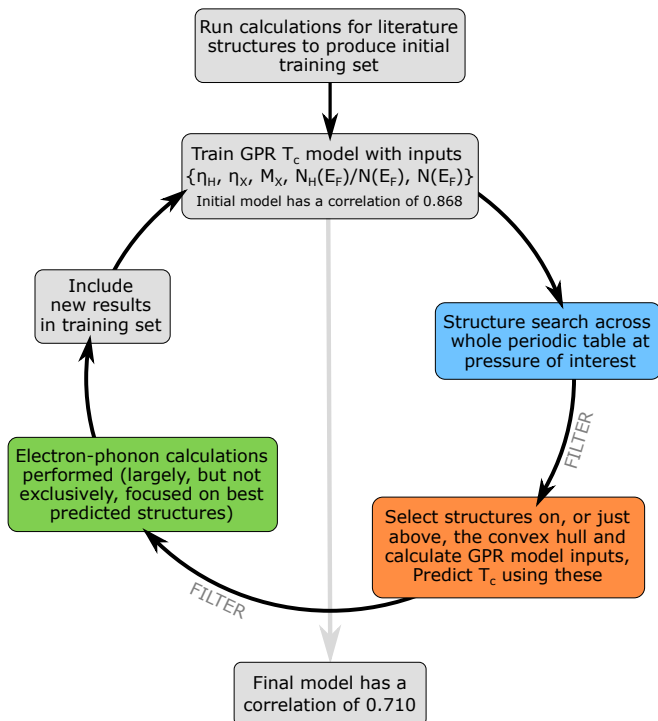


FIG. 1. A flowchart summarising our methodology.

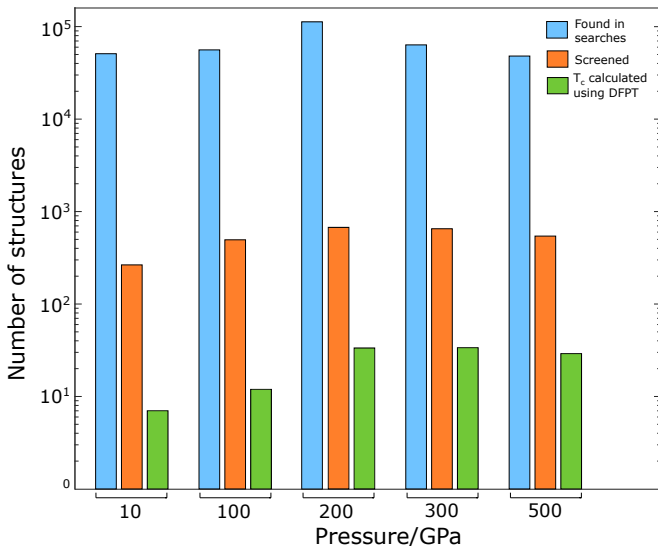


FIG. 2. A summary of the number of structures studied at each stage of the training process - note the logarithmic scale.

were performed for hydrides of Na, Ca, La, Ac, and K at 100 GPa, hydrides of La, Ac, S, Mg, and Na at 200 GPa, hydrides of Li, Sr, K, Mg, Na, and Sc at 300 GPa, and hydrides of Li, Sr, Mg, Na, Yb, Y, and Ca at 500 GPa. For these calculations, the earlier symmetry constraints were relaxed, but all other parameters remained the same. These composition choices reflect a bias towards elements from the left-hand side of the periodic table amongst the most promising candidates from the

training stage. However, this is not to say that only the compositions that we study further in this work are capable of supporting high- T_c superconductivity. Future studies, with a different focus, could potentially identify more candidates. No additional searches were performed at 10 GPa as the highest T_c calculated at this pressure in the training phase was only 12-15 K (belonging to $Fm\bar{3}m$ -CaH₂) and a large proportion of the 245 structures screened were only weakly metallic (in fact, 48 of them were insulating).

On completion of the focused searches, we again calculated η_H , η_X , $N(E_F)$, and $N_H(E_F)/N(E_F)$ for the stable and metastable structures found. Stoichiometries with $E_{stoic} \leq 25$ meV/formula unit were selected for further study. For the stoichiometries on the hull ($E_{stoic} = 0$), 2-5 of the most stable structures were chosen. For the selected off-hull stoichiometries, only the lowest energy structure ($E_{struc} = 0$) was chosen. The inputs were then fed into the final T_c model trained in Sec. III and fully converged electron-phonon calculations were performed for the structures with the highest predicted T_c values at each pressure (as well as for the most promising candidates already identified during training). These results are shown in Figs. 3 and 4. Promising structures that remained dynamically stable after convergence of the \mathbf{q} -point grids are listed in Table I. We find near room-temperature superconductors at every pressure considered, which we elaborate on in the following sections. Unless otherwise stated, all critical temperatures reported in the following sections are from direct solution of the Eliashberg equations.

A. 100GPa

Of particular note at 100 GPa is a $Pm\bar{3}m$ structure of NaH₆, a stoichiometry which we find to lie above the convex hull, in agreement with Ref. [92] (although they find that the $Pm\bar{3}m$ structure is not the lowest energy structure until 150 GPa). This structure consists of a cubic lattice of H octahedra with Na at the body-centred positions (see Fig. 5). Indeed, as we will see throughout this work, many of the best candidate systems contain hydrogen in such polyhedral clusters. While experimental synthesis of sodium polyhydrides has been demonstrated [93], superconductivity in the system seems under-studied given its promise here with a calculated T_c of 248-279 K. This places the structure at a crucial position in pressure- T_c space, strongly influencing the apparent low-pressure trend of maximum T_c (see Figs. 3 and 4) and hinting at the exciting possibility of other low-pressure high- T_c superconductors. Such high-temperature superconductivity is only possible with both high average phonon frequencies and strong electron-phonon coupling. Indeed, the logarithmic average phonon frequency, $\omega_{ln} = 870$ cm⁻¹, and electron-phonon coupling constant, $\lambda = 2.54$, of $Pm\bar{3}m$ -NaH₆ at 100 GPa are comparable to the values for the $Fm\bar{3}m$ -

Stoichiometry	Space Group	Pressure (GPa)	Allen-Dynes T_c (K)	Eliashberg T_c (K)	λ	E_{stoic} (meV/unit)	E_{struc} (meV/unit)
<u>NaH₆</u>	<u>$Pm\bar{3}m$</u>	100	228-267	248-279	2.54	28	0
CaH ₆	$Im\bar{3}m$	100	150-179	216-253	5.81	9	137
<u>Na₂H₁₁</u>	<u>$Cmmm$</u>	100	127-156	134-161	1.28	0	0
<u>KH₁₀</u>	<u>$C2/m$</u>	100	105-124	134-157	2.45	0	0
NaH ₁₆	$Fmm2$	100	47-60	61-75	1.10	0	0
AcH ₅	$P\bar{1}$	100	48-65	49-69	0.91	0	0
LaH ₅	$P\bar{1}$	100	37-55	40-58	0.83	0	0
NaH ₂₄	$R\bar{3}$	100	40-57	40-55	0.82	0	0
AcH ₁₁	$C2/m$	100	14-23	13-20	0.71	0	0
<u>NaH₆</u>	<u>$Pm\bar{3}m$</u>	200	235-275	260-288	2.06	39	16
<u>AcH₁₂</u>	<u>$P6_3mc$</u>	200	197-231	245-280	3.92	11	0
<u>MgH₁₃</u>	<u>$Fm\bar{3}m$</u>	200	179-210	196-224	1.98	17	635
SH ₃	$Im\bar{3}m$	200	173-203	196-219	1.77	0	0
AcH ₆	$Fmmm$	200	110-140	169-204	2.01	0	14
<u>NaH₈</u>	<u>$I4/mmm$</u>	200	146-171	152-175	1.63	26	124
<u>Na₂H₁₁</u>	<u>$Cmmm$</u>	200	120-156	129-162	1.11	0	0
<u>MgH₁₄</u>	<u>$P\bar{1}$</u>	200	106-132	112-134	1.35	23	0
LaH ₇	$C2/m$	200	98-120	105-134	1.23	3	0
MgH ₄	$I4/mmm$	200	63-88	73-94	0.98	0	101
SH ₇	$Fmmm$	200	57-78	58-78	0.91	29	0
Mg ₂ H ₇	$C2/m$	200	55-75	56-75	0.98	22	0
AcH ₄	$Cmcm$	200	35-54	42-58	0.99	19	0
Mg ₂ H ₅	$R\bar{3}m$	200	22-39	24-39	0.74	139	21
MgH ₆	$Im\bar{3}m$	300	248-284	271-301	2.28	19	437
<u>YH₉</u>	<u>$F\bar{4}3m$</u>	300	220-255	261-293	2.58	2	0
ScH ₈	$Immm$	300	185-217	212-233	2.06	3	0
<u>LiH₂</u>	<u>$P6/mmm$</u>	300	162-193	177-207	1.45	40	75
<u>NaH₇</u>	<u>$C2/m$</u>	300	157-190	167-198	1.48	3	0
<u>ScH₁₂</u>	<u>$P\bar{1}$</u>	300	127-157	137-165	1.28	0	103
<u>NaH₅</u>	<u>$P4/mmm$</u>	300	121-144	138-164	1.92	1	0
<u>LiH₆</u>	<u>$C2/m$</u>	300	109-142	130-163	1.16	0	14
LiH ₆	$R\bar{3}m$	300	121-152	130-161	1.30	0	0
ScH ₆	$Im\bar{3}m$	300	118-150	135-161	1.26	0	0
<u>LiH₃</u>	<u>$Cmcm$</u>	300	104-137	112-140	1.06	1	0
<u>ScH₁₄</u>	<u>$P\bar{1}$</u>	300	87-109	91-115	1.20	6	0
MgH ₄	$I4/mmm$	300	53-81	59-84	0.76	0	0
<u>MgH₁₂</u>	<u>$Pm\bar{3}$</u>	500	294-340	360-402	2.65	0	259
<u>SrH₁₀</u>	<u>$Fm\bar{3}m$</u>	500	239-275	285-319	2.22	8	120
<u>MgH₁₃</u>	<u>$P3m1$</u>	500	239-275	257-287	2.21	12	0
<u>MgH₁₀</u>	<u>$C2/m$</u>	500	209-250	232-270	1.63	9	0
<u>NaH₉</u>	<u>$P6_3/mmc$</u>	500	218-256	235-269	1.67	0	0
<u>YH₁₈</u>	<u>$P\bar{1}$</u>	500	179-212	213-246	1.99	25	0
<u>SrH₂₄</u>	<u>$R\bar{3}$</u>	500	195-227	218-245	1.88	9	0
<u>YH₂₀</u>	<u>$P\bar{1}$</u>	500	176-205	212-244	2.21	39	0
SrH ₁₀	$R\bar{3}m$	500	165-199	190-228	1.31	8	0
CaH ₁₀	$R\bar{3}m$	500	155-187	184-220	1.51	3	0
<u>Na₂H₁₁</u>	<u>$Cmmm$</u>	500	132-166	141-180	1.12	0	0
<u>CaH₁₅</u>	<u>$P\bar{6}2m$</u>	500	120-160	134-167	1.01	0	0
<u>SrH₁₅</u>	<u>$P\bar{6}2m$</u>	500	100-136	110-139	0.93	0	0
<u>MgH₈</u>	<u>$C2/m$</u>	500	82-110	91-121	0.96	0	0
Na ₂ H ₁₁	$I4/mmm$	500	72-105	76-104	0.80	0	297

TABLE I. Allen-Dynes and Eliashberg T_c values for dynamically stable superconductors found in this work, along with calculated λ and stability measures. Structures that are underlined have a calculated T_c above 100 K and have either not been reported in the literature before or have not had their superconducting properties studied before (to the best of our knowledge) - more details are given in the Supplementary Information [90]. Structures available online [91].

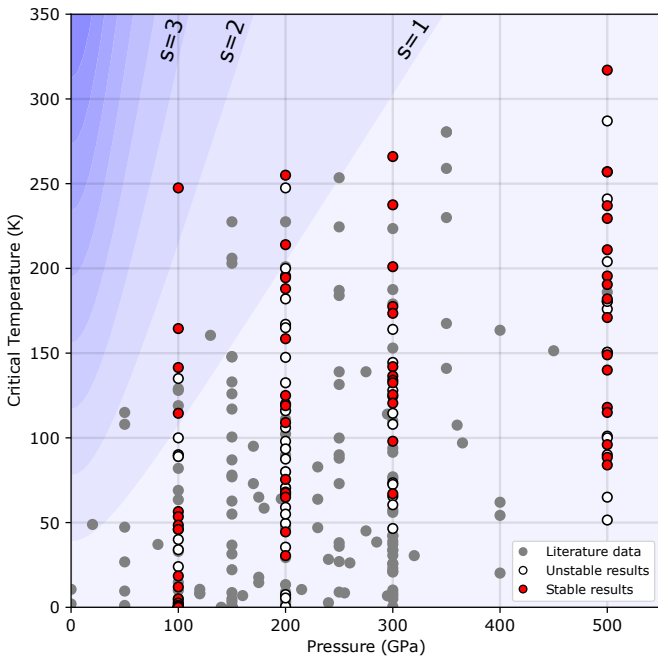


FIG. 3. Critical temperatures obtained from converged DFPT calculations for the most promising candidates according to our screening process (calculated using the Allen-Dynes equation to facilitate comparison with the literature). Both dynamically stable and dynamically unstable results are shown. The background is shaded according to the figure of merit S , introduced in Ref. [6].

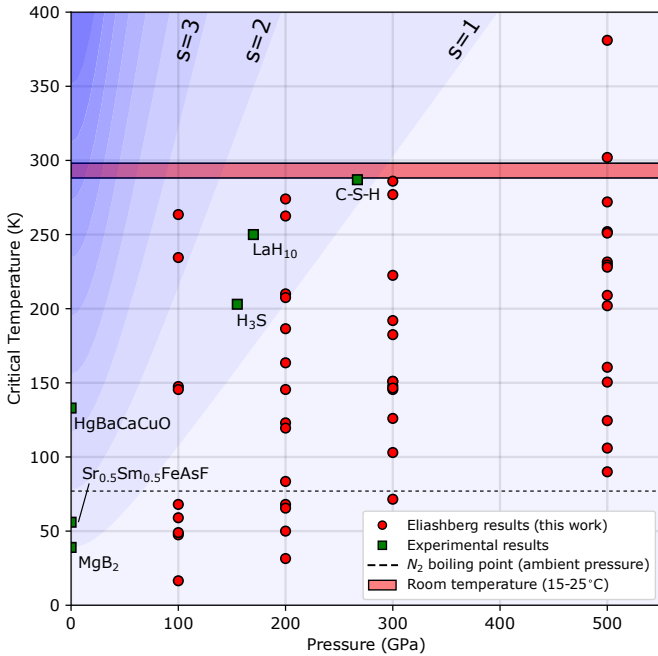


FIG. 4. As Fig. 3, but showing the Eliashberg results from Table I (dynamically stable structures only) alongside experimental results for specific superconductors (in order of increasing T_c : [86], [87], [88], [75], [74] and [89]).

LaH₁₀ clathrate superconductor at 250 GPa ($\omega_{\text{ln}} = 871 \text{ cm}^{-1}$, $\lambda = 2.29$ [50]). The ability of $Pm\bar{3}m$ -NaH₆ to maintain a high average phonon frequency at such low pressures is due to its compact structure, with a shortest hydrogen-hydrogen bond length of only $d_{\text{HH}} = 0.85 \text{ \AA}$ (shown on Fig. 5) - significantly shorter than in $Fm\bar{3}m$ -LaH₁₀, where $d_{\text{HH}} > 1 \text{ \AA}$ up to pressures as high as 300 GPa [94].

Also of interest at 100 GPa is a cage-like $Im\bar{3}m$ structure of CaH₆ (see Fig. 3 of Ref. [35]). As was the case with NaH₆, this stoichiometry is found to be slightly above the static-lattice convex hull, in agreement with previous calculations [35]. However, despite strong electron-phonon coupling, its critical temperature (216-253 K) is found to be slightly lower than that of $Pm\bar{3}m$ -NaH₆ due to a lower average phonon frequency. Indeed, our CaH₆ phonons are significantly softer than those calculated at 150 GPa in Ref. [35], resulting in a much higher λ value (5.81 vs. 2.69 from [35]), suggesting that the structure is on the verge of a mechanical instability at 100 GPa. Fig. 7 illustrates this, highlighting the strong dependence of both λ and the Allen-Dynes T_c on the low-frequency portion of $\alpha^2F(\omega)$ and, in particular, the appearance of a peak in $\alpha^2F(\omega)$ at very low frequencies. This is unsurprising as the Allen-Dynes equation is known to be sensitive to small changes in $\alpha^2F(\omega)$ at low frequencies (in particular, the functional derivative $\delta T_c(\text{AD})/\delta \alpha^2F(\omega)$ diverges as $\omega \rightarrow 0$ [95], in this case towards $-\infty$). However, the full Eliashberg calculation of T_c is much less sensitive and the 100 GPa result calculated here (216-253 K) is comparable to the critical temperature of 220-235 K calculated at 150 GPa in Ref. [35], also via solution of the Eliashberg equations.

Fig. 6 also demonstrates that while the next best structures, $Cmmm$ -Na₂H₁₁ and $C2/m$ -KH₁₀, have similar average phonon frequencies to $Pm\bar{3}m$ -NaH₆, they do not exhibit such high coupling strengths. This leads to lower T_c values of 134-161 K and 134-157 K, respectively. KH₁₀ adopts a cage like structure, whilst the Na₂H₁₁ structure contains broken octahedral hydrogen clusters (see Fig. 6 inset). Superconductivity in the KH₁₀ stoichiometry has been studied previously [70]; it was found to be on the convex hull at 150 GPa (and off-hull at 50 GPa) where an Allen-Dynes T_c of 148 K was calculated for an $Immm$ structure. Ref. [96] found KH₁₀ to be above the convex hull at 100 GPa and instead found metastable metallic structures of other stoichiometries, but superconductivity was not directly investigated.

B. 200GPa

At 200 GPa, the $Pm\bar{3}m$ structure of NaH₆ remains the highest T_c structure found, rising slightly from its 100 GPa value to 260-288 K. However, as pressure increases we find this stoichiometry to be less stable with respect to decomposition. Similarly to Ref. [28], we find several actinium hydrides to be high-temperature superconduc-

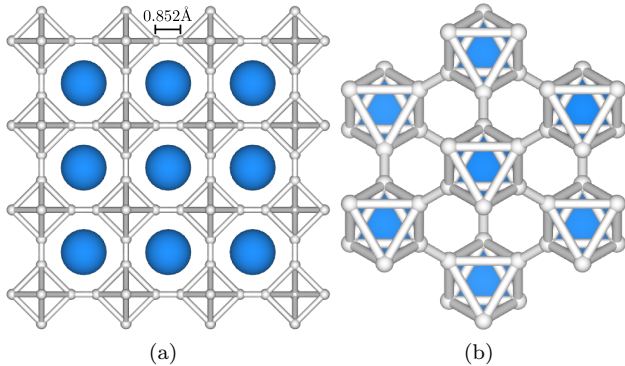


FIG. 5. The 100 GPa structure of $Pm\bar{3}m$ NaH_6 as viewed along the (a) [100] and (b) [111] directions of the standardized cell.

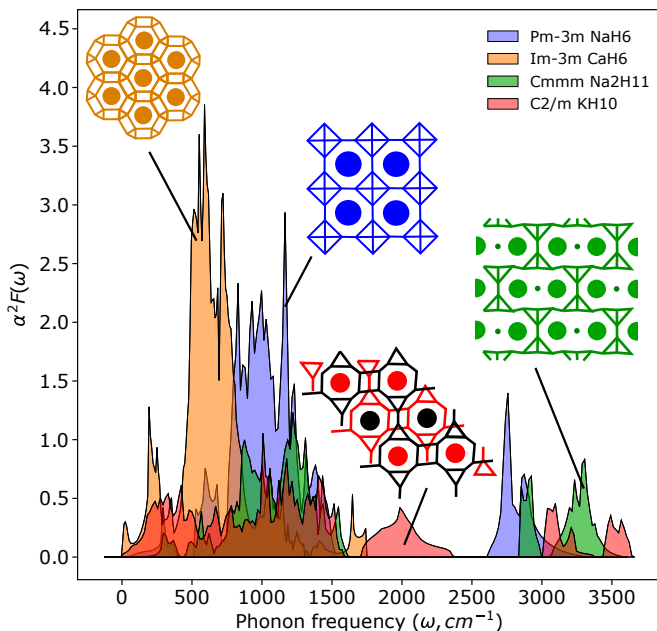


FIG. 6. The highest- T_c structures and corresponding Eliashberg functions at 100 GPa.

tors at this pressure, most notably a $P6_3mc$ structure of AcH_{12} with a critical temperature of 245-280 K. This structure is best described as cage-like, but with hydrogen atoms concentrated along specific channels along the c axis (see Fig. 9).

200 GPa also marks the appearance of magnesium hydrides, which become increasingly prevalent in our results with pressure. Of particular note is a cubic structure of MgH_{13} with the space group $Fm\bar{3}m$, which possesses a slightly higher calculated T_c (196-224 K) than the experimentally-verified [75] $Im\bar{3}m$ - H_3S at the same pressure (196-219 K). The MgH_{13} structure consists of axis-aligned cuboctahedral hydrogen clusters (see Fig. 8). In agreement with Ref. [84], we find MgH_{13} to lie above the convex hull at 200 GPa. They report significantly lower critical temperatures for on-hull structures.

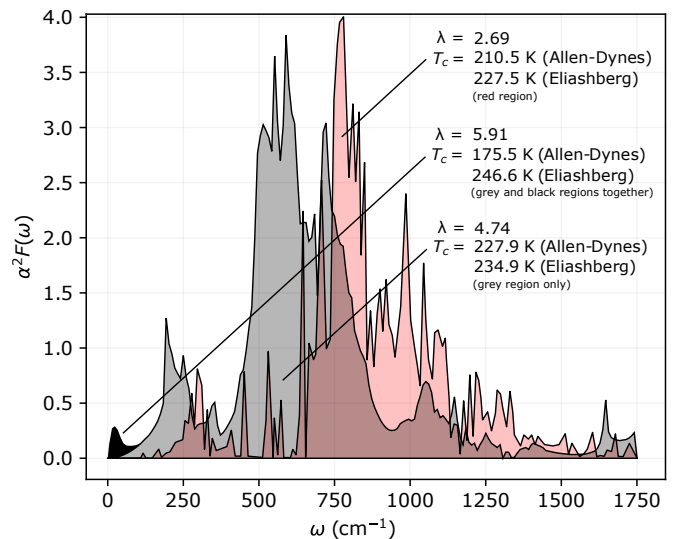


FIG. 7. Grey and black: The Eliashberg function of $Im\bar{3}m$ CaH_6 at 100GPa, demonstrating the suppression of the Allen-Dynes T_c relative to the one obtained by solving the Eliashberg equations. This suppression is due to electrons coupling to soft phonon modes. Red: The Eliashberg function of the same material at 150GPa from Ref. [35].

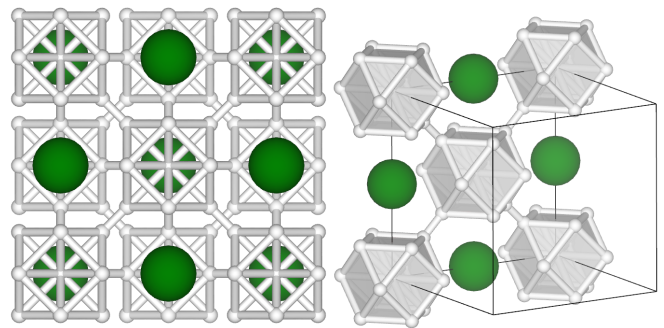


FIG. 8. The 200 GPa $Fm\bar{3}m$ structure of MgH_{13} . The structure consists of Mg atoms and axis-aligned cuboctahedra of hydrogen in a checkerboard pattern. Each cuboctahedra has an additional hydrogen atom at its centre to make up the necessary 13.

A notable absence from the 200 GPa results is LaH_{10} . Several structures of LaH_{10} (including the experimentally-verified $Fm\bar{3}m$ structure [74, 80]) were found in our structure searches and flagged as good candidates by our T_c model, but were dynamically unstable at the harmonic level. This has been noted previously for the cubic structure [26, 97, 98]. We elaborate on our treatment of structures with dynamical instabilities in Sec. IV E.

C. 300GPa

At 300 GPa, an $Im\bar{3}m$ structure of MgH_6 exhibits the highest T_c value - 271-301 K (in agreement with previous

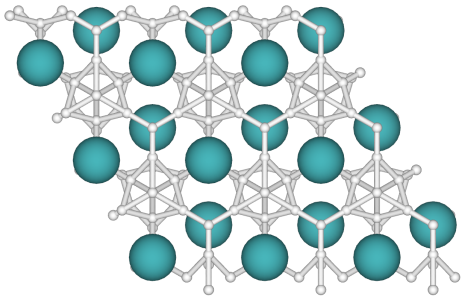


FIG. 9. The 200 GPa $P6_3mc$ structure of AcH_{12} as viewed along the $[001]$ direction of the standardized cell.

work [83]). This structure can be obtained by substituting Ca for Mg in the CaH_6 structure investigated at 100 GPa. By instead substituting only half of the Ca atoms at 200 GPa, it has been reported that one obtains an even higher critical temperature ternary superconductor [99]. Hybridizing compatible binary crystal structures in this way could provide an efficient method to design future high-temperature ternary hydride superconductors.

With a critical temperature of 261-293 K, a cage-like $F\bar{4}3m$ structure of YH_9 (shown in Fig. 10(a)) is the next highest temperature superconductor found at 300 GPa. This stoichiometry (although with $P6_3/mmc$ symmetry) has been synthesised experimentally, confirming theoretical predictions [76], and was found to exhibit a critical temperature of 243 K at 201 GPa [85]. Y-H systems have been extensively studied [26, 100–102] with critical temperatures in excess of 200 K predicted over large pressure ranges.

We find that an $Immm$ structure of ScH_8 with a similar motif to $F\bar{4}3m$ - YH_9 (see Fig. 10(b)) is also a high-temperature superconductor at this pressure with a T_c of 212-233 K. This is significantly higher than the (Allen-Dynes) value of ~ 115 K obtained in Ref. [103]; we elaborate on the source of this discrepancy in the Supplementary Information [90].

The next structure of note is a metastable $P6/mmm$ structure of LiH_2 , which is interesting both because of its relatively low hydrogen content and because its structure is analogous to the well-known ambient-pressure superconductor, MgB_2 [86] (see Fig. 11). Superconductivity in Li-H systems has been investigated previously at lower pressures [77], where it was found that the LiH_2 stoichiometry did not exhibit superconductivity at 150 GPa. We find that the LiH_2 stoichiometry lies above the static-lattice convex hull at 300 GPa. However, we find this stoichiometry is stabilised (and lies on the hull, in agreement with Ref. [104]) when using harder pseudopotentials with denser \mathbf{k} -point grids.

D. 500GPa

As we increase pressure further, hydrides with higher hydrogen content can be metallised. In particular, at 500

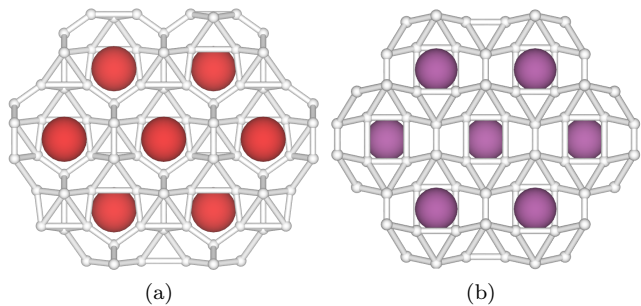


FIG. 10. (a) The 300 GPa $F\bar{4}3m$ structure of YH_9 as viewed along the $[110]$ direction of the standardized cell. (b) The 300 GPa $Immm$ structure of ScH_8 as viewed along the $[100]$ direction of the standardized cell.

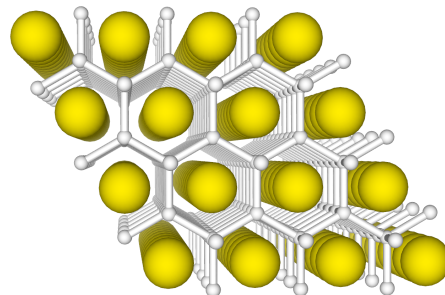


FIG. 11. The 300 GPa $P6/mmm$ structure of LiH_2 as viewed with perspective along the $[001]$ direction of the standardized cell.

GPa we see the appearance of several MgH_n structures with $n > 10$. The highest critical temperature of these belongs to MgH_{12} , which we find to be on the convex hull at this pressure, where a $Pm\bar{3}$ structure (see Fig. 12(a)) exhibits hot superconductivity with a critical temperature of 360-402 K (87-129°C). This extremely high critical temperature is due to strong electron-phonon coupling that persists over the entire phonon spectrum, extending to very high frequencies (see Fig. 13). Despite increased hydrogen content, $P3m1$ - MgH_{13} (see Fig. 12(b)) exhibits a lower T_c of 257-287 K due to reduced (but still extended) electron-phonon coupling (see Fig. 13). Superconductivity in the Mg-H system appears to be enhanced substantially with increased pressure; the MgH_{12} stoichiometry has been previously investigated at lower pressures [84], where it was also found to lie on the convex hull, but with a much reduced T_c of 47-60 K at 140 GPa.

At 500 GPa, we also find that a high-symmetry metastable $Fm\bar{3}m$ phase of SrH_{10} exhibits room-temperature superconductivity with a T_c of 285-319 K (12-46°C). This is significantly higher than the 190-228 K we calculate for the ground-state structure of this stoichiometry, which we find to have $R\bar{3}m$ symmetry in agreement with previous calculations at 300 GPa [105]. A T_c of 259 K had been calculated for the $R\bar{3}m$ structure previously at this lower pressure [82].

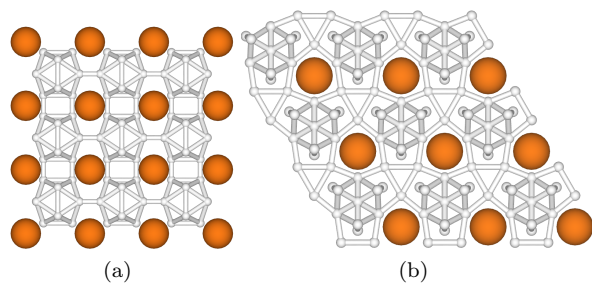


FIG. 12. (a) The 500 GPa $Pm\bar{3}$ structure of MgH_{12} as viewed along the $[010]$ direction of the standardized cell. (b) The 500 GPa $P3m1$ structure of MgH_{13} as viewed along the $[001]$ direction of the standardized cell.

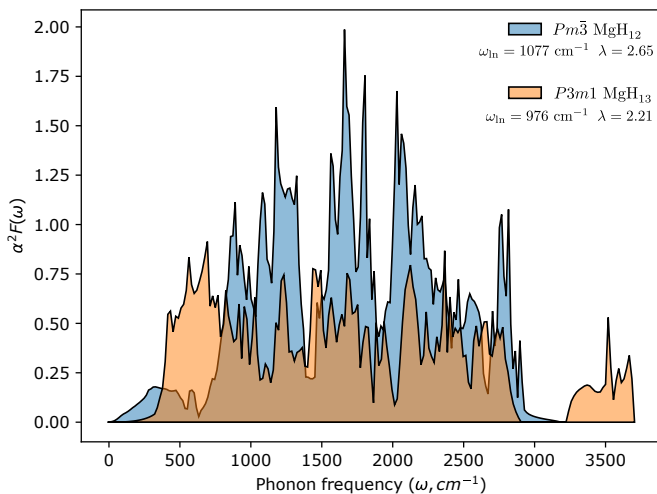


FIG. 13. The Eliashberg functions of the $Pm\bar{3}$ structure of MgH_{12} (a hot superconductor with a T_c of 360–402 K) and the $P3m1$ structure of MgH_{13} , both at 500 GPa.

E. Dynamically unstable structures

Structures that are found to be dynamically unstable correspond to saddle-points, rather than minima, of the potential energy surface. Such structures can be stabilized by anharmonic or thermal effects, as is the case in $Fm\bar{3}m$ - LaH_{10} at 200 GPa [26, 74, 106], and locating them is the goal of sp-AIRSS [12]. The calculations required to filter out, or correctly treat [107–110], dynamically unstable superconductors are expensive; the solution of this problem will be important in the further development of high-throughput workflows. However, one can roughly establish the promise of a saddle-point superconductor by simply neglecting unstable modes in the calculation of the Eliashberg function [26, 111]. We provide the results of this procedure for dynamically unstable structures that were flagged by the final model in the Supplementary Information [90] (see also Fig. 3), along with a short discussion of the validity of this procedure.

F. A modified Allen-Dynes equation

Having a large number of superconductors for which the Eliashberg equations have been solved directly (see Table I) provides a unique opportunity to test the Allen-Dynes equation. This comparison is made in Fig. 14 (a), where it is clear to see that, while the Allen-Dynes result correlates well with the Eliashberg result, it systematically underestimates its value (at least for the binary hydride superconductors studied in this work). We fit a modified version of the Allen-Dynes equation of the form

$$T_c = T_c^{(AD)}(a + b\lambda) \quad (4)$$

to the data given in Table I, which gives $a = 1.0061$ and $b = 0.0663$. As we can see in Fig. 14 (b) this removes the systematic underestimation and slightly reduces the variance of the prediction. However, given access to $\alpha^2 F(\omega)$, we recommend that the Eliashberg equations be solved directly, to remove the need for approximate T_c predictors entirely.

V. CONCLUSIONS

In this work, we demonstrate a high-throughput method to efficiently discover high- T_c binary hydrides. We construct a T_c model based on physically-motivated descriptors, trained initially on superconductivity data from the literature and iteratively updated using the results of our own DFPT calculations. Following extensive structure searching, a two-step screening process (based on stability criteria and the predictions of our model) allows us to identify energetically-competitive high- T_c candidates from the large volume of search data. The best candidates include hydrides of sodium, calcium, actinium, lanthanum, magnesium, yttrium, scandium, lithium and strontium.

We have performed a total of 240 T_c calculations using DFPT, split roughly equally between the training phase and final results. This was made possible by optimizing the QUANTUM ESPRESSO electron-phonon code. In the final results, we identify 36 dynamically stable superconductors with $T_c > 100$ K of which 18 have $T_c > 200$ K (see Table I). To the best of our knowledge, superconductivity has not been investigated previously in 27 of the 36 (see Table I and the Supplementary Information [90]). These findings add considerably to the known pressure- T_c behaviour of the binary hydrides. Of particular note, we find a $Pm\bar{3}m$ structure of NaH_6 to have a T_c of 248–279 K at 100 GPa, suggesting the exciting possibility of other low-pressure high- T_c hydride superconductors. We also identify $Pm\bar{3}$ - MgH_{12} and $Fm\bar{3}m$ - SrH_{10} as above-room-temperature superconductors at 500 GPa, as well as several near-room-temperature superconductors at lower pressures.

Throughout this work, our aim has been to consider as wide a range of binary compositions as possible; since

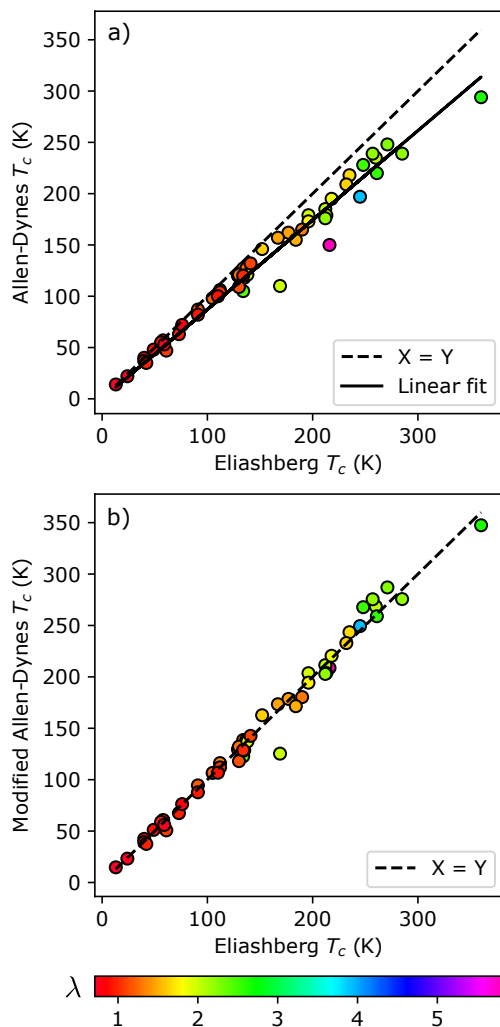


FIG. 14. (a) Allen-Dynes critical temperatures, plotted against critical temperatures from solution of the Eliashberg equations (data from Table I). (b) The same as (a), but using the modified Allen-Dynes equation (Eq. 4).

our focus is on breadth, we make no claim that this study is exhaustive. Despite this, we identify a large num-

ber of high- T_c candidates, suggesting the binaries have more to offer in future, more focused, studies. We also note that the highest critical temperature results at each pressure arise from metastable structures or off-hull stoichiometries. Many of these were introduced into the study during the training phase by focusing on high-symmetry structures using sp-AIRSS. This suggests that the additional freedom afforded by allowing some degree of metastability can reveal higher critical temperature superconductors. For example, in the case of SrH_{10} at 500 GPa we see that the ground state $R\bar{3}m$ structure has a critical temperature nearly 100 K lower than a metastable $Fm\bar{3}m$ structure. Exploring avenues such as metastability will be important in future work in order to push the boundaries of high-temperature superconductivity.

Future work on superconducting hydrides is likely to focus on ternary hydrides and higher order systems. Given the increased complexity of these systems, high-throughput screening approaches, such as the one presented here, are likely to become increasingly important. Our high-throughput methodology could be extended to ternary hydrides, although it may be desirable to redefine these systems as effective binaries in order make use of the extensive binary hydride literature data during model training.

VI. ACKNOWLEDGEMENTS

AMS is funded by an EPSRC studentship. MJH acknowledges the EPSRC Centre for Doctoral Training in Computational Methods for Materials Science for funding under grant number EP/L015552/1. RJN is supported by EPSRC under Critical Mass Grant EP/P034616/1 and the UKCP consortium grant EP/P022596/1. CJP was supported by the Royal Society through a Royal Society Wolfson Research Merit award. This work has been performed using resources provided by the Cambridge Tier-2 system operated by the University of Cambridge Research Computing Service (<http://www.hpc.cam.ac.uk>) funded by EPSRC Tier-2 capital grant EP/P020259/1.

-
- [1] D. Duan, Y. Liu, Y. Ma, Z. Shao, B. Liu, and T. Cui, Structure and superconductivity of hydrides at high pressures, *National Science Review* **4**, 121 (2017).
 - [2] E. Zurek and T. Bi, High-temperature superconductivity in alkaline and rare earth polyhydrides at high pressure: A theoretical perspective, *The Journal of chemical physics* **150**, 050901 (2019).
 - [3] J. A. Flores-Livas, L. Boeri, A. Sanna, G. Profeta, R. Arita, and M. Eremets, A perspective on conventional high-temperature superconductors at high pressure: Methods and materials, *Physics Reports* (2020).
 - [4] L. Boeri and G. B. Bachelet, Viewpoint: the road to room-temperature conventional superconductivity, *J. Phys: Condens. Matt.* **31**, 234002 (2019).
 - [5] A. R. Oganov, C. J. Pickard, Q. Zhu, and R. J. Needs, Structure prediction drives materials discovery, *Nature Reviews Materials* **4**, 331 (2019).
 - [6] C. J. Pickard, I. Errea, and M. I. Eremets, Superconducting hydrides under pressure, *Annual Review of Condensed Matter Physics* **11**, 57 (2020).
 - [7] G. D. Gaspari and B. L. Gyorffy, Electron-phonon interactions, d resonances, and superconductivity in transition metals, *Phys. Rev. Lett.* **28**, 801 (1972).

- [8] C. J. Pickard and R. J. Needs, High-pressure phases of silane, *Phys. Rev. Lett.* **97**, 045504 (2006).
- [9] C. J. Pickard and R. J. Needs, Ab initio random structure searching, *J. Phys: Condens. Matt.* **23**, 053201 (2011).
- [10] S. J. Clark, M. D. Segall, C. J. Pickard, P. J. Hasnip, M. I. J. Probert, K. Refson, and M. C. Payne, First principles methods using CASTEP, *Zeitschrift für Kristallographie-Crystalline Materials* **220**, 567 (2005).
- [11] J. P. Perdew, K. Burke, and M. Ernzerhof, Generalized gradient approximation made simple, *Phys. Rev. Lett.* **77**, 3865 (1996).
- [12] B. Monserrat, N. D. Drummond, P. Dalladay-Simpson, R. T. Howie, P. López Ríos, E. Gregoryanz, C. J. Pickard, and R. J. Needs, Structure and metallicity of phase v of hydrogen, *Phys. Rev. Lett* **120**, 255701 (2018).
- [13] W. L. McMillan, Transition temperature of strong-coupled superconductors, *Physical Review* **167**, 331 (1968).
- [14] J. J. Hopfield, Angular momentum and transition-metal superconductivity, *Physical Review* **186**, 443 (1969).
- [15] J. C. Slater, Wave functions in a periodic potential, *Physical Review* **51**, 846 (1937).
- [16] D. A. Papaconstantopoulos, B. Klein, M. J. Mehl, and W. E. Pickett, Cubic H₃S around 200GPa: An atomic hydrogen superconductor stabilized by sulfur, *Phys. Rev. B* **91**, 184511 (2015).
- [17] P.-H. Chang, S. Silayi, D. Papaconstantopoulos, and M. Mehl, Pressure-induced high-temperature superconductivity in hypothetical h₃x (x=as, se, br, sb, te and i) in the h₃s structure with im $\bar{3}$ m symmetry, *Journal of Physics and Chemistry of Solids* **139**, 109315 (2020).
- [18] J. J. Sakurai and J. Napolitano, Scattering theory, in *Modern Quantum Mechanics* (Cambridge University Press, 2017) p. 386–445, 2nd ed.
- [19] <http://elk.sourceforge.net/>, the ELK FP-LAPW code.
- [20] M. J. Hutcheon, A. M. Shipley, and R. J. Needs, Predicting novel superconducting hydrides using machine learning approaches, *Phys. Rev. B* **101**, 144505 (2020).
- [21] P. B. Allen and R. C. Dynes, Transition temperature of strong-coupled superconductors reanalyzed, *Phys. Rev. B* **12**, 905 (1975).
- [22] P. Giannozzi, S. Baroni, N. Bonini, M. Calandra, R. Car, C. Cavazzoni, D. Ceresoli, G. L. Chiarotti, M. Cococcioni, I. Dabo, A. Dal Corso, S. de Gironcoli, S. Fabris, G. Fratesi, R. Gebauer, U. Gerstmann, C. Gougoussis, A. Kokalj, M. Lazzeri, L. Martin-Samos, N. Marzari, F. Mauri, R. Mazzarello, S. Paolini, A. Pasquarello, L. Paulatto, C. Sbraccia, S. Scandolo, G. Sclauzero, A. P. Seitsonen, A. Smogunov, P. Umari, and R. M. Wentzcovitch, QUANTUM ESPRESSO: a modular and open-source software project for quantum simulations of materials, *Journal of Physics: Condensed Matter* **21**, 395502 (19pp) (2009).
- [23] P. Giannozzi, O. Andreussi, T. Brumme, O. Bunau, M. B. Nardelli, M. Calandra, R. Car, C. Cavazzoni, D. Ceresoli, M. Cococcioni, N. Colonna, I. Carnimeo, A. D. Corso, S. de Gironcoli, P. Delugas, R. A. DiStasio, A. Ferretti, A. Floris, G. Fratesi, G. Fugallo, R. Gebauer, U. Gerstmann, F. Giustino, T. Gorni, J. Jia, M. Kawamura, H.-Y. Ko, A. Kokalj, E. Küçükbenli, M. Lazzeri, M. Marsili, N. Marzari, F. Mauri, N. L. Nguyen, H.-V. Nguyen, A. O. de-la Roza, L. Paulatto, S. Poncé, D. Rocca, R. Sabatini, B. Santra, M. Schlipf, A. P. Seitsonen, A. Smogunov, I. Timrov, T. Thonhauser, P. Umari, N. Vast, X. Wu, and S. Baroni, Advanced capabilities for materials modelling with quantum ESPRESSO, *Journal of Physics: Condensed Matter* **29**, 465901 (2017).
- [24] G. M. Eliashberg, Interactions between electrons and lattice vibrations in a superconductor, *Sov. Phys. JETP* **11**, 696 (1960).
- [25] M. Wierzbowska, S. de Gironcoli, and P. Giannozzi, Origins of low-and high-pressure discontinuities of t_c in niobium, [arXiv:cond-mat/0504077](https://arxiv.org/abs/cond-mat/0504077) (2005).
- [26] A. M. Shipley, M. J. Hutcheon, M. S. Johnson, R. J. Needs, and C. J. Pickard, Stability and superconductivity of lanthanum and yttrium decahydrides, *Phys. Rev. B* **101**, 224511 (2020).
- [27] The optimizations to QUANTUM ESPRESSO resulting from this work have been submitted to the developers (see <https://gitlab.com/miicck/q-e>).
- [28] D. V. Semenov, A. G. Kvasnin, I. A. Kruglov, and A. R. Oganov, Actinium hydrides ach10, ach12, and ach16 as high-temperature conventional superconductors, *The journal of physical chemistry letters* **9**, 1920 (2018).
- [29] P. Hou, X. Zhao, F. Tian, D. Li, D. Duan, Z. Zhao, B. Chu, B. Liu, and T. Cui, High pressure structures and superconductivity of alh₃ (h₂) predicted by first principles, *RSC Advances* **5**, 5096 (2015).
- [30] Y. Fu, X. Du, L. Zhang, F. Peng, M. Zhang, C. J. Pickard, R. J. Needs, D. J. Singh, W. Zheng, and Y. Ma, High-pressure phase stability and superconductivity of pnictogen hydrides and chemical trends for compressed hydrides, *Chemistry of Materials* **28**, 1746 (2016).
- [31] K. Abe and N. Ashcroft, Crystalline diborane at high pressures, *Physical Review B* **84**, 104118 (2011).
- [32] S. Yu, Q. Zeng, A. R. Oganov, C. Hu, G. Frapper, and L. Zhang, Exploration of stable compounds, crystal structures, and superconductivity in the be-h system, *AIP Advances* **4**, 107118 (2014).
- [33] C.-H. Hu, A. R. Oganov, Q. Zhu, G.-R. Qian, G. Frapper, A. O. Lyakhov, and H.-Y. Zhou, Pressure-induced stabilization and insulator-superconductor transition of bh, *Physical review letters* **110**, 165504 (2013).
- [34] Y. Ma, D. Duan, D. Li, Y. Liu, F. Tian, H. Yu, C. Xu, Z. Shao, B. Liu, and T. Cui, High-pressure structures and superconductivity of bismuth hydrides, [arXiv preprint arXiv:1511.05291](https://arxiv.org/abs/1511.05291) (2015).
- [35] H. Wang, S. T. John, K. Tanaka, T. Iitaka, and Y. Ma, Superconductive sodalite-like clathrate calcium hydride at high pressures, *Proceedings of the National Academy of Sciences* **109**, 6463 (2012).
- [36] N. P. Salke, M. M. D. Esfahani, Y. Zhang, I. A. Kruglov, J. Zhou, Y. Wang, E. Greenberg, V. B. Prakapenka, J. Liu, A. R. Oganov, and J.-F. Lin, Synthesis of clathrate cerium superhydride ceh₉ at 80-100 gpa with atomic hydrogen sublattice, *Nature communications* **10**, 1 (2019).
- [37] S. Yu, X. Jia, G. Frapper, D. Li, A. R. Oganov, Q. Zeng, and L. Zhang, Pressure-driven formation and stabilization of superconductive chromium hydrides, *Scientific reports* **5**, 17764 (2015).
- [38] C. Heil, G. B. Bachelet, and L. Boeri, Absence of superconductivity in iron polyhydrides at high pressures, *Physical Review B* **97**, 214510 (2018).

- [39] M. M. D. Esfahani, A. R. Oganov, H. Niu, and J. Zhang, Superconductivity and unexpected chemistry of germanium hydrides under pressure, *Physical Review B* **95**, 134506 (2017).
- [40] G. Gao, A. R. Oganov, A. Bergara, M. Martinez-Canales, T. Cui, T. Iitaka, Y. Ma, and G. Zou, Superconducting high pressure phase of germane, *Physical review letters* **101**, 107002 (2008).
- [41] G. Zhong, C. Zhang, X. Chen, Y. Li, R. Zhang, and H. Lin, Structural, electronic, dynamical, and superconducting properties in dense GeH_4 , *The Journal of Physical Chemistry C* **116**, 5225 (2012).
- [42] D. Duan, F. Tian, Y. Liu, X. Huang, D. Li, H. Yu, Y. Ma, B. Liu, and T. Cui, Enhancement of T_c in the atomic phase of iodine-doped hydrogen at high pressures, *Physical Chemistry Chemical Physics* **17**, 32335 (2015).
- [43] A. Champ and E. Zurek, Superconducting high-pressure phases composed of hydrogen and iodine, *The journal of physical chemistry letters* **6**, 4067 (2015).
- [44] D. Duan, Y. Liu, F. Tian, D. Li, X. Huang, Z. Zhao, H. Yu, B. Liu, W. Tian, and T. Cui, Pressure-induced metallization of dense H_2 with high- T_c superconductivity, *Scientific reports* **4**, 6968 (2014).
- [45] I. Errea, M. Calandra, C. J. Pickard, J. Nelson, R. J. Needs, Y. Li, H. Liu, Y. Zhang, Y. Ma, and F. Mauri, High-pressure hydrogen sulfide from first principles: A strongly anharmonic phonon-mediated superconductor, *Physical review letters* **114**, 157004 (2015).
- [46] S. Zhang, Y. Wang, J. Zhang, H. Liu, X. Zhong, H.-F. Song, G. Yang, L. Zhang, and Y. Ma, Phase diagram and high-temperature superconductivity of compressed selenium hydrides, *Scientific reports* **5**, 15433 (2015).
- [47] Y. Liu, D. Duan, F. Tian, C. Wang, G. Wu, Y. Ma, H. Yu, D. Li, B. Liu, and T. Cui, Prediction of stoichiometric PbH_n compounds: crystal structures and properties, *RSC Advances* **5**, 103445 (2015).
- [48] X. Zhong, H. Wang, J. Zhang, H. Liu, S. Zhang, H.-F. Song, G. Yang, L. Zhang, and Y. Ma, Tellurium hydrides at high pressures: High-temperature superconductors, *Physical review letters* **116**, 057002 (2016).
- [49] D. Zhou, X. Jin, X. Meng, G. Bao, Y. Ma, B. Liu, and T. Cui, Ab initio study revealing a layered structure in hydrogen-rich KH_6 under high pressure, *Physical Review B* **86**, 014118 (2012).
- [50] I. A. Kruglov, D. V. Semenok, H. Song, R. L. Szczeniak, I. A. Wrona, R. Akashi, M. M. D. Esfahani, D. Duan, T. Cui, A. G. Kvashnin, and A. R. Oganov, Superconductivity of LaH_{10} and LaH_{16} polyhydrides, *Phys. Rev. B* **101**, 024508 (2020).
- [51] G. Gao, R. Hoffmann, N. W. Ashcroft, H. Liu, A. Bergara, and Y. Ma, Theoretical study of the ground-state structures and properties of niobium hydrides under pressure, *Physical Review B* **88**, 184104 (2013).
- [52] D. Zhou, D. V. Semenok, H. Xie, X. Huang, D. Duan, A. Aperis, P. M. Oppeneer, M. Galasso, A. I. Kartsev, A. G. Kvashnin, A. R. Oganov, and T. Cui, High-pressure synthesis of magnetic neodymium polyhydrides, *Journal of the American Chemical Society* **142**, 2803 (2020).
- [53] Y. Liu, D. Duan, X. Huang, F. Tian, D. Li, X. Sha, C. Wang, H. Zhang, T. Yang, B. Liu, and T. Cui, Structures and properties of osmium hydrides under pressure from first principle calculation, *The Journal of Physical Chemistry C* **119**, 15905 (2015).
- [54] D. Zhou, D. V. Semenok, D. Duan, H. Xie, W. Chen, X. Huang, X. Li, B. Liu, A. R. Oganov, and T. Cui, Superconducting praseodymium superhydrides, *Science Advances* **6** (2020).
- [55] Y. Liu, D. Duan, F. Tian, C. Wang, Y. Ma, D. Li, X. Huang, B. Liu, and T. Cui, Stability and properties of the Ru-H system at high pressure, *Physical Chemistry Chemical Physics* **18**, 1516 (2016).
- [56] Y. Ma, D. Duan, D. Li, Y. Liu, F. Tian, X. Huang, Z. Zhao, H. Yu, B. Liu, and T. Cui, The unexpected binding and superconductivity in SbH_4 at high pressure, *arXiv preprint arXiv:1506.03889* (2015).
- [57] X. Ye, N. Zarifi, E. Zurek, R. Hoffmann, and N. Ashcroft, High hydrides of scandium under pressure: potential superconductors, *The Journal of Physical Chemistry C* **122**, 6298 (2018).
- [58] X. Jin, X. Meng, Z. He, Y. Ma, B. Liu, T. Cui, G. Zou, and H.-k. Mao, Superconducting high-pressure phases of disilane, *Proceedings of the National Academy of Sciences* **107**, 9969 (2010).
- [59] M. M. D. Esfahani, Z. Wang, A. R. Oganov, H. Dong, Q. Zhu, S. Wang, M. S. Rakin, and X.-F. Zhou, Superconductivity of novel tin hydrides (Sn_nH_m) under pressure, *Scientific reports* **6**, 22873 (2016).
- [60] Q. Zhuang, X. Jin, T. Cui, Y. Ma, Q. Lv, Y. Li, H. Zhang, X. Meng, and K. Bao, Pressure-stabilized superconductive ionic tantalum hydrides, *Inorganic chemistry* **56**, 3901 (2017).
- [61] X. Li, H. Liu, and F. Peng, Crystal structures and superconductivity of technetium hydrides under pressure, *Physical Chemistry Chemical Physics* **18**, 28791 (2016).
- [62] A. G. Kvashnin, D. V. Semenok, I. A. Kruglov, I. A. Wrona, and A. R. Oganov, High-temperature superconductivity in a Th-H system under pressure conditions, *ACS applied materials & interfaces* **10**, 43809 (2018).
- [63] D. V. Semenok, A. G. Kvashnin, A. G. Ivanova, V. Svitlyk, V. Y. Fomin, A. V. Sadakov, O. A. Sobolevskiy, V. M. Pudalov, I. A. Troyan, and A. R. Oganov, Superconductivity at 161k in thorium hydride ThH_{10} : Synthesis and properties, *Materials Today* **33**, 36 (2020).
- [64] I. A. Kruglov, A. G. Kvashnin, A. F. Goncharov, A. R. Oganov, S. S. Lobanov, N. Holtgrewe, S. Jiang, V. B. Prakapenka, E. Greenberg, and A. V. Yanilkin, Uranium polyhydrides at moderate pressures: Prediction, synthesis, and expected superconductivity, *Science advances* **4** (2018).
- [65] X. Li and F. Peng, Superconductivity of pressure-stabilized vanadium hydrides, *Inorganic chemistry* **56**, 13759 (2017).
- [66] S. Zheng, S. Zhang, Y. Sun, J. Zhang, J. Lin, G. Yang, and A. Bergara, Structural and superconducting properties of tungsten hydrides under high pressure, *Frontiers in Physics* **6**, 101 (2018).
- [67] L.-L. Liu, H.-J. Sun, C. Wang, and W.-C. Lu, High-pressure structures of yttrium hydrides, *Journal of Physics: Condensed Matter* **29**, 325401 (2017).
- [68] X.-F. Li, Z.-Y. Hu, and B. Huang, Phase diagram and superconductivity of compressed zirconium hydrides, *Physical Chemistry Chemical Physics* **19**, 3538 (2017).
- [69] K. Abe, High-pressure properties of dense metallic zirconium hydrides studied by ab initio calculations, *Physical Review B* **98**, 134103 (2018).

- [70] D. V. Semenov, I. A. Kruglov, I. A. Savkin, A. G. Kvashnin, and A. R. Oganov, On distribution of superconductivity in metal hydrides, *Current Opinion in Solid State and Materials Science*, 100808 (2020).
- [71] Q. Gu, P. Lu, K. Xia, J. Sun, and D. Xing, High-temperature superconducting phase of hbr under pressure predicted by first-principles calculations, *Physical Review B* **96**, 064517 (2017).
- [72] T. Bi, N. Zarifi, T. Terpstra, and E. Zurek, The search for superconductivity in high pressure hydrides, in *Reference Module in Chemistry, Molecular Sciences and Chemical Engineering* (Elsevier, 2019).
- [73] <https://uk.mathworks.com/help/stats/fitrgp.html>, MATLAB GPR fitting documentation.
- [74] A. Drozdov, P. Kong, V. Minkov, S. Besedin, M. Kuzovnikov, S. Mozaffari, L. Balicas, F. Balakirev, D. Graf, V. Prakapenka, E. Greenberg, D. Knyazev, M. Tkacz, and M. Eremets, Superconductivity at 250 k in lanthanum hydride under high pressures, *Nature* **569**, 528 (2019).
- [75] A. Drozdov, M. Eremets, I. Troyan, V. Ksenofontov, and S. Shylin, Conventional superconductivity at 203 kelvin at high pressures in the sulfur hydride system, *Nature* **525**, 73 (2015).
- [76] F. Peng, Y. Sun, C. J. Pickard, R. J. Needs, Q. Wu, and Y. Ma, Hydrogen clathrate structures in rare earth hydrides at high pressures: possible route to room-temperature superconductivity, *Physical review letters* **119**, 107001 (2017).
- [77] Y. Xie, Q. Li, A. Oganov, and H. Wang, Superconductivity of lithium-doped hydrogen under high pressure, *Acta Crystallographica Section C: Structural Chemistry* **70**, 104 (2014).
- [78] R. T. Howie, O. Narygina, C. L. Guillaume, S. Evans, and E. Gregoryanz, High-pressure synthesis of lithium hydride, *Physical Review B* **86**, 064108 (2012).
- [79] H. Liu, I. I. Naumov, R. Hoffmann, N. Ashcroft, and R. J. Hemley, Potential high- T_c superconducting lanthanum and yttrium hydrides at high pressure, *Proceedings of the National Academy of Sciences* **114**, 6990 (2017).
- [80] M. Somayazulu, M. Ahart, A. K. Mishra, Z. M. Geballe, M. Baldini, Y. Meng, V. V. Struzhkin, and R. J. Hemley, Evidence for superconductivity above 260 k in lanthanum superhydride at megabar pressures, *Physical review letters* **122**, 027001 (2019).
- [81] K. Abe, Hydrogen-rich scandium compounds at high pressures, *Physical Review B* **96**, 144108 (2017).
- [82] K. Tanaka, J. Tse, and H. Liu, Electron-phonon coupling mechanisms for hydrogen-rich metals at high pressure, *Physical Review B* **96**, 100502 (2017).
- [83] X. Feng, J. Zhang, G. Gao, H. Liu, and H. Wang, Compressed sodalite-like mgh6 as a potential high-temperature superconductor, *RSC Advances* **5**, 59292 (2015).
- [84] D. C. Lonie, J. Hooper, B. Altintas, and E. Zurek, Metallization of magnesium polyhydrides under pressure, *Physical Review B* **87**, 054107 (2013).
- [85] P. Kong, V. Minkov, M. Kuzovnikov, S. Besedin, A. Drozdov, S. Mozaffari, L. Balicas, F. Balakirev, V. Prakapenka, E. Greenberg, D. Knyazev, and E. M. I., Superconductivity up to 243 k in yttrium hydrides under high pressure, arXiv preprint arXiv:1909.10482 (2019).
- [86] J. Nagamatsu, N. Nakagawa, T. Muranaka, Y. Zenitani, and J. Akimitsu, Superconductivity at 39 k in magnesium diboride, *Nature* **410**, 63 (2001).
- [87] G. Wu, Y. L. Xie, H. Chen, M. Zhong, R. H. Liu, B. C. Shi, Q. J. Li, X. F. Wang, T. Wu, Y. J. Yan, J. J. Ying, and X. H. Chen, Superconductivity at 56 k in samarium-doped SrFeAsF, *Journal of Physics: Condensed Matter* **21**, 142203 (2009).
- [88] A. Schilling, M. Cantoni, J. D. Guo, and H. R. Ott, Superconductivity above 130 k in the hg-ba-ca-cu-o system, *Nature* **363**, 56 (1993).
- [89] E. Snider, N. Dasenbrock-Gammon, R. McBride, M. Debessai, H. Vindana, K. Venkatasamy, K. V. Lawler, A. Salamat, and R. P. Dias, Room-temperature superconductivity in a carbonaceous sulfur hydride, *Nature* **586**, 373 (2020).
- [90] See supplementary information, which includes refs. [112–121].
- [91] Structures from table 1 (cambridge online data repository), <https://doi.org/10.17863/CAM.72574>.
- [92] P. Baettig and E. Zurek, Pressure-stabilized sodium polyhydrides: NaH_n ($n > 1$), *Phys. Rev. Lett.* **106**, 237002 (2011).
- [93] V. V. Struzhkin, D. Y. Kim, E. Stavrou, T. Muramatsu, H.-k. Mao, C. J. Pickard, R. J. Needs, V. B. Prakapenka, and A. F. Goncharov, Synthesis of sodium polyhydrides at high pressures, *Nature Communications* **7**, 12267 (2016).
- [94] C. Wang, S. Yi, and J.-H. Cho, Pressure dependence of the superconducting transition temperature of compressed LaH_{10} , *Phys. Rev. B* **100**, 060502 (2019).
- [95] G. Bergmann and D. Rainer, The sensitivity of the transition temperature to changes in $\alpha^2 f(\omega)$, *Zeitschrift für Physik* **263**, 59 (1973).
- [96] J. Hooper and E. Zurek, High pressure potassium polyhydrides: A chemical perspective, *The Journal of Physical Chemistry C* **116**, 13322 (2012).
- [97] Z. M. Geballe, H. Liu, A. K. Mishra, M. Ahart, M. Somayazulu, Y. Meng, M. Baldini, and R. J. Hemley, Synthesis and stability of lanthanum superhydrides, *Angewandte Chemie International Edition* **57**, 688 (2018).
- [98] H. Liu, I. I. Naumov, Z. M. Geballe, M. Somayazulu, S. T. John, and R. J. Hemley, Dynamics and superconductivity in compressed lanthanum superhydride, *Physical Review B* **98**, 100102 (2018).
- [99] W. Sukmas, P. Tsuppayakorn-aek, U. Pinsook, and T. Bovornratanarak, Near-room-temperature superconductivity of mg/ca substituted metal hexahydride under pressure, *Journal of Alloys and Compounds* **849**, 156434 (2020).
- [100] C. Heil, S. Di Cataldo, G. B. Bachelet, and L. Boeri, Superconductivity in sodalite-like yttrium hydride clathrates, *Physical Review B* **99**, 220502 (2019).
- [101] I. A. Troyan, D. V. Semenov, A. G. Kvashnin, A. V. Sadakov, O. A. Sobolevskiy, V. M. Pudalov, A. G. Ivanova, V. B. Prakapenka, E. Greenberg, A. G. Gavriliuk, I. S. Lyubutin, V. V. Struzhkin, A. Bergara, I. Errea, R. Bianco, M. Calandra, F. Mauri, L. Monacelli, R. Akashi, and A. R. Oganov, Anomalous high-temperature superconductivity in yh6, *Advanced Materials* **33**, 2006832 (2021).
- [102] Y. Li, J. Hao, H. Liu, S. T. John, Y. Wang, and Y. Ma, Pressure-stabilized superconductive yttrium hydrides, *Scientific reports* **5**, 9948 (2015).

- [103] S. Qian, X. Sheng, X. Yan, Y. Chen, and B. Song, Theoretical study of stability and superconductivity of Sc_n ($n=4-8$) at high pressure, *Physical Review B* **96**, 094513 (2017).
- [104] E. Zurek, R. Hoffmann, N. W. Ashcroft, A. R. Oganov, and A. O. Lyakhov, A little bit of lithium does a lot for hydrogen, *Proceedings of the National Academy of Sciences* **106**, 17640 (2009).
- [105] Y. Wang, H. Wang, S. T. John, T. Iitaka, and Y. Ma, Structural morphologies of high-pressure polymorphs of strontium hydrides, *Physical Chemistry Chemical Physics* **17**, 19379 (2015).
- [106] I. Errea, F. Belli, L. Monacelli, A. Sanna, T. Koretsune, T. Tadano, R. Bianco, M. Calandra, R. Arita, F. Mauri, and J. A. Flores-Livas, Quantum crystal structure in the 250-kelvin superconducting lanthanum hydride, *Nature* **578**, 66 (2020).
- [107] I. Errea, M. Calandra, C. J. Pickard, J. R. Nelson, R. J. Needs, Y. Li, H. Liu, Y. Zhang, Y. Ma, and F. Mauri, Quantum hydrogen-bond symmetrization in the superconducting hydrogen sulfide system, *Nature* **532**, 81 (2016).
- [108] I. Errea, M. Calandra, and F. Mauri, Anharmonic free energies and phonon dispersions from the stochastic self-consistent harmonic approximation: Application to platinum and palladium hydrides, *Phys. Rev. B* **89**, 064302 (2014).
- [109] J. C. K. Hui and P. B. Allen, Effect of lattice anharmonicity on superconductivity, *Journal of Physics F: Metal Physics* **4**, L42 (1974).
- [110] V. Mereghalli and S. Y. Savrasov, Electron-phonon coupling and properties of doped BaBiO_3 , *Phys. Rev. B* **57**, 14453 (1998).
- [111] X. Wan, H.-C. Ding, S. Y. Savrasov, and C.-G. Duan, Electron-phonon superconductivity near charge-density-wave instability in $\text{LaO}_{0.5}\text{F}_{0.5}\text{BiS}_2$: Density-functional calculations, *Phys. Rev. B* **87**, 115124 (2013).
- [112] H. Xie, D. Duan, Z. Shao, H. Song, Y. Wang, X. Xiao, D. Li, F. Tian, B. Liu, and T. Cui, High-temperature superconductivity in ternary clathrate YCaH_{12} under high pressures, *Journal of Physics: Condensed Matter* **31**, 245404 (2019).
- [113] Y. Sun, J. Lv, Y. Xie, H. Liu, and Y. Ma, Route to a superconducting phase above room temperature in electron-doped hydride compounds under high pressure, *Phys. Rev. Lett.* **123**, 097001 (2019).
- [114] R. Szczesniak and A. Durajski, Superconductivity well above room temperature in compressed MgH_6 , *Frontiers of Physics* **11**, 117406 (2016).
- [115] Y. Chen, H. Y. Geng, X. Yan, Y. Sun, Q. Wu, and X. Chen, Prediction of stable ground-state lithium polyhydrides under high pressures, *Inorganic Chemistry* **56**, 3867 (2017).
- [116] J. A. Camargo-Martínez, G. I. González-Pedrerros, and F. Mesa, The higher superconducting transition temperature T_c and the functional derivative of T_c with $\alpha^2F(\omega)$ for electron-phonon superconductors, *Journal of Physics: Condensed Matter* **32**, 505901 (2020).
- [117] Y.-K. Wei, J.-N. Yuan, F. I. Khan, G.-F. Ji, Z.-W. Gu, and D.-Q. Wei, Pressure induced superconductivity and electronic structure properties of scandium hydrides using first principles calculations, *RSC Advances* **6**, 81534 (2016).
- [118] J. S. Smith, S. Desgreniers, D. D. Klug, and S. T. John, High-density strontium hydride: An experimental and theoretical study, *Solid state communications* **149**, 830 (2009).
- [119] Z. Shao, D. Duan, Y. Ma, H. Yu, H. Song, H. Xie, D. Li, F. Tian, B. Liu, and T. Cui, Unique phase diagram and superconductivity of calcium hydrides at high pressures, *Inorganic chemistry* **58**, 2558 (2019).
- [120] H. Xie, Y. Yao, X. Feng, D. Duan, H. Song, Z. Zhang, S. Jiang, S. A. T. Redfern, V. Z. Kresin, C. J. Pickard, and T. Cui, Hydrogen pentagraphenelike structure stabilized by hafnium: A high-temperature conventional superconductor, *Phys. Rev. Lett.* **125**, 217001 (2020).
- [121] J. Hooper, T. Terpstra, A. Shamp, and E. Zurek, Composition and constitution of compressed strontium polyhydrides, *The Journal of Physical Chemistry C* **118**, 6433 (2014).

SUPPLEMENTARY INFORMATION

**VII. THE CRITICAL TEMPERATURE OF
Immm-ScH₈**

We find that an *Immm* structure of ScH₈ exhibits superconductivity at 300 GPa with a T_c of 212-233 K. This is significantly higher than the (Allen-Dynes) value of ~ 115 K obtained in Ref. [103] using a $16 \times 16 \times 16$ **k**-point grid and norm-conserving pseudopotentials with 3 valence electrons for Sc. In contrast, we use a $36 \times 36 \times 36$ **k**-point grid and ultrasoft pseudopotentials with 11 valence electrons for Sc; a more substantial investigation into pseudopotentials is therefore needed to fully resolve this discrepancy. While they did not calculate T_c for ScH₈, critical temperatures of 213 K and 233 K were obtained at 300 GPa for ScH₇ and ScH₉, respectively, in Ref. [57] (remarkably close to our range for ScH₈).

VIII. DYNAMICALLY UNSTABLE CRITICAL TEMPERATURES

For dynamically unstable structures, a large amount of spectral weight can be introduced to the Eliashberg function near to $\omega = 0$ due to the unstable modes. Similarly to what was seen for *Im $\bar{3}m$* CaH₆ at 100 GPa in Fig. 7 of the main text, this strongly affects the Allen-Dynes critical temperature ($T_c^{(AD)}$), because the functional derivative $\delta T_c^{(AD)}/\delta\alpha^2 F(\omega)$ diverges (towards $-\infty$) as $\omega \rightarrow 0$. However, the critical temperature derived from solution of the Eliashberg equations ($T_c^{(E)}$) is much less sensitive ($\delta T_c^{(E)}/\delta\alpha^2 F(\omega) \rightarrow 0$ as $\omega \rightarrow 0$ [116]). Therefore, if one of these unstable superconductors is in reality stabilized by anharmonic effects (as is the case for *Fm $\bar{3}m$* -LaH₁₀ at 200 GPa [26, 74, 106]), then a rough estimate of its promise as a high-temperature superconductor can be estimated by simply neglecting unstable modes in a harmonic calculation of $T_c^{(E)}$. The results of this procedure are shown in Table. II, along with the same procedure for $T_c^{(AD)}$ for comparison. In carrying out a harmonic calculation, we are neglecting anharmonic renormalization of the phonon frequencies, which may affect the critical temperatures, especially if there is a large amount of spectral weight near to $\omega = 0$ to be renormalized. Therefore, an anharmonic treatment is needed to determine the stability and critical temperatures more accurately, especially when the Allen-Dynes and Eliashberg results strongly disagree (as they do in many cases). These results might therefore be used to identify interesting systems to investigate with anharmonic methods.

Stoichiometry	Space group	P(GPa)	$T_c^{(AD)}$ (K)	$T_c^{(E)}$ (K)	E_{stoic} (meV/unit)
LaH ₆	<i>Im$\bar{3}m$</i>	100	119-151	226-250	12*
AcH ₁₀	<i>Fm$\bar{3}m$</i>	100	75-125	171-203	8*
NaH ₁₆	<i>P$\bar{3}1m$</i>	100	81-99	138-163	0*
CaH ₁₁	<i>R$\bar{3}c$</i>	100	30-50	128-161	28*
LaH ₁₄	<i>R$\bar{3}m$</i>	100	80-98	99-123	33*
LaH ₂₄	<i>C2</i>	100	37-55	64-82	0
AcH ₂₁	<i>P$\bar{1}$</i>	100	28-40	28-41	0
CaH ₂₄	<i>Cmcm</i>	100	19-29	19-32	0*
AcH ₆	<i>I4/mmm</i>	200	129-166	279-315	0*
LaH ₁₀	<i>Fm$\bar{3}m$</i>	200	235-260	269-279	0
LaH ₁₀	<i>Immm</i>	200	60-180	265-296	0*
AcH ₆	<i>Cmcm</i>	200	171-220	248-304	0
NaH ₁₀	<i>Cmmm</i>	200	160-170	243-283	8
ScH ₈	<i>R$\bar{3}m$</i>	200	86-179	242-271	-
AcH ₆	<i>Im$\bar{3}m$</i>	200	63-78	241-265	0*
LaH ₁₀	<i>R$\bar{3}m$</i>	200	45-54	225-270	0*
LaH ₁₀	<i>C222₁</i>	200	169-195	221-248	0*
H ₃ S	<i>Fmmm</i>	200	154-180	216-246	0*
AcH ₆	<i>Pmmm</i>	200	67-69	208-238	0*
NaH ₄	<i>Immm</i>	200	106-126	191-218	61*
MgH ₇	<i>C2/m</i>	200	85-102	188-220	29*
AcH ₆	<i>C2/m</i>	200	100-112	184-214	0*
AcH ₁₁	<i>Imm2</i>	200	88-108	165-184	0*
NaH ₅	<i>P4/mmm</i>	200	66-75	134-163	21*
NaH ₁₂	<i>R$\bar{3}m$</i>	200	50-60	122-151	4
MgH ₆	<i>P$\bar{1}$</i>	200	71-104	98-121	19*
MgH ₅	<i>C2/m</i>	200	58-75	71-95	30
Na ₂ H ₇	<i>P$\bar{1}$</i>	200	20-140	57-169	98*
ScH ₁₂	<i>P4/mcc</i>	300	120-136	302-332	0*
NaH ₁₀	<i>Cmmm</i>	300	151-177	243-283	3
KH ₁₁	<i>P4/nmm</i>	300	109-140	233-256	7*
NaH ₁₄	<i>P4/mmm</i>	300	103-126	220-245	1*
SrH ₁₀	<i>Cmcm</i>	300	133-156	215-250	0*
Na ₂ H ₁₁	<i>P2/m</i>	300	60-71	154-185	0*
NaH ₉	<i>P2/m</i>	300	67-80	151-186	0*
LiH ₄	<i>C2/m</i>	300	93-123	131-168	17
MgH ₁₄	<i>P$\bar{1}$</i>	300	55-66	117-143	14
NaH ₁₂	<i>R$\bar{3}m$</i>	300	66-79	88-115	2
KH ₆	<i>Immm</i>	300	40-53	46-64	3
LiH ₁₂	<i>Pm$\bar{3}m$</i>	500	244-330	433-485	26*
NaH ₆	<i>Im$\bar{3}m$</i>	500	215-267	357-406	30*
YH ₁₇	<i>R32</i>	500	137-164	287-331	29
MgH ₉	<i>Cmmm</i>	500	133-168	284-336	7
CaH ₁₀	<i>Fm$\bar{3}m$</i>	500	157-195	238-279	3*
SrH ₂₂	<i>R32</i>	500	167-194	227-266	0*
Y ₂ H ₁₉	<i>C2</i>	500	188-220	214-251	37
MgH ₁₂	<i>Fmmm</i>	500	161-200	208-245	0
YH ₂₂	<i>P$\bar{1}$</i>	500	90-110	203-234	34
NaH ₄	<i>I4₁/amd</i>	500	83-97	193-233	25
YbH ₁₀	<i>R$\bar{3}m$</i>	500	94-136	176-207	0*
YbH ₁₀	<i>Fm$\bar{3}m$</i>	500	76-92	164-202	0
NaH ₅	<i>P4/mmm</i>	500	86-116	85-118	26
MgH ₄	<i>Immm</i>	500	60-70	66-90	0*
MgH ₄	<i>I4/mmm</i>	500	40-63	48-77	0

TABLE II. Dynamically unstable candidate superconductors. Those structures marked with * are not the lowest energy structure for the given stoichiometry (i.e. have non-zero E_{struc}). The Sc-H system was not in the focused searches at 200 GPa.

**IX. 100 K+ DYNAMICALLY STABLE
SUPERCONDUCTORS**

Stoichiometry	Space group	P(GPa)	T_c (K)	Comments
NaH6	$Pm\bar{3}m$	100	263.5	Superconductivity not previously studied to the best of our knowledge. Ref. [93] found NaH ₆ off hull at 50 GPa. Ref. [92] found $Pm\bar{3}m$ -NaH ₆ becomes stable with respect to $P1$ above 150 GPa.
CaH6	$Im\bar{3}m$	100	234.5	Superconductivity studied previously for this structure in Ref. [35]. Ref. [119] found CaH ₆ slightly above the hull at 100 GPa.
NaH6	$Pm\bar{3}m$	200	274	See above comments for NaH ₆ at 100 GPa.
AcH12	$P63mc$	200	262.5	Space group not studied elsewhere to the best of our knowledge. Ref. [28] studies $I4/mmm$ AcH ₁₂ (T_c =148-173 K at 150 GPa). They find AcH ₁₂ on hull at 150 GPa, slightly above at 250 GPa.
MgH13	$Fm\bar{3}m$	200	210	Space group not studied elsewhere to the best of our knowledge. Refs. [84] and [113] predict MgH ₁₃ above hull at 200 and 300 GPa, respectively.
SH3	$Im\bar{3}m$	200	207.5	Well-known structure from experiment [75] and theory [44, 45].
MgH6	$Im\bar{3}m$	300	286	Superconductivity studied previously for this structure. Ref. [83] found MgH ₆ thermodynamically stable above 263 GPa relative to MgH ₂ and H ₂ , and T_c =260 K for the $Im\bar{3}m$ structure above 300 GPa. Ref. [114] calculated much higher T_c for this structure - 420 K at 300 GPa.
YH9	$F\bar{4}3m$	300	277	Space group not studied elsewhere to the best of our knowledge. Ref. [76] predicted YH ₉ stoichiometry on hull 100-400 GPa, with $P63/mmc$ symmetry at 300 GPa. Ref. [26] found YH ₉ on hull at 400 GPa with $P63/mmc$ lowest in energy. Ref. [85] synthesised YH ₉ in $P63/mmc$ structure.
ScH8	$Immm$	300	222.5	Superconductivity studied previously for this structure. Ref. [57] found ScH ₈ above static-lattice convex hull at 150-350 GPa, but on hull at 350-400 GPa when ZPE included. Their predicted phase behaviour is $Immm$ above 320 GPa. Ref. [103] found $Immm$ ScH ₈ stable above 300 GPa, with $T_c \approx 115$ K at 300 GPa. Ref. [76] found ScH ₈ above hull at 100, 200 and 300 GPa.
MgH12	$Pm\bar{3}$	500	381	Space group not studied elsewhere to the best of our knowledge. Ref. [84] looked at lower pressures, calculated T_c =47-60 K for $R3$ MgH ₁₂ at 140 GPa. Ref. [113] found MgH ₁₂ on hull at 300 GPa.
MgH13	$P3m1$	500	272	Space group not studied elsewhere to the best of our knowledge. Ref. [113] finds MgH ₁₃ above hull at 300 GPa.
SrH10	$Fm\bar{3}m$	500	302	Space group not studied elsewhere to the best of our knowledge. Ref. [105] found a $P21/m$ structure at 50 GPa, a $P2/c$ structure at 150 GPa and transition to $R\bar{3}m$ at 300 GPa. Ref. [70] found $C2/m$ SrH ₁₀ at much lower pressures of 100 GPa.
NaH9	$P63/mmc$	500	252	Space group not studied elsewhere to the best of our knowledge. Ref. [92] found a 25-300+ GPa stability range for NaH ₉ (though 500 GPa seems to be outside range of study) with $Cmc21$ -NaH ₉ stable at 300 GPa.
MgH10	$C2/m$	500	251	Space group not studied elsewhere to the best of our knowledge. Ref. [120] found a $P63/mmc$ structure of MgH ₁₀ which was dynamically unstable at 300 GPa. Ref. [113] predicts MgH ₁₀ to be above the hull at 300 GPa.
SrH24	$R\bar{3}$	500	231.5	Stoichiometry not studied elsewhere to the best of our knowledge. Refs. [105, 121] both study Sr-H structures, but don't look at hydrogen content this high.
YH18	$P\bar{1}$	500	229.5	Space group not studied elsewhere to the best of our knowledge. YH ₁₈ stoichiometry mentioned in Fig. 3b of Ref. [85].
YH20	$P\bar{1}$	500	228	Stoichiometry not studied elsewhere to the best of our knowledge. No high hydrogen content on/near hull up to 300 GPa in Ref. [79]. Higher H content YH ₂₄ on hull at 200 and 300 GPa in Ref. [76].
SrH10	$R\bar{3}m$	500	209	Superconductivity studied previously for this structure. Ref. [105] found a $P21/m$ structure at 50 GPa, a $P2/c$ structure at 150 GPa and transition to $R\bar{3}m$ at 300 GPa. Ref. [82] calculated T_c =259 K for $R\bar{3}m$ at 300 GPa.
CaH10	$R\bar{3}m$	500	202	Superconductivity studied previously for this structure. Ref. [119] found $R\bar{3}m$ -CaH ₁₀ metastable at 400 GPa with T_c =157-175 K. They find CaH ₁₀ lies above the hull at 50-400 GPa,

Stoichiometry	Space group	P(GPa)	T_c (K)	Comments
Na2H11	$Cmmm$	100	147.5	Stoichiometry not studied elsewhere to the best of our knowledge.
KH10	$C2/m$	100	145.5	Space group not studied elsewhere to the best of our knowledge. Ref. [70] finds KH10 not on hull at 50 GPa, but $Immm$ -KH10 stable at 150 GPa with an Allen-Dynes T_c of 148K.
NaH8	$I4/mmm$	200	163.5	Space group not studied elsewhere to the best of our knowledge. Ref. [92] finds $P1$ structure below 180 GPa, and $Cmcm$ above.
AcH6	$Fmmm$	200	186.5	Space group not studied elsewhere to the best of our knowledge. Ref. [28] finds this stoichiometry is not on hull at 150 or 250 GPa.
Na2H11	$Cmmm$	200	145.5	Stoichiometry not studied elsewhere to the best of our knowledge.
MgH14	$P\bar{1}$	200	123	Stoichiometry not studied elsewhere to the best of our knowledge. Ref. [113] did not find MgH14 on the hull at 300 GPa.
LaH7	$C2/m$	200	119.5	Superconductivity studied previously for this structure. Ref. [50] found LaH7 not on hull at 200 GPa. They report metastable $C2/m$ LaH7 (17meV/atom above the hull at 150 GPa) with Allen-Dynes $T_c=158-185$ K at 180 GPa.
LiH2	$P6/mmm$	300	192	Space group not studied elsewhere to the best of our knowledge. Ref. [104] predicted 130-300+ GPa stability range for LiH2, with lowest energy structure having $P4/mbm$ symmetry. Ref. [77] found that LiH2 does not exhibit superconductivity at 150 GPa. Ref. [115] looked at lower pressures, found LiH2 to be stable at 130-200 GPa and also looked at $P4/mbm$.
NaH7	$C2/m$	300	182.5	Superconductivity not previously studied to the best of our knowledge. Stability range of NaH7 from Ref. [92] is 25-100 GPa; they study a Cc structure at low pressures and predict a transition to $C2/m$ at 245 GPa.
ScH12	$P\bar{1}$	300	151	Space group not studied elsewhere to the best of our knowledge. Ref. [57] found $Immm$ -ScH12 stable above 320 GPa with $T_c=141-194$ K at 350 GPa. They found the ScH12 stoichiometry to be on the static-lattice hull at 350 GPa and above, close at 300 GPa. Ref. [76] found ScH12 on the hull at 300 GPa, identifying a $C2/c$ structure at this pressure.
LiH6	$R\bar{3}m$	300	145.5	Superconductivity studied previously for this structure. Ref. [104] found a 140-300+ GPa region of stability for LiH6 and found $R\bar{3}m$. Ref. [77] calculated $T_c=82$ K at 300 GPa for $R\bar{3}m$ LiH6. Ref. [115] also studied the $R\bar{3}m$ structure.
ScH6	$Im\bar{3}m$	300	148	Superconductivity studied previously for this structure. Ref. [81] predicted $Im\bar{3}m$ ScH6 stable above 265 GPa with $T_c=130$ K at 285 GPa. Ref. [76] found ScH6 on hull at 300 GPa and identified the $Im\bar{3}m$ structure. Ref. [57] predicted a region of stability for $Im\bar{3}m$ ScH6 above 350 GPa.
NaH5	$P4/mmm$	300	151	Space group not studied elsewhere to the best of our knowledge. Ref. [93] studied lower pressures region, finding a structure with $P-1$ symmetry.
LiH6	$C2/m$	300	146.5	Space group not studied elsewhere to the best of our knowledge. See entry for $R\bar{3}m$ LiH6, $C2/m$ structure of LiH6 not mentioned in these references.
LiH3	$Cmcm$	300	126	Space group not studied elsewhere to the best of our knowledge. LiH3 found to be off-hull in Ref. [104] but no structure given, same as in Ref. [115].
ScH14	$P\bar{1}$	300	103	Stoichiometry not studied elsewhere to the best of our knowledge. Refs. [57], [81] and [117] do not study hydrogen content this high.
Na2H11	$Cmmm$	500	160.5	Stoichiometry not studied elsewhere to the best of our knowledge.
CaH15	$P\bar{6}2m$	500	150.5	Superconductivity not previously studied to the best of our knowledge. Structure found at 200 GPa in Ref. [112], but superconductivity not studied.
SrH15	$P\bar{6}2m$	500	124.5	Stoichiometry not studied elsewhere to the best of our knowledge. Refs. [82, 105, 118, 121] do not study hydrogen content this high.
MgH8	$C2/m$	500	106	Space group not studied elsewhere to the best of our knowledge. MgH8 found to lie off of the convex hull at the lower pressures of 100/200 GPa in Ref. [84].

TABLE IV. Dynamically stable superconductors with T_c between 100 and 200 K found in this work, along with their converged (average) Eliashberg T_c values and notes on findings for these systems in previous work.

X. CONVEX HULLS

On the following pages, we include the static-lattice convex hulls used to assess the stability of structures in the results stage of this work. These are produced from our focused searches as described in Section IV of the main text. To the right of each hull is a list of the on-hull stoichiometries and the space groups of the corresponding on-hull structures. The four columns in this list are stoichiometry, number of formula units in the cell, space group and composition label (x), respectively.

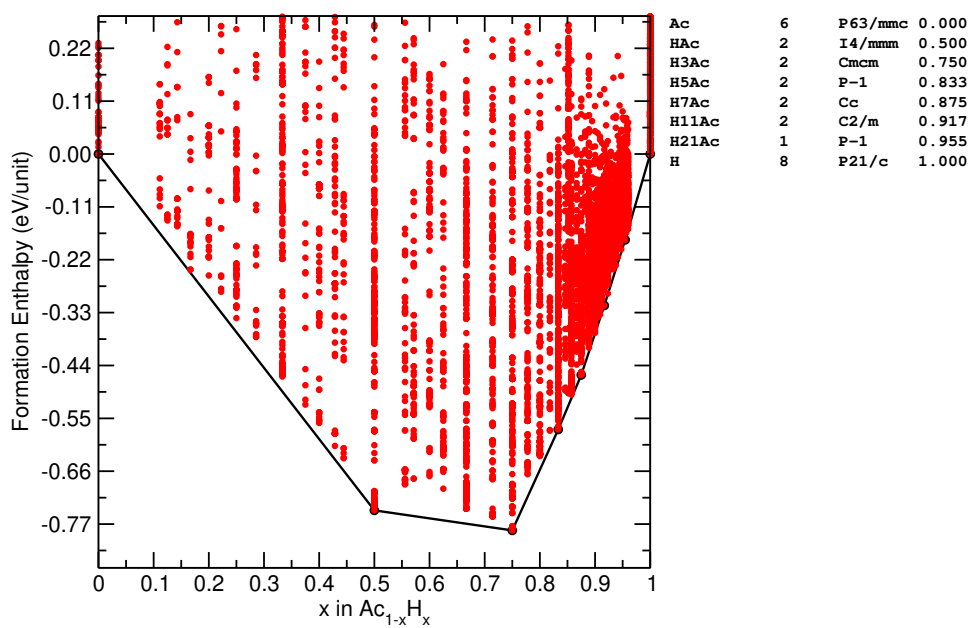


FIG. 15. The convex hull of Ac-H at 100 GPa.

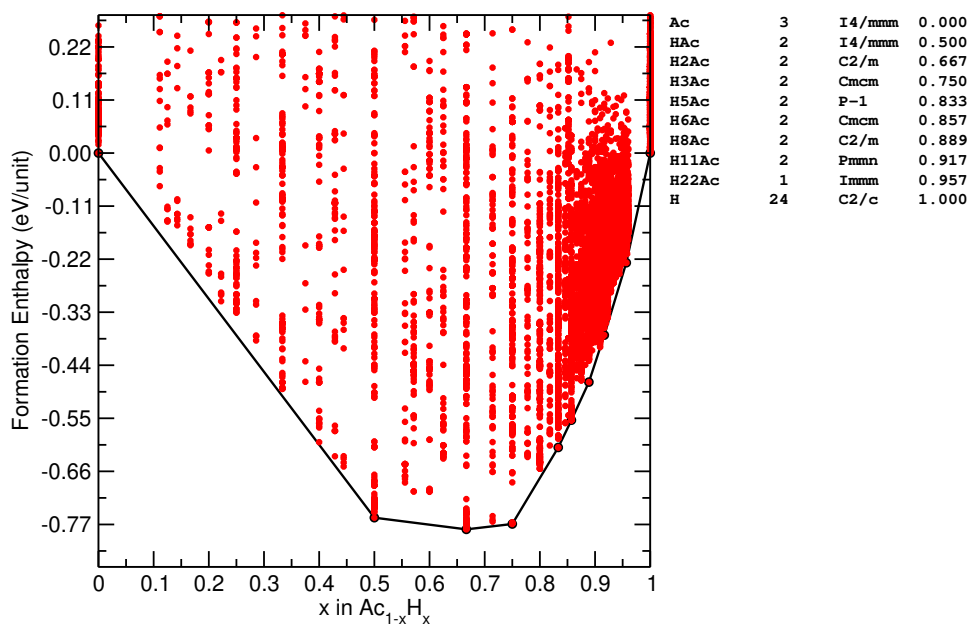


FIG. 16. The convex hull of Ac-H at 200 GPa.

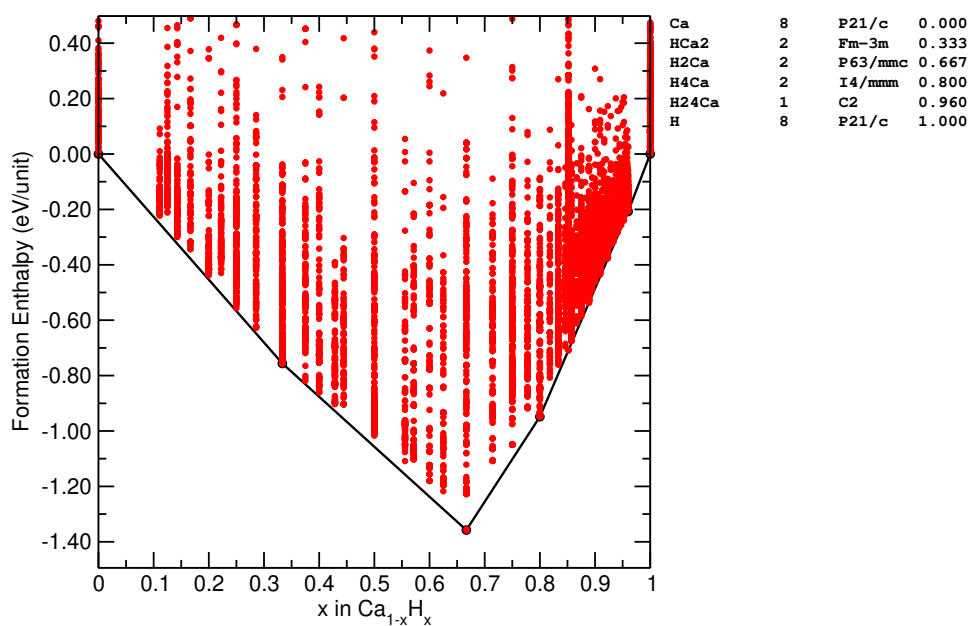


FIG. 17. The convex hull of Ca-H at 100 GPa.

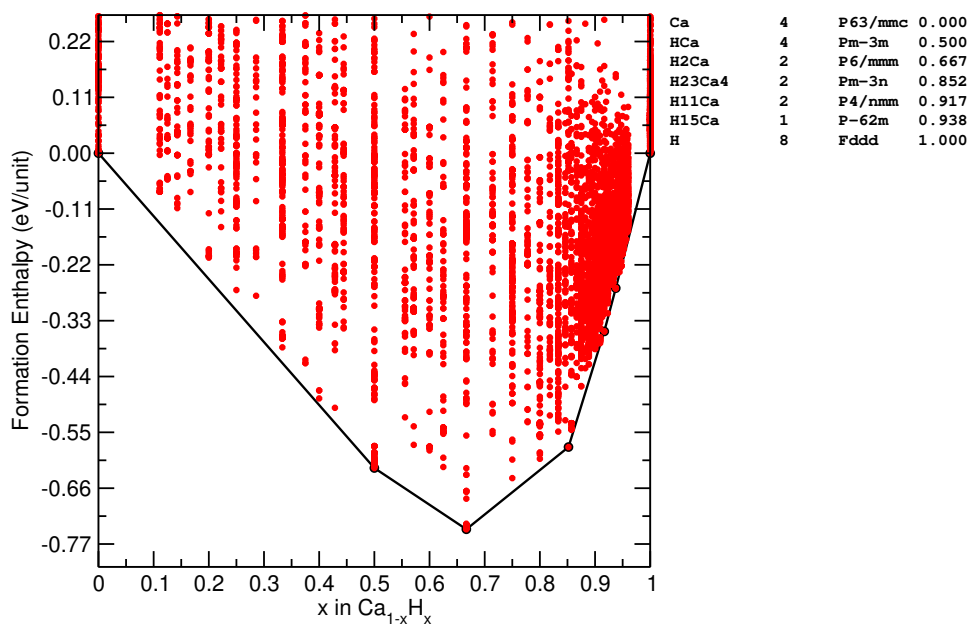


FIG. 18. The convex hull of Ca-H at 500 GPa.

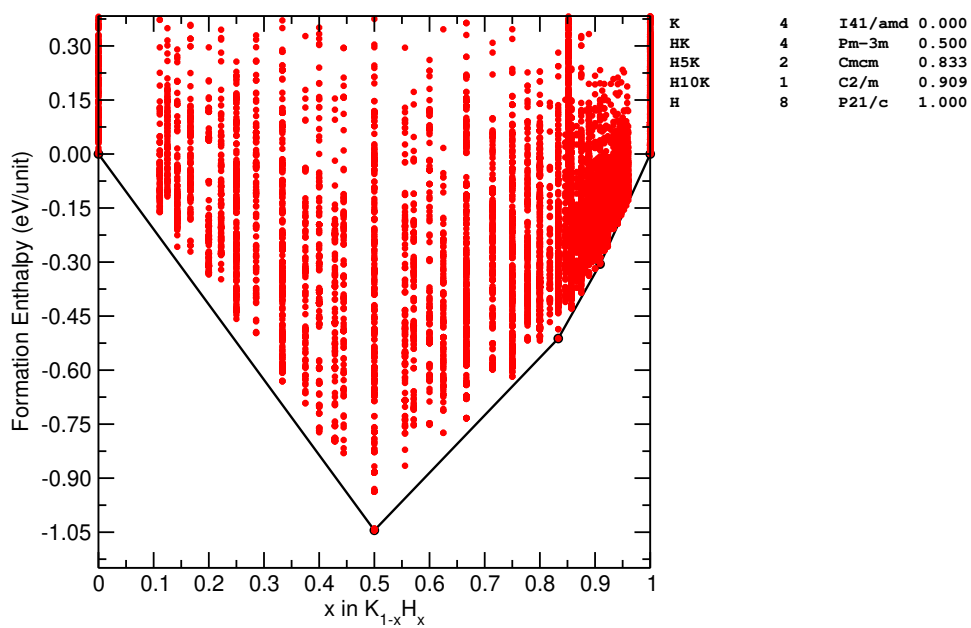


FIG. 19. The convex hull of K-H at 100 GPa.

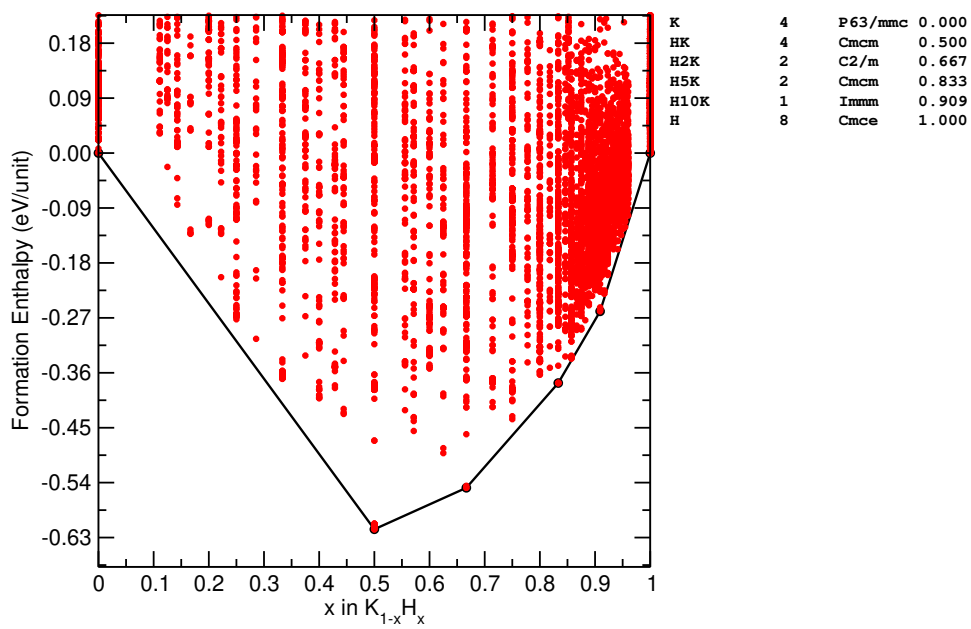


FIG. 20. The convex hull of K-H at 300 GPa.

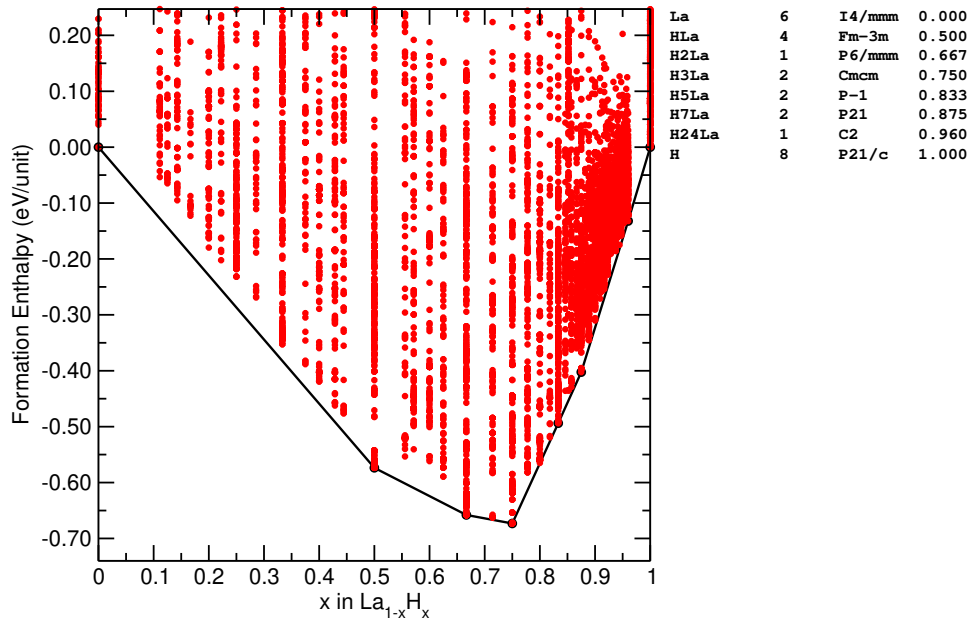


FIG. 21. The convex hull of La-H at 100 GPa.

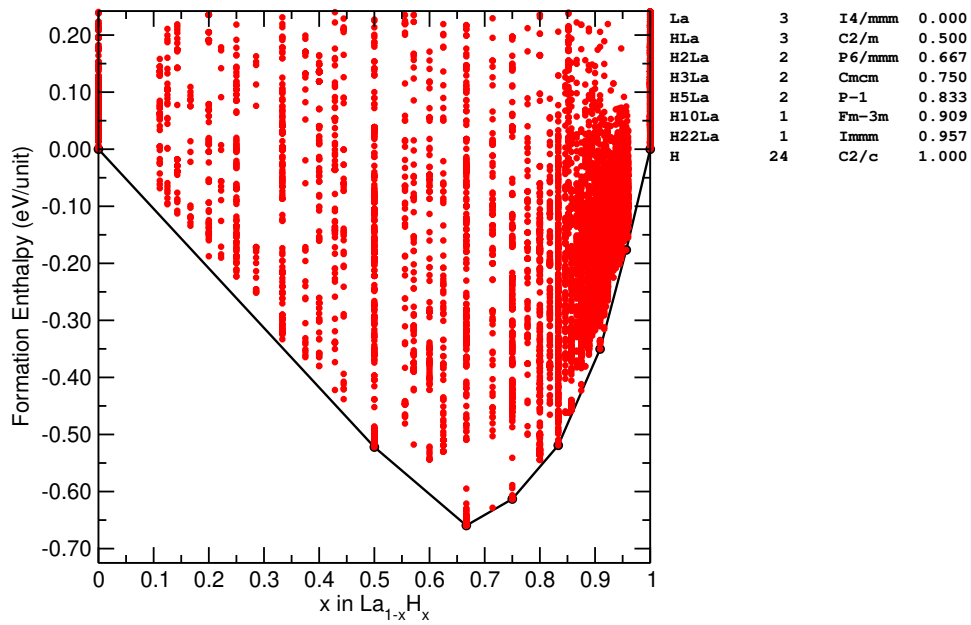


FIG. 22. The convex hull of La-H at 200 GPa.

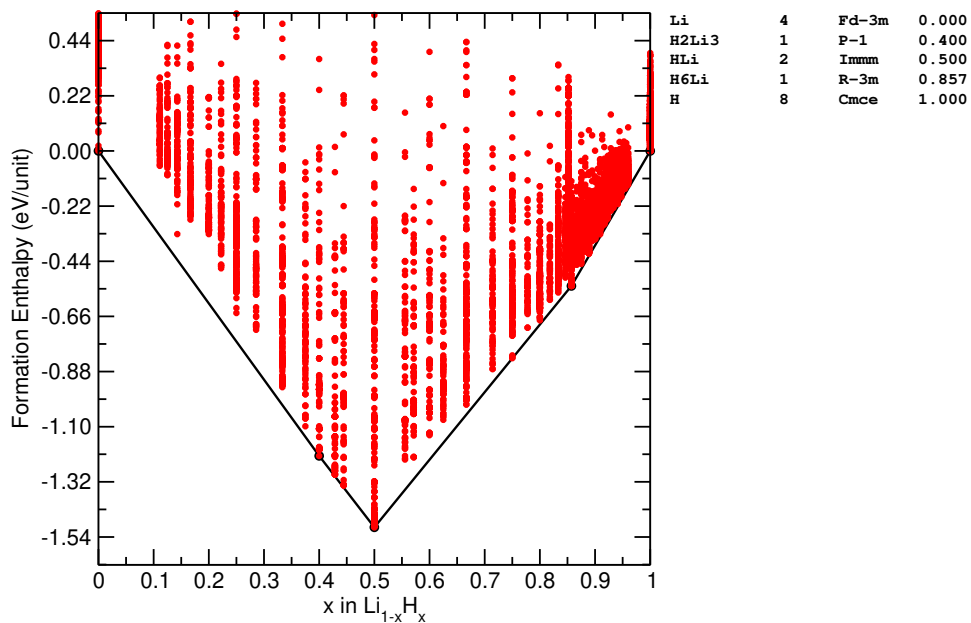


FIG. 23. The convex hull of Li-H at 300 GPa.

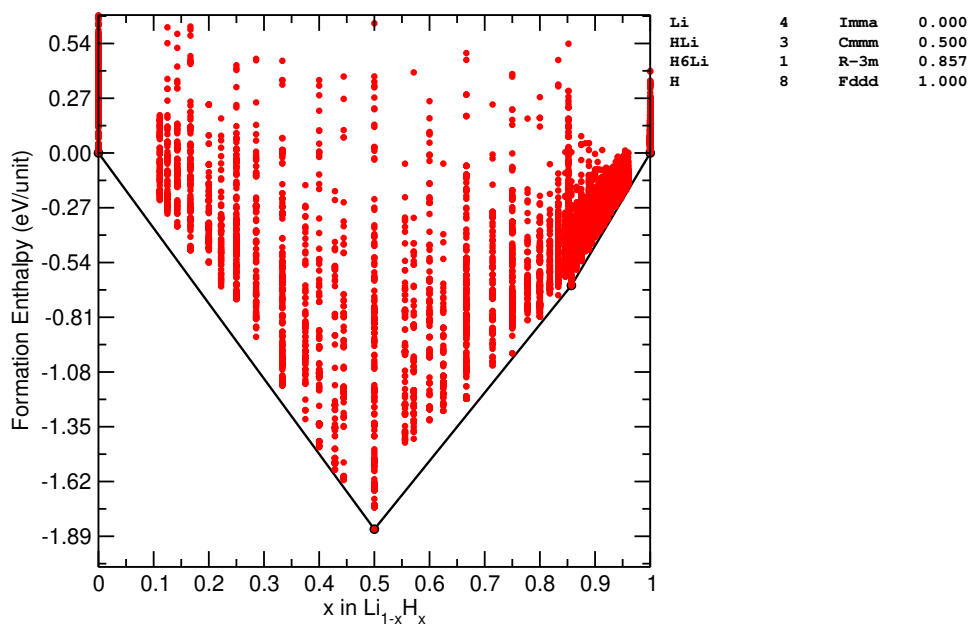


FIG. 24. The convex hull of Li-H at 500 GPa.

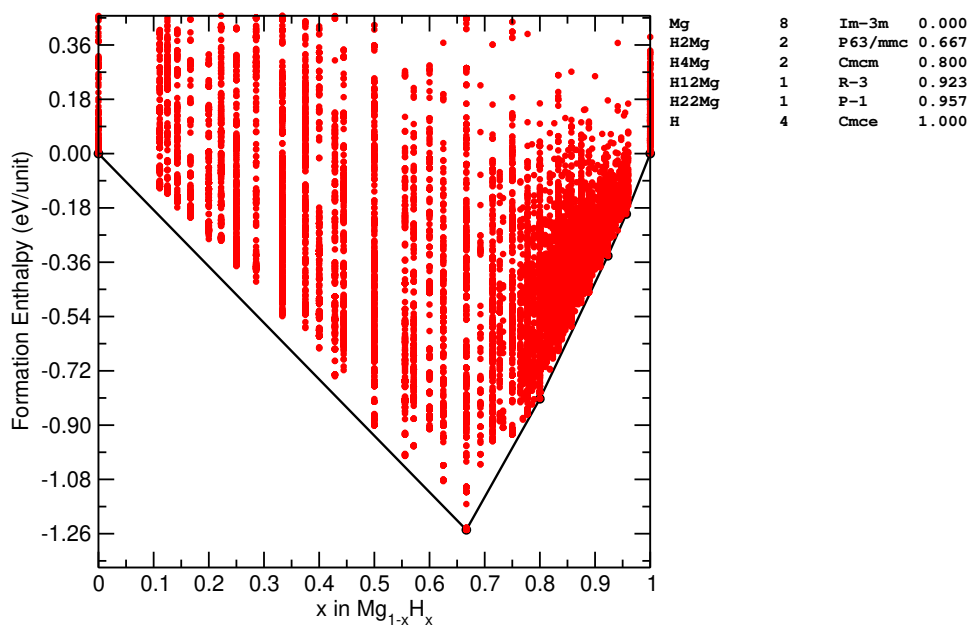


FIG. 25. The convex hull of Mg-H at 200 GPa.

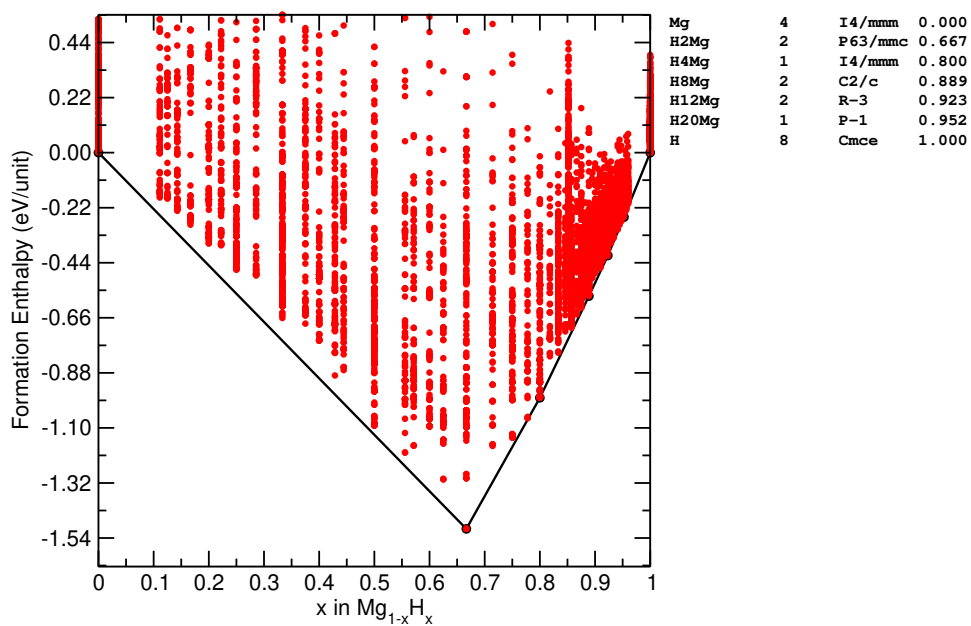


FIG. 26. The convex hull of Mg-H at 300 GPa.

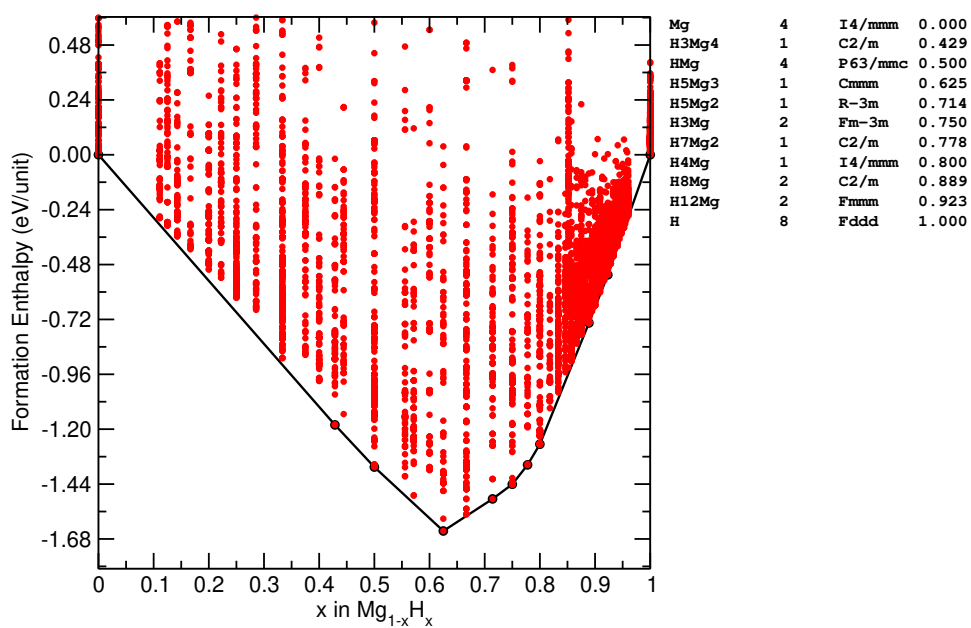


FIG. 27. The convex hull of Mg-H at 500 GPa.

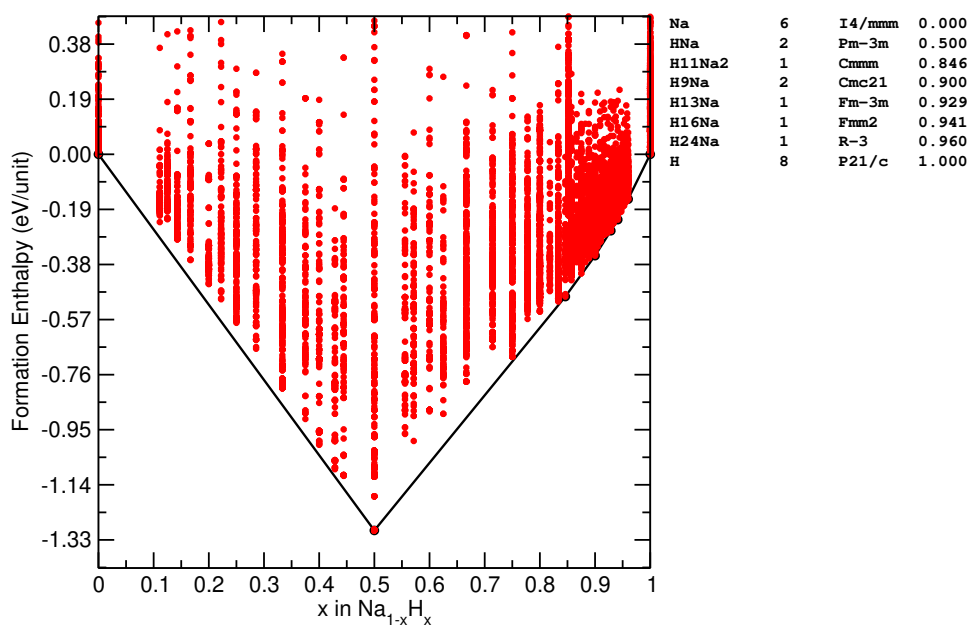


FIG. 28. The convex hull of Na-H at 100 GPa.

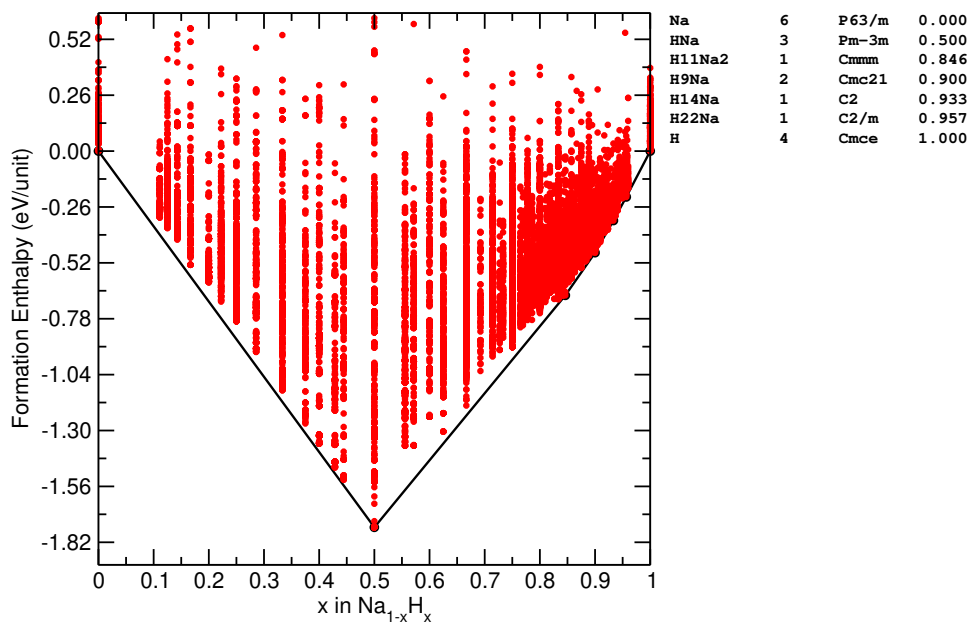


FIG. 29. The convex hull of Na-H at 200 GPa.

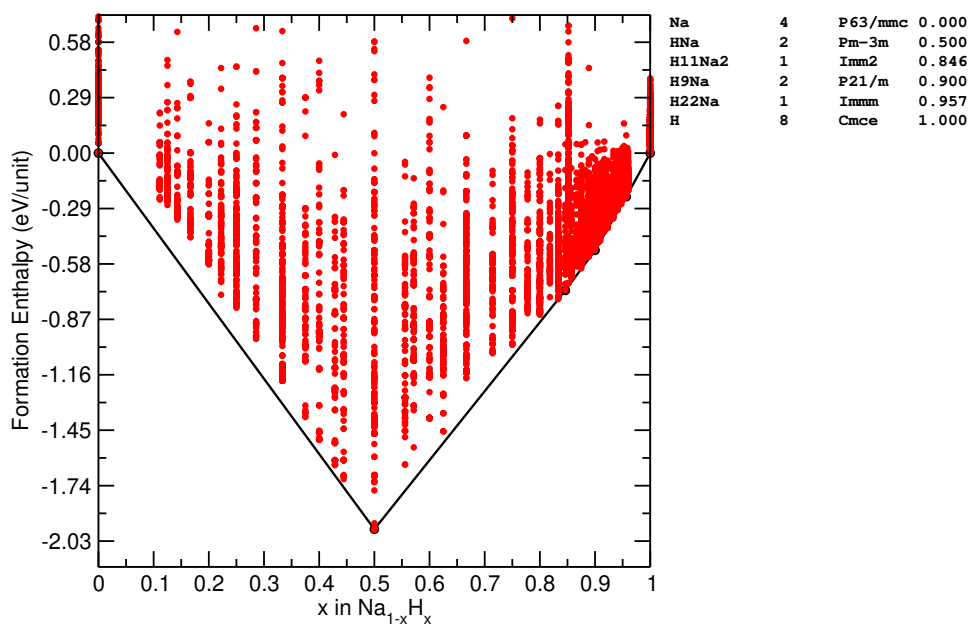


FIG. 30. The convex hull of Na-H at 300 GPa.

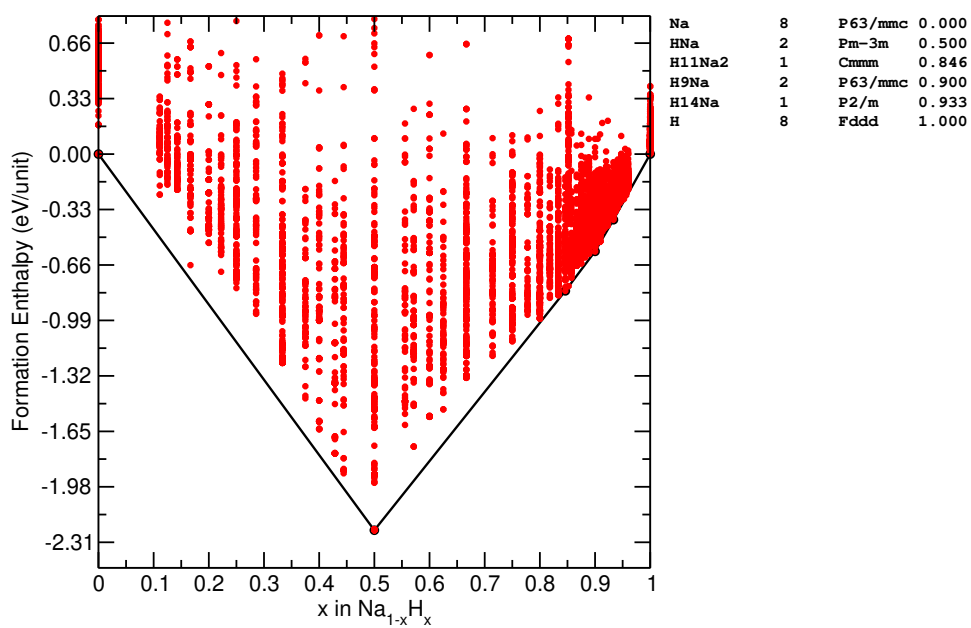


FIG. 31. The convex hull of Na-H at 500 GPa.

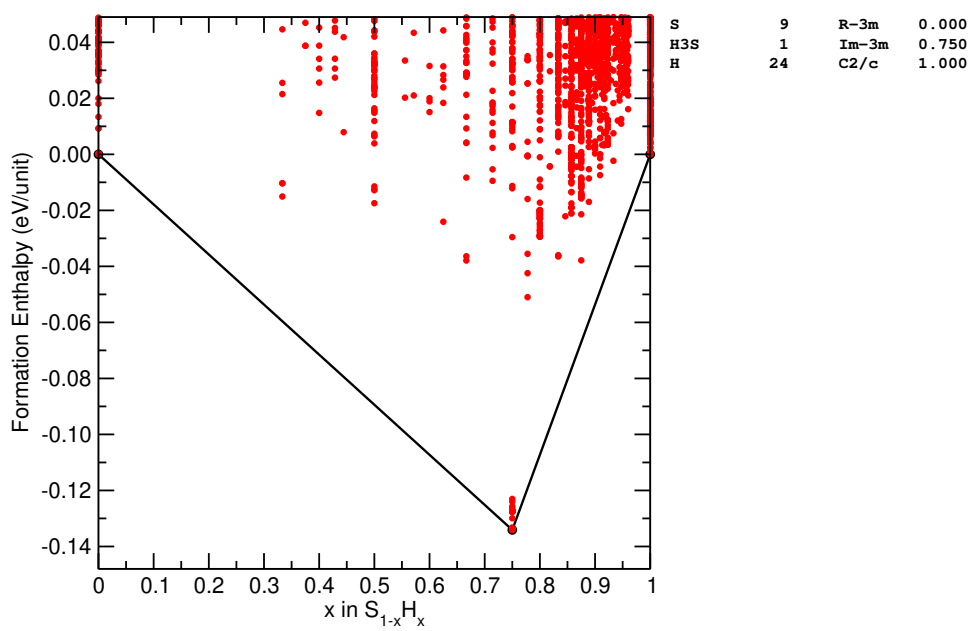


FIG. 32. The convex hull of S-H at 200 GPa.

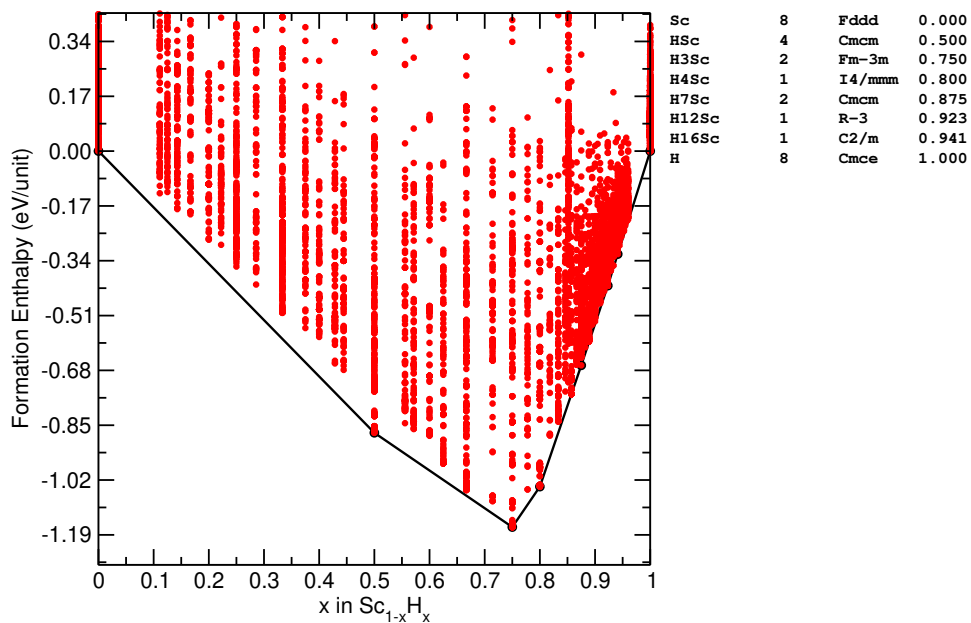


FIG. 33. The convex hull of Sc-H at 300 GPa.

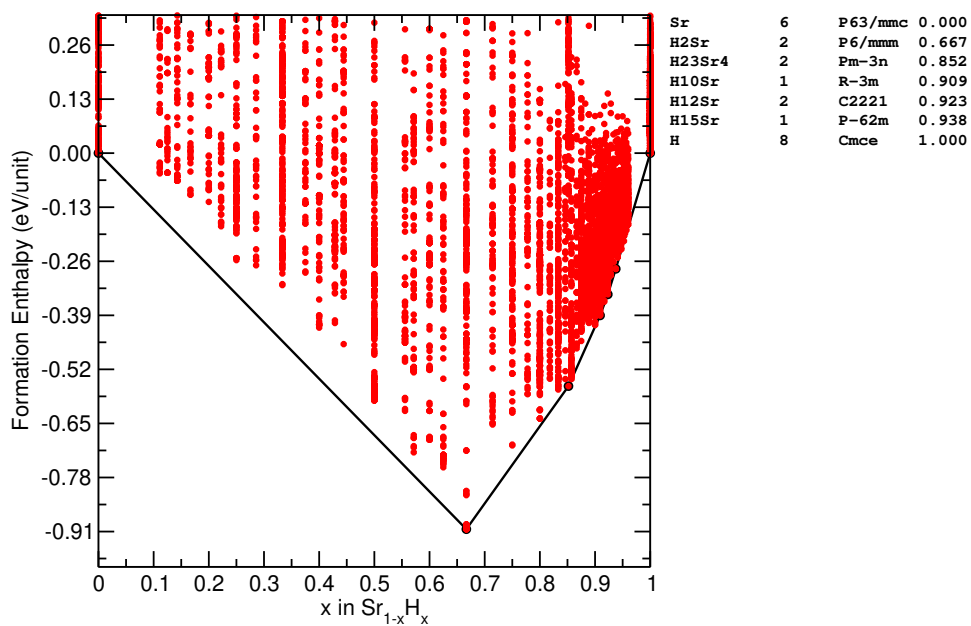


FIG. 34. The convex hull of Sr-H at 300 GPa.

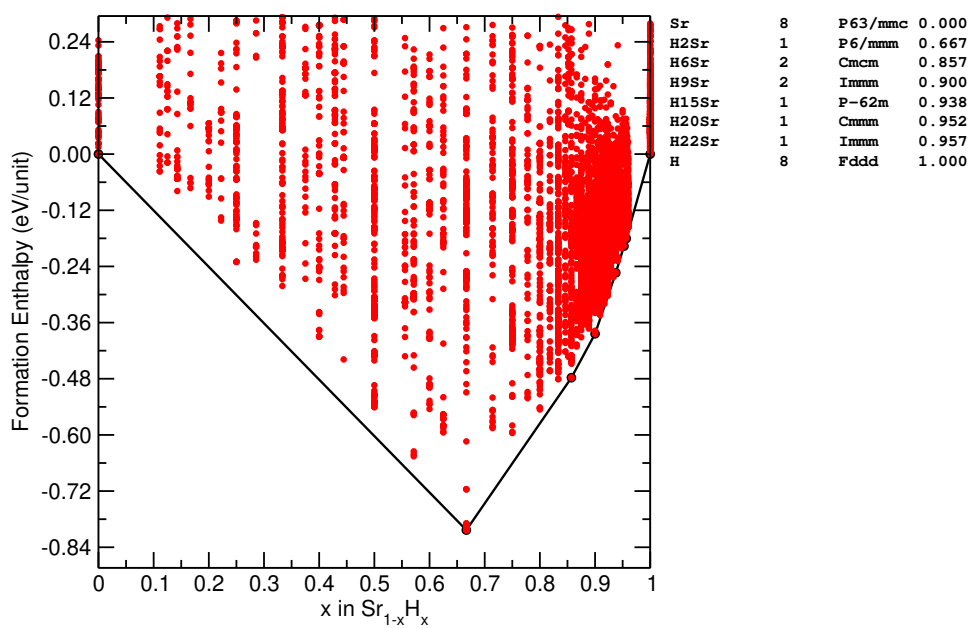


FIG. 35. The convex hull of Sr-H at 500 GPa.

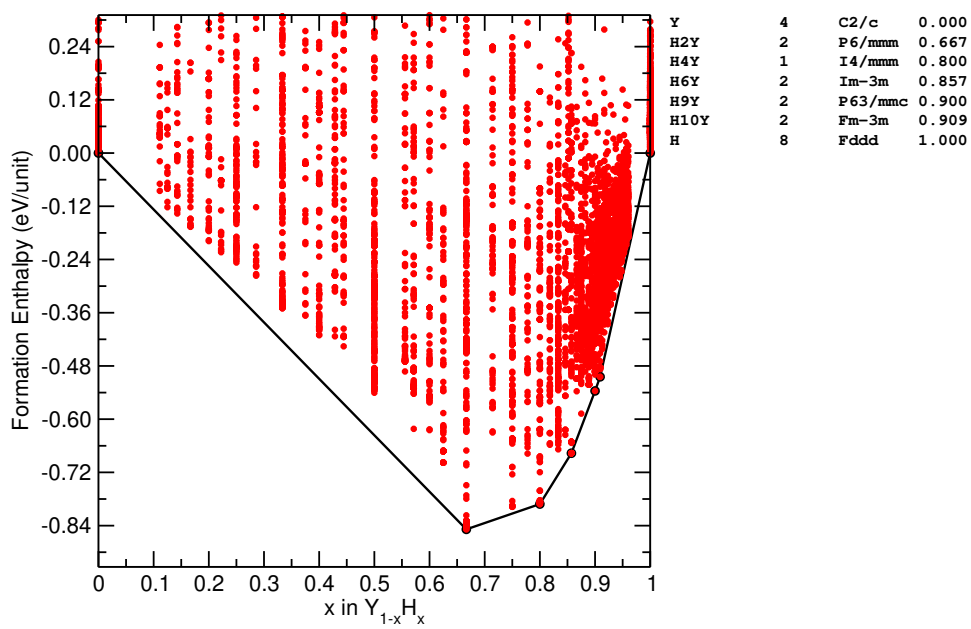


FIG. 36. The convex hull of Y-H at 500 GPa.

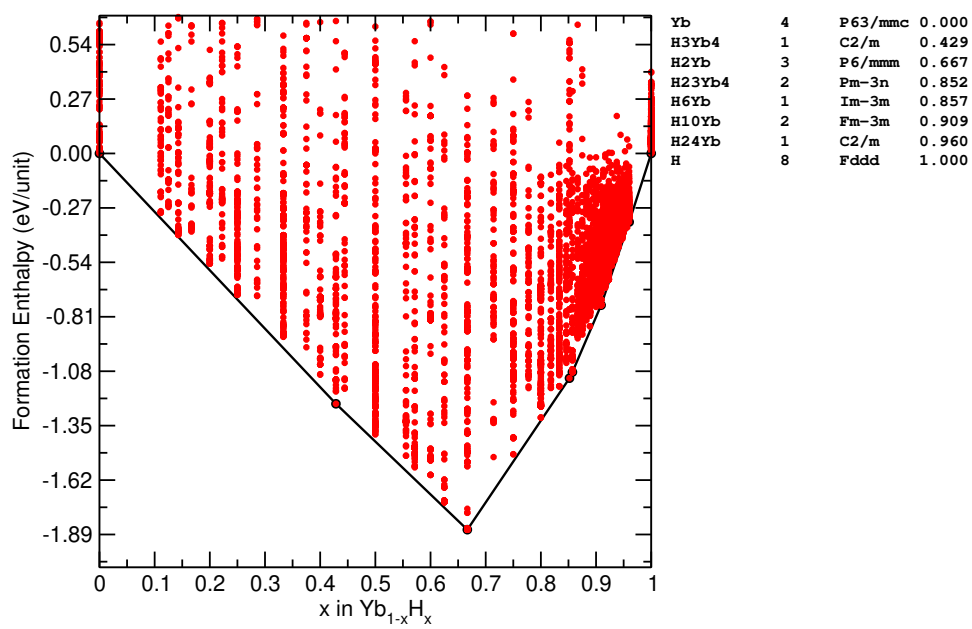


FIG. 37. The convex hull of Yb-H at 500 GPa.

- [1] D. Duan, Y. Liu, Y. Ma, Z. Shao, B. Liu, and T. Cui, Structure and superconductivity of hydrides at high pressures, *National Science Review* **4**, 121 (2017).
- [2] E. Zurek and T. Bi, High-temperature superconductivity in alkaline and rare earth polyhydrides at high pressure: A theoretical perspective, *The Journal of chemical physics* **150**, 050901 (2019).
- [3] J. A. Flores-Livas, L. Boeri, A. Sanna, G. Profeta, R. Arita, and M. Eremets, A perspective on conventional high-temperature superconductors at high pressure: Methods and materials, *Physics Reports* (2020).
- [4] L. Boeri and G. B. Bachelet, Viewpoint: the road to room-temperature conventional superconductivity, *J. Phys: Condens. Matt.* **31**, 234002 (2019).
- [5] A. R. Oganov, C. J. Pickard, Q. Zhu, and R. J. Needs, Structure prediction drives materials discovery, *Nature Reviews Materials* **4**, 331 (2019).
- [6] C. J. Pickard, I. Errea, and M. I. Eremets, Superconducting hydrides under pressure, *Annual Review of Condensed Matter Physics* **11**, 57 (2020).
- [7] G. D. Gaspari and B. L. Gyorffy, Electron-phonon interactions, d resonances, and superconductivity in transition metals, *Phys. Rev. Lett.* **28**, 801 (1972).
- [8] C. J. Pickard and R. J. Needs, High-pressure phases of silane, *Phys. Rev. Lett.* **97**, 045504 (2006).
- [9] C. J. Pickard and R. J. Needs, Ab initio random structure searching, *J. Phys: Condens. Matt.* **23**, 053201 (2011).
- [10] S. J. Clark, M. D. Segall, C. J. Pickard, P. J. Hasnip, M. I. J. Probert, K. Refson, and M. C. Payne, First principles methods using CASTEP, *Zeitschrift für Kristallographie-Crystalline Materials* **220**, 567 (2005).
- [11] J. P. Perdew, K. Burke, and M. Ernzerhof, Generalized gradient approximation made simple, *Phys. Rev. Lett.* **77**, 3865 (1996).
- [12] B. Monserrat, N. D. Drummond, P. Dalladay-Simpson, R. T. Howie, P. López Ríos, E. Gregoryanz, C. J. Pickard, and R. J. Needs, Structure and metallicity of phase v of hydrogen, *Phys. Rev. Lett* **120**, 255701 (2018).
- [13] W. L. McMillan, Transition temperature of strongly-coupled superconductors, *Physical Review* **167**, 331 (1968).
- [14] J. J. Hopfield, Angular momentum and transition-metal superconductivity, *Physical Review* **186**, 443 (1969).
- [15] J. C. Slater, Wave functions in a periodic potential, *Physical Review* **51**, 846 (1937).
- [16] D. A. Papaconstantopoulos, B. Klein, M. J. Mehl, and W. E. Pickett, Cubic H₃S around 200GPa: An atomic hydrogen superconductor stabilized by sulfur, *Phys. Rev. B* **91**, 184511 (2015).
- [17] P.-H. Chang, S. Silayi, D. Papaconstantopoulos, and M. Mehl, Pressure-induced high-temperature superconductivity in hypothetical h₃x (x=as, se, br, sb, te and i) in the h₃s structure with im $\bar{3}$ m symmetry, *Journal of Physics and Chemistry of Solids* **139**, 109315 (2020).
- [18] J. J. Sakurai and J. Napolitano, Scattering theory, in *Modern Quantum Mechanics* (Cambridge University Press, 2017) p. 386–445, 2nd ed.
- [19] <http://elk.sourceforge.net/>, the ELK FP-LAPW code.
- [20] M. J. Hutcheon, A. M. Shipley, and R. J. Needs, Predicting novel superconducting hydrides using machine learning approaches, *Phys. Rev. B* **101**, 144505 (2020).
- [21] P. B. Allen and R. C. Dynes, Transition temperature of strong-coupled superconductors reanalyzed, *Phys. Rev. B* **12**, 905 (1975).
- [22] P. Giannozzi, S. Baroni, N. Bonini, M. Calandra, R. Car, C. Cavazzoni, D. Ceresoli, G. L. Chiarotti, M. Cococcioni, I. Dabo, A. Dal Corso, S. de Gironcoli, S. Fabris, G. Fratesi, R. Gebauer, U. Gerstmann, C. Gougoussis, A. Kokalj, M. Lazzeri, L. Martin-Samos, N. Marzari, F. Mauri, R. Mazzarello, S. Paolini, A. Pasquarello, L. Paulatto, C. Sbraccia, S. Scandolo, G. Sclauzero, A. P. Seitsonen, A. Smogunov, P. Umari, and R. M. Wentzcovitch, QUANTUM ESPRESSO: a modular and open-source software project for quantum simulations of materials, *Journal of Physics: Condensed Matter* **21**, 395502 (19pp) (2009).
- [23] P. Giannozzi, O. Andreussi, T. Brumme, O. Bunau, M. B. Nardelli, M. Calandra, R. Car, C. Cavazzoni, D. Ceresoli, M. Cococcioni, N. Colonna, I. Carnimeo, A. D. Corso, S. de Gironcoli, P. Delugas, R. A. DiStasio, A. Ferretti, A. Floris, G. Fratesi, G. Fugallo, R. Gebauer, U. Gerstmann, F. Giustino, T. Gorni, J. Jia, M. Kawamura, H.-Y. Ko, A. Kokalj, E. Küçükbenli, M. Lazzeri, M. Marsili, N. Marzari, F. Mauri, N. L. Nguyen, H.-V. Nguyen, A. O. de-la Roza, L. Paulatto, S. Poncè, D. Rocca, R. Sabatini, B. Santra, M. Schlipf, A. P. Seitsonen, A. Smogunov, I. Timrov, T. Thonhauser, P. Umari, N. Vast, X. Wu, and S. Baroni, Advanced capabilities for materials modelling with quantum ESPRESSO, *Journal of Physics: Condensed Matter* **29**, 465901 (2017).
- [24] G. M. Eliashberg, Interactions between electrons and lattice vibrations in a superconductor, *Sov. Phys. JETP* **11**, 696 (1960).
- [25] M. Wierzbowska, S. de Gironcoli, and P. Giannozzi, Origins of low-and high-pressure discontinuities of t_c in niobium, *arXiv:cond-mat/0504077* (2005).
- [26] A. M. Shipley, M. J. Hutcheon, M. S. Johnson, R. J. Needs, and C. J. Pickard, Stability and superconductivity of lanthanum and yttrium decahydrides, *Phys. Rev. B* **101**, 224511 (2020).
- [27] The optimizations to QUANTUM ESPRESSO resulting from this work have been submitted to the developers (see <https://gitlab.com/miicck/q-e>).
- [28] D. V. Semenov, A. G. Kvashnin, I. A. Kruglov, and A. R. Oganov, Actinium hydrides ach₁₀, ach₁₂, and ach₁₆ as high-temperature conventional superconductors, *The journal of physical chemistry letters* **9**, 1920 (2018).
- [29] P. Hou, X. Zhao, F. Tian, D. Li, D. Duan, Z. Zhao, B. Chu, B. Liu, and T. Cui, High pressure structures and superconductivity of alh₃ (h₂) predicted by first principles, *RSC Advances* **5**, 5096 (2015).
- [30] Y. Fu, X. Du, L. Zhang, F. Peng, M. Zhang, C. J. Pickard, R. J. Needs, D. J. Singh, W. Zheng, and Y. Ma, High-pressure phase stability and superconductivity of pnictogen hydrides and chemical trends for compressed hydrides, *Chemistry of Materials* **28**, 1746 (2016).

- [31] K. Abe and N. Ashcroft, Crystalline diborane at high pressures, *Physical Review B* **84**, 104118 (2011).
- [32] S. Yu, Q. Zeng, A. R. Oganov, C. Hu, G. Frapper, and L. Zhang, Exploration of stable compounds, crystal structures, and superconductivity in the be-h system, *AIP Advances* **4**, 107118 (2014).
- [33] C.-H. Hu, A. R. Oganov, Q. Zhu, G.-R. Qian, G. Frapper, A. O. Lyakhov, and H.-Y. Zhou, Pressure-induced stabilization and insulator-superconductor transition of bh, *Physical review letters* **110**, 165504 (2013).
- [34] Y. Ma, D. Duan, D. Li, Y. Liu, F. Tian, H. Yu, C. Xu, Z. Shao, B. Liu, and T. Cui, High-pressure structures and superconductivity of bismuth hydrides, *arXiv preprint arXiv:1511.05291* (2015).
- [35] H. Wang, S. T. John, K. Tanaka, T. Iitaka, and Y. Ma, Superconductive sodalite-like clathrate calcium hydride at high pressures, *Proceedings of the National Academy of Sciences* **109**, 6463 (2012).
- [36] N. P. Salke, M. M. D. Esfahani, Y. Zhang, I. A. Kruglov, J. Zhou, Y. Wang, E. Greenberg, V. B. Prakapenka, J. Liu, A. R. Oganov, and J.-F. Lin, Synthesis of clathrate cerium superhydride ceh 9 at 80-100 gpa with atomic hydrogen sublattice, *Nature communications* **10**, 1 (2019).
- [37] S. Yu, X. Jia, G. Frapper, D. Li, A. R. Oganov, Q. Zeng, and L. Zhang, Pressure-driven formation and stabilization of superconductive chromium hydrides, *Scientific reports* **5**, 17764 (2015).
- [38] C. Heil, G. B. Bachelet, and L. Boeri, Absence of superconductivity in iron polyhydrides at high pressures, *Physical Review B* **97**, 214510 (2018).
- [39] M. M. D. Esfahani, A. R. Oganov, H. Niu, and J. Zhang, Superconductivity and unexpected chemistry of germanium hydrides under pressure, *Physical Review B* **95**, 134506 (2017).
- [40] G. Gao, A. R. Oganov, A. Bergara, M. Martinez-Canales, T. Cui, T. Iitaka, Y. Ma, and G. Zou, Superconducting high pressure phase of germane, *Physical review letters* **101**, 107002 (2008).
- [41] G. Zhong, C. Zhang, X. Chen, Y. Li, R. Zhang, and H. Lin, Structural, electronic, dynamical, and superconducting properties in dense geh₄ (h₂)₂, *The Journal of Physical Chemistry C* **116**, 5225 (2012).
- [42] D. Duan, F. Tian, Y. Liu, X. Huang, D. Li, H. Yu, Y. Ma, B. Liu, and T. Cui, Enhancement of t_c in the atomic phase of iodine-doped hydrogen at high pressures, *Physical Chemistry Chemical Physics* **17**, 32335 (2015).
- [43] A. Shamp and E. Zurek, Superconducting high-pressure phases composed of hydrogen and iodine, *The journal of physical chemistry letters* **6**, 4067 (2015).
- [44] D. Duan, Y. Liu, F. Tian, D. Li, X. Huang, Z. Zhao, H. Yu, B. Liu, W. Tian, and T. Cui, Pressure-induced metallization of dense (h₂s)₂h₂ with high-t_c superconductivity, *Scientific reports* **4**, 6968 (2014).
- [45] I. Errea, M. Calandra, C. J. Pickard, J. Nelson, R. J. Needs, Y. Li, H. Liu, Y. Zhang, Y. Ma, and F. Mauri, High-pressure hydrogen sulfide from first principles: A strongly anharmonic phonon-mediated superconductor, *Physical review letters* **114**, 157004 (2015).
- [46] S. Zhang, Y. Wang, J. Zhang, H. Liu, X. Zhong, H.-F. Song, G. Yang, L. Zhang, and Y. Ma, Phase diagram and high-temperature superconductivity of compressed selenium hydrides, *Scientific reports* **5**, 15433 (2015).
- [47] Y. Liu, D. Duan, F. Tian, C. Wang, G. Wu, Y. Ma, H. Yu, D. Li, B. Liu, and T. Cui, Prediction of stoichiometric polyn compounds: crystal structures and properties, *RSC Advances* **5**, 103445 (2015).
- [48] X. Zhong, H. Wang, J. Zhang, H. Liu, S. Zhang, H.-F. Song, G. Yang, L. Zhang, and Y. Ma, Tellurium hydrides at high pressures: High-temperature superconductors, *Physical review letters* **116**, 057002 (2016).
- [49] D. Zhou, X. Jin, X. Meng, G. Bao, Y. Ma, B. Liu, and T. Cui, Ab initio study revealing a layered structure in hydrogen-rich kh₆ under high pressure, *Physical Review B* **86**, 014118 (2012).
- [50] I. A. Kruglov, D. V. Semenov, H. Song, R. L. Szczeniak, I. A. Wrona, R. Akashi, M. M. D. Esfahani, D. Duan, T. Cui, A. G. Kvashnin, and A. R. Oganov, Superconductivity of lah 10 and lah 16 polyhydrides, *Phys. Rev. B* **101**, 024508 (2020).
- [51] G. Gao, R. Hoffmann, N. W. Ashcroft, H. Liu, A. Bergara, and Y. Ma, Theoretical study of the ground-state structures and properties of niobium hydrides under pressure, *Physical Review B* **88**, 184104 (2013).
- [52] D. Zhou, D. V. Semenov, H. Xie, X. Huang, D. Duan, A. Aperis, P. M. Oppeneer, M. Galasso, A. I. Kartsev, A. G. Kvashnin, A. R. Oganov, and T. Cui, High-pressure synthesis of magnetic neodymium polyhydrides, *Journal of the American Chemical Society* **142**, 2803 (2020).
- [53] Y. Liu, D. Duan, X. Huang, F. Tian, D. Li, X. Sha, C. Wang, H. Zhang, T. Yang, B. Liu, and T. Cui, Structures and properties of osmium hydrides under pressure from first principle calculation, *The Journal of Physical Chemistry C* **119**, 15905 (2015).
- [54] D. Zhou, D. V. Semenov, D. Duan, H. Xie, W. Chen, X. Huang, X. Li, B. Liu, A. R. Oganov, and T. Cui, Superconducting praseodymium superhydrides, *Science Advances* **6** (2020).
- [55] Y. Liu, D. Duan, F. Tian, C. Wang, Y. Ma, D. Li, X. Huang, B. Liu, and T. Cui, Stability and properties of the ru-h system at high pressure, *Physical Chemistry Chemical Physics* **18**, 1516 (2016).
- [56] Y. Ma, D. Duan, D. Li, Y. Liu, F. Tian, X. Huang, Z. Zhao, H. Yu, B. Liu, and T. Cui, The unexpected binding and superconductivity in sbh₄ at high pressure, *arXiv preprint arXiv:1506.03889* (2015).
- [57] X. Ye, N. Zarifi, E. Zurek, R. Hoffmann, and N. Ashcroft, High hydrides of scandium under pressure: potential superconductors, *The Journal of Physical Chemistry C* **122**, 6298 (2018).
- [58] X. Jin, X. Meng, Z. He, Y. Ma, B. Liu, T. Cui, G. Zou, and H.-k. Mao, Superconducting high-pressure phases of disilane, *Proceedings of the National Academy of Sciences* **107**, 9969 (2010).
- [59] M. M. D. Esfahani, Z. Wang, A. R. Oganov, H. Dong, Q. Zhu, S. Wang, M. S. Rakinin, and X.-F. Zhou, Superconductivity of novel tin hydrides (sn_nh_m) under pressure, *Scientific reports* **6**, 22873 (2016).
- [60] Q. Zhuang, X. Jin, T. Cui, Y. Ma, Q. Lv, Y. Li, H. Zhang, X. Meng, and K. Bao, Pressure-stabilized superconductive ionic tantalum hydrides, *Inorganic chemistry* **56**, 3901 (2017).
- [61] X. Li, H. Liu, and F. Peng, Crystal structures and superconductivity of technetium hydrides under pressure, *Physical Chemistry Chemical Physics* **18**, 28791 (2016).

- [62] A. G. Kvashnin, D. V. Semenov, I. A. Kruglov, I. A. Wrona, and A. R. Oganov, High-temperature superconductivity in a th-h system under pressure conditions, *ACS applied materials & interfaces* **10**, 43809 (2018).
- [63] D. V. Semenov, A. G. Kvashnin, A. G. Ivanova, V. Svitlyk, V. Y. Fominski, A. V. Sadakov, O. A. Sobolevskiy, V. M. Pudalov, I. A. Troyan, and A. R. Oganov, Superconductivity at 161k in thorium hydride thh10: Synthesis and properties, *Materials Today* **33**, 36 (2020).
- [64] I. A. Kruglov, A. G. Kvashnin, A. F. Goncharov, A. R. Oganov, S. S. Lobanov, N. Holtgrewe, S. Jiang, V. B. Prakapenka, E. Greenberg, and A. V. Yanilkin, Uranium polyhydrides at moderate pressures: Prediction, synthesis, and expected superconductivity, *Science advances* **4** (2018).
- [65] X. Li and F. Peng, Superconductivity of pressure-stabilized vanadium hydrides, *Inorganic chemistry* **56**, 13759 (2017).
- [66] S. Zheng, S. Zhang, Y. Sun, J. Zhang, J. Lin, G. Yang, and A. Bergara, Structural and superconducting properties of tungsten hydrides under high pressure, *Frontiers in Physics* **6**, 101 (2018).
- [67] L.-L. Liu, H.-J. Sun, C. Wang, and W.-C. Lu, High-pressure structures of yttrium hydrides, *Journal of Physics: Condensed Matter* **29**, 325401 (2017).
- [68] X.-F. Li, Z.-Y. Hu, and B. Huang, Phase diagram and superconductivity of compressed zirconium hydrides, *Physical Chemistry Chemical Physics* **19**, 3538 (2017).
- [69] K. Abe, High-pressure properties of dense metallic zirconium hydrides studied by ab initio calculations, *Physical Review B* **98**, 134103 (2018).
- [70] D. V. Semenov, I. A. Kruglov, I. A. Savkin, A. G. Kvashnin, and A. R. Oganov, On distribution of superconductivity in metal hydrides, *Current Opinion in Solid State and Materials Science*, 100808 (2020).
- [71] Q. Gu, P. Lu, K. Xia, J. Sun, and D. Xing, High-temperature superconducting phase of hbr under pressure predicted by first-principles calculations, *Physical Review B* **96**, 064517 (2017).
- [72] T. Bi, N. Zarifi, T. Terpstra, and E. Zurek, The search for superconductivity in high pressure hydrides, in *Reference Module in Chemistry, Molecular Sciences and Chemical Engineering* (Elsevier, 2019).
- [73] <https://uk.mathworks.com/help/stats/fitrgp.html>, MATLAB GPR fitting documentation.
- [74] A. Drozdov, P. Kong, V. Minkov, S. Besedin, M. Kuzovnikov, S. Mozaffari, L. Balicas, F. Balakirev, D. Graf, V. Prakapenka, E. Greenberg, D. Knyazev, M. Tkacz, and M. Eremets, Superconductivity at 250 k in lanthanum hydride under high pressures, *Nature* **569**, 528 (2019).
- [75] A. Drozdov, M. Eremets, I. Troyan, V. Ksenofontov, and S. Shylin, Conventional superconductivity at 203 kelvin at high pressures in the sulfur hydride system, *Nature* **525**, 73 (2015).
- [76] F. Peng, Y. Sun, C. J. Pickard, R. J. Needs, Q. Wu, and Y. Ma, Hydrogen clathrate structures in rare earth hydrides at high pressures: possible route to room-temperature superconductivity, *Physical review letters* **119**, 107001 (2017).
- [77] Y. Xie, Q. Li, A. Oganov, and H. Wang, Superconductivity of lithium-doped hydrogen under high pressure, *Acta Crystallographica Section C: Structural Chemistry* **70**, 104 (2014).
- [78] R. T. Howie, O. Narygina, C. L. Guillaume, S. Evans, and E. Gregoryanz, High-pressure synthesis of lithium hydride, *Physical Review B* **86**, 064108 (2012).
- [79] H. Liu, I. I. Naumov, R. Hoffmann, N. Ashcroft, and R. J. Hemley, Potential high- T_c superconducting lanthanum and yttrium hydrides at high pressure, *Proceedings of the National Academy of Sciences* **114**, 6990 (2017).
- [80] M. Somayazulu, M. Ahart, A. K. Mishra, Z. M. Geballe, M. Baldini, Y. Meng, V. V. Struzhkin, and R. J. Hemley, Evidence for superconductivity above 260 k in lanthanum superhydride at megabar pressures, *Physical review letters* **122**, 027001 (2019).
- [81] K. Abe, Hydrogen-rich scandium compounds at high pressures, *Physical Review B* **96**, 144108 (2017).
- [82] K. Tanaka, J. Tse, and H. Liu, Electron-phonon coupling mechanisms for hydrogen-rich metals at high pressure, *Physical Review B* **96**, 100502 (2017).
- [83] X. Feng, J. Zhang, G. Gao, H. Liu, and H. Wang, Compressed sodalite-like mgh6 as a potential high-temperature superconductor, *RSC Advances* **5**, 59292 (2015).
- [84] D. C. Lonie, J. Hooper, B. Altintas, and E. Zurek, Metallization of magnesium polyhydrides under pressure, *Physical Review B* **87**, 054107 (2013).
- [85] P. Kong, V. Minkov, M. Kuzovnikov, S. Besedin, A. Drozdov, S. Mozaffari, L. Balicas, F. Balakirev, V. Prakapenka, E. Greenberg, D. Knyazev, and E. M. I., Superconductivity up to 243 k in yttrium hydrides under high pressure, arXiv preprint arXiv:1909.10482 (2019).
- [86] J. Nagamatsu, N. Nakagawa, T. Muranaka, Y. Zenitani, and J. Akimitsu, Superconductivity at 39 k in magnesium diboride, *Nature* **410**, 63 (2001).
- [87] G. Wu, Y. L. Xie, H. Chen, M. Zhong, R. H. Liu, B. C. Shi, Q. J. Li, X. F. Wang, T. Wu, Y. J. Yan, J. J. Ying, and X. H. Chen, Superconductivity at 56 k in samarium-doped SrFeAsF, *Journal of Physics: Condensed Matter* **21**, 142203 (2009).
- [88] A. Schilling, M. Cantoni, J. D. Guo, and H. R. Ott, Superconductivity above 130 k in the hg-ba-ca-cu-o system, *Nature* **363**, 56 (1993).
- [89] E. Snider, N. Dasenbrock-Gammon, R. McBride, M. Debessai, H. Vindana, K. Vencatasamy, K. V. Lawler, A. Salamat, and R. P. Dias, Room-temperature superconductivity in a carbonaceous sulfur hydride, *Nature* **586**, 373 (2020).
- [90] See supplementary information, which includes refs. [112–121].
- [91] Structures from table 1 (cambridge online data repository), <https://doi.org/10.17863/CAM.72574>.
- [92] P. Baettig and E. Zurek, Pressure-stabilized sodium polyhydrides: NaH_n ($n > 1$), *Phys. Rev. Lett.* **106**, 237002 (2011).
- [93] V. V. Struzhkin, D. Y. Kim, E. Stavrou, T. Muramatsu, H.-k. Mao, C. J. Pickard, R. J. Needs, V. B. Prakapenka, and A. F. Goncharov, Synthesis of sodium polyhydrides at high pressures, *Nature Communications* **7**, 12267 (2016).
- [94] C. Wang, S. Yi, and J.-H. Cho, Pressure dependence of the superconducting transition temperature of compressed LaH_{10} , *Phys. Rev. B* **100**, 060502 (2019).
- [95] G. Bergmann and D. Rainer, The sensitivity of the transition temperature to changes in $\alpha^2 f(\omega)$, *Zeitschrift für*

- Physik **263**, 59 (1973).
- [96] J. Hooper and E. Zurek, High pressure potassium polyhydrides: A chemical perspective, *The Journal of Physical Chemistry C* **116**, 13322 (2012).
- [97] Z. M. Geballe, H. Liu, A. K. Mishra, M. Ahart, M. Somayazulu, Y. Meng, M. Baldini, and R. J. Hemley, Synthesis and stability of lanthanum superhydrides, *Angewandte Chemie International Edition* **57**, 688 (2018).
- [98] H. Liu, I. I. Naumov, Z. M. Geballe, M. Somayazulu, S. T. John, and R. J. Hemley, Dynamics and superconductivity in compressed lanthanum superhydride, *Physical Review B* **98**, 100102 (2018).
- [99] W. Sukmas, P. Tsuppayakorn-ae, U. Pinsook, and T. Bovornratanaraks, Near-room-temperature superconductivity of mg/ca substituted metal hexahydride under pressure, *Journal of Alloys and Compounds* **849**, 156434 (2020).
- [100] C. Heil, S. Di Cataldo, G. B. Bachelet, and L. Boeri, Superconductivity in sodalite-like yttrium hydride clathrates, *Physical Review B* **99**, 220502 (2019).
- [101] I. A. Troyan, D. V. Semenov, A. G. Kvashnin, A. V. Sadakov, O. A. Sobolevskiy, V. M. Pudalov, A. G. Ivanova, V. B. Prakapenka, E. Greenberg, A. G. Gavriliuk, I. S. Lyubutin, V. V. Struzhkin, A. Bergara, I. Errea, R. Bianco, M. Calandra, F. Mauri, L. Monacelli, R. Akashi, and A. R. Oganov, Anomalous high-temperature superconductivity in yh₆, *Advanced Materials* **33**, 2006832 (2021).
- [102] Y. Li, J. Hao, H. Liu, S. T. John, Y. Wang, and Y. Ma, Pressure-stabilized superconductive yttrium hydrides, *Scientific reports* **5**, 9948 (2015).
- [103] S. Qian, X. Sheng, X. Yan, Y. Chen, and B. Song, Theoretical study of stability and superconductivity of sch_n (n= 4-8) at high pressure, *Physical Review B* **96**, 094513 (2017).
- [104] E. Zurek, R. Hoffmann, N. W. Ashcroft, A. R. Oganov, and A. O. Lyakhov, A little bit of lithium does a lot for hydrogen, *Proceedings of the National Academy of Sciences* **106**, 17640 (2009).
- [105] Y. Wang, H. Wang, S. T. John, T. Iitaka, and Y. Ma, Structural morphologies of high-pressure polymorphs of strontium hydrides, *Physical Chemistry Chemical Physics* **17**, 19379 (2015).
- [106] I. Errea, F. Belli, L. Monacelli, A. Sanna, T. Koretsune, T. Tadano, R. Bianco, M. Calandra, R. Arita, F. Mauri, and J. A. Flores-Livas, Quantum crystal structure in the 250-kelvin superconducting lanthanum hydride, *Nature* **578**, 66 (2020).
- [107] I. Errea, M. Calandra, C. J. Pickard, J. R. Nelson, R. J. Needs, Y. Li, H. Liu, Y. Zhang, Y. Ma, and F. Mauri, Quantum hydrogen-bond symmetrization in the superconducting hydrogen sulfide system, *Nature* **532**, 81 (2016).
- [108] I. Errea, M. Calandra, and F. Mauri, Anharmonic free energies and phonon dispersions from the stochastic self-consistent harmonic approximation: Application to platinum and palladium hydrides, *Phys. Rev. B* **89**, 064302 (2014).
- [109] J. C. K. Hui and P. B. Allen, Effect of lattice anharmonicity on superconductivity, *Journal of Physics F: Metal Physics* **4**, L42 (1974).
- [110] V. Meregalli and S. Y. Savrasov, Electron-phonon coupling and properties of doped babio₃, *Phys. Rev. B* **57**, 14453 (1998).
- [111] X. Wan, H.-C. Ding, S. Y. Savrasov, and C.-G. Duan, Electron-phonon superconductivity near charge-density-wave instability in lao_{0.5}f_{0.5}bis₂: Density-functional calculations, *Phys. Rev. B* **87**, 115124 (2013).
- [112] H. Xie, D. Duan, Z. Shao, H. Song, Y. Wang, X. Xiao, D. Li, F. Tian, B. Liu, and T. Cui, High-temperature superconductivity in ternary clathrate ycah₁₂ under high pressures, *Journal of Physics: Condensed Matter* **31**, 245404 (2019).
- [113] Y. Sun, J. Lv, Y. Xie, H. Liu, and Y. Ma, Route to a superconducting phase above room temperature in electron-doped hydride compounds under high pressure, *Phys. Rev. Lett.* **123**, 097001 (2019).
- [114] R. Szczesniak and A. Durajski, Superconductivity well above room temperature in compressed mgh₆, *Frontiers of Physics* **11**, 117406 (2016).
- [115] Y. Chen, H. Y. Geng, X. Yan, Y. Sun, Q. Wu, and X. Chen, Prediction of stable ground-state lithium polyhydrides under high pressures, *Inorganic Chemistry* **56**, 3867 (2017).
- [116] J. A. Camargo-Martínez, G. I. González-Pedrerros, and F. Mesa, The higher superconducting transition temperature T_c and the functional derivative of T_c with $\alpha^2F(\omega)$ for electron-phonon superconductors, *Journal of Physics: Condensed Matter* **32**, 505901 (2020).
- [117] Y.-K. Wei, J.-N. Yuan, F. I. Khan, G.-F. Ji, Z.-W. Gu, and D.-Q. Wei, Pressure induced superconductivity and electronic structure properties of scandium hydrides using first principles calculations, *RSC Advances* **6**, 81534 (2016).
- [118] J. S. Smith, S. Desgreniers, D. D. Klug, and S. T. John, High-density strontium hydride: An experimental and theoretical study, *Solid state communications* **149**, 830 (2009).
- [119] Z. Shao, D. Duan, Y. Ma, H. Yu, H. Song, H. Xie, D. Li, F. Tian, B. Liu, and T. Cui, Unique phase diagram and superconductivity of calcium hydrides at high pressures, *Inorganic chemistry* **58**, 2558 (2019).
- [120] H. Xie, Y. Yao, X. Feng, D. Duan, H. Song, Z. Zhang, S. Jiang, S. A. T. Redfern, V. Z. Kresin, C. J. Pickard, and T. Cui, Hydrogen pentagraphenelike structure stabilized by hafnium: A high-temperature conventional superconductor, *Phys. Rev. Lett.* **125**, 217001 (2020).
- [121] J. Hooper, T. Terpstra, A. Shamp, and E. Zurek, Composition and constitution of compressed strontium polyhydrides, *The Journal of Physical Chemistry C* **118**, 6433 (2014).

Supplementary material for: High-throughput discovery of high-temperature conventional superconductors

Alice M. Shipley, Michael J. Hutcheon, and Richard J. Needs
*Theory of Condensed Matter Group, Cavendish Laboratory,
J. J. Thomson Avenue, Cambridge CB3 0HE, United Kingdom*

Chris J. Pickard
*Department of Materials Science and Metallurgy,
27 Charles Babbage Rd, Cambridge CB3 0FS, United Kingdom and
Advanced Institute for Materials Research, Tohoku University,
2-1-1 Katahira, Aoba, Sendai, 980-8577, Japan*
(Dated: August 6, 2021)

I. THE CRITICAL TEMPERATURE OF $Immm$ -ScH₈

We find that an $Immm$ structure of ScH₈ exhibits superconductivity at 300 GPa with a T_c of 212-233 K. This is significantly higher than the (Allen-Dynes) value of ~ 115 K obtained in Ref. [?] using a $16 \times 16 \times 16$ \mathbf{k} -point grid and norm-conserving pseudopotentials with 3 valence electrons for Sc. In contrast, we use a $36 \times 36 \times 36$ \mathbf{k} -point grid and ultrasoft pseudopotentials with 11 valence electrons for Sc; a more substantial investigation into pseudopotentials is therefore needed to fully resolve this discrepancy. While they did not calculate T_c for ScH₈, critical temperatures of 213 K and 233 K were obtained at 300 GPa for ScH₇ and ScH₉, respectively, in Ref. [?] (remarkably close to our range for ScH₈).

II. DYNAMICALLY UNSTABLE CRITICAL TEMPERATURES

For dynamically unstable structures, a large amount of spectral weight can be introduced to the Eliashberg function near to $\omega = 0$ due to the unstable modes. Similarly to what was seen for $Im\bar{3}m$ CaH₆ at 100 GPa in Fig. 7 of the main text, this strongly affects the Allen-Dynes critical temperature ($T_c^{(AD)}$), because the functional derivative $\delta T_c^{(AD)}/\delta\alpha^2 F(\omega)$ diverges (towards $-\infty$) as $\omega \rightarrow 0$. However, the critical temperature derived from solution of the Eliashberg equations ($T_c^{(E)}$) is much less sensitive ($\delta T_c^{(E)}/\delta\alpha^2 F(\omega) \rightarrow 0$ as $\omega \rightarrow 0$ [?]). Therefore, if one of these unstable superconductors is in reality stabilized by anharmonic effects (as is the case for $Fm\bar{3}m$ -LaH₁₀ at 200 GPa [? ?]), then a rough estimate of its promise as a high-temperature superconductor can be estimated by simply neglecting unstable modes in a harmonic calculation of $T_c^{(E)}$. The results of this procedure are shown in Table. I, along with the same procedure for $T_c^{(AD)}$ for comparison. In carrying out a harmonic calculation, we are neglecting anharmonic renormalization of the phonon frequencies, which may affect the critical temperatures, especially if there is a large amount of spectral weight near to $\omega = 0$ to be renormalized. Therefore, an anharmonic treatment is needed to determine the stability and critical temperatures more accurately, especially when the Allen-Dynes and Eliashberg results strongly disagree (as they do in many cases). These results might therefore be used to identify interesting systems to investigate with anharmonic methods.

Stoichiometry	Space group	P(GPa)	$T_c^{(AD)}$ (K)	$T_c^{(E)}$ (K)	E_{stoic} (meV/unit)
LaH ₆	$Im\bar{3}m$	100	119-151	226-250	12*
AcH ₁₀	$Fm\bar{3}m$	100	75-125	171-203	8*
NaH ₁₆	$P\bar{3}1m$	100	81-99	138-163	0*
CaH ₁₁	$R\bar{3}c$	100	30-50	128-161	28*
LaH ₁₄	$R\bar{3}m$	100	80-98	99-123	33*
LaH ₂₄	$C2$	100	37-55	64-82	0
AcH ₂₁	$P\bar{1}$	100	28-40	28-41	0
CaH ₂₄	$Cmcm$	100	19-29	19-32	0*
AcH ₆	$I4/mmm$	200	129-166	279-315	0*
LaH ₁₀	$Fm\bar{3}m$	200	235-260	269-279	0
LaH ₁₀	$Immm$	200	60-180	265-296	0*
AcH ₆	$Cmcm$	200	171-220	248-304	0
NaH ₁₀	$Cmmm$	200	160-170	243-283	8
ScH ₈	$R\bar{3}m$	200	86-179	242-271	-
AcH ₆	$Im\bar{3}m$	200	63-78	241-265	0*
LaH ₁₀	$R\bar{3}m$	200	45-54	225-270	0*
LaH ₁₀	$C222_1$	200	169-195	221-248	0*
H ₃ S	$Fmmm$	200	154-180	216-246	0*
AcH ₆	$Pmmn$	200	67-69	208-238	0*
NaH ₄	$Immm$	200	106-126	191-218	61*
MgH ₇	$C2/m$	200	85-102	188-220	29*
AcH ₆	$C2/m$	200	100-112	184-214	0*
AcH ₁₁	$Imm2$	200	88-108	165-184	0*
NaH ₅	$P4/mmm$	200	66-75	134-163	21*
NaH ₁₂	$R\bar{3}m$	200	50-60	122-151	4
MgH ₆	$P\bar{1}$	200	71-104	98-121	19*
MgH ₅	$C2/m$	200	58-75	71-95	30
Na ₂ H ₇	$P\bar{1}$	200	20-140	57-169	98*
ScH ₁₂	$P4/mcc$	300	120-136	302-332	0*
NaH ₁₀	$Cmmm$	300	151-177	243-283	3
KH ₁₁	$P4/nmm$	300	109-140	233-256	7*
NaH ₁₄	$P4/mmm$	300	103-126	220-245	1*
SrH ₁₀	$Cmcm$	300	133-156	215-250	0*
Na ₂ H ₁₁	$P2/m$	300	60-71	154-185	0*
NaH ₉	$P2/m$	300	67-80	151-186	0*
LiH ₄	$C2/m$	300	93-123	131-168	17
MgH ₁₄	$P\bar{1}$	300	55-66	117-143	14
NaH ₁₂	$R\bar{3}m$	300	66-79	88-115	2
KH ₆	$Immm$	300	40-53	46-64	3
LiH ₁₂	$Pm\bar{3}m$	500	244-330	433-485	26*
NaH ₆	$Im\bar{3}m$	500	215-267	357-406	30*
YH ₁₇	$R32$	500	137-164	287-331	29
MgH ₉	$Cmmm$	500	133-168	284-336	7
CaH ₁₀	$Fm\bar{3}m$	500	157-195	238-279	3*
SrH ₂₂	$R32$	500	167-194	227-266	0*
Y ₂ H ₁₉	$C2$	500	188-220	214-251	37
MgH ₁₂	$Fmmm$	500	161-200	208-245	0
YH ₂₂	$P\bar{1}$	500	90-110	203-234	34
NaH ₄	$I4_1/amd$	500	83-97	193-233	25
YbH ₁₀	$R\bar{3}m$	500	94-136	176-207	0*
YbH ₁₀	$Fm\bar{3}m$	500	76-92	164-202	0
NaH ₅	$P4/mmm$	500	86-116	85-118	26
MgH ₄	$Immm$	500	60-70	66-90	0*
MgH ₄	$I4/mmm$	500	40-63	48-77	0

TABLE I. Dynamically unstable candidate superconductors. Those structures marked with * are not the lowest energy structure for the given stoichiometry (i.e. have non-zero E_{struc}). The Sc-H system was not in the focused searches at 200 GPa.

III. 100 K+ DYNAMICALLY STABLE SUPERCONDUCTORS

Stoichiometry	Space group	P(GPa)	T_c (K)	Comments
NaH6	$Pm\bar{3}m$	100	263.5	Superconductivity not previously studied to the best of our knowledge. Ref. [?] found NaH ₆ off hull at 50 GPa. Ref. [?] found $Pm\bar{3}m$ -NaH6 becomes stable with respect to $P1$ above 150 GPa.
CaH6	$Im\bar{3}m$	100	234.5	Superconductivity studied previously for this structure in Ref. [?]. Ref. [?] found CaH6 slightly above the hull at 100 GPa.
NaH6	$Pm\bar{3}m$	200	274	See above comments for NaH ₆ at 100 GPa.
AcH12	$P63mc$	200	262.5	Space group not studied elsewhere to the best of our knowledge. Ref. [?] studies $I4/mmm$ AcH12 ($T_c=148-173$ K at 150 GPa). They find AcH12 on hull at 150 GPa, slightly above at 250 GPa.
MgH13	$Fm\bar{3}m$	200	210	Space group not studied elsewhere to the best of our knowledge. Refs. [?] and [?] predict MgH13 above hull at 200 and 300 GPa, respectively.
SH3	$Im\bar{3}m$	200	207.5	Well-known structure from experiment [?] and theory [? ?].
MgH6	$Im\bar{3}m$	300	286	Superconductivity studied previously for this structure. Ref. [?] found MgH6 thermodynamically stable above 263 GPa relative to MgH2 and H2, and $T_c=260$ K for the $Im\bar{3}m$ structure above 300 GPa. Ref. [?] calculated much higher T_c for this structure - 420 K at 300 GPa.
YH9	$F\bar{4}3m$	300	277	Space group not studied elsewhere to the best of our knowledge. Ref. [?] predicted YH9 stoichiometry on hull 100-400 GPa, with $P63/mmc$ symmetry at 300 GPa. Ref. [?] found YH9 on hull at 400 GPa with $P63/mmc$ lowest in energy. Ref. [?] synthesised YH9 in $P63/mmc$ structure.
ScH8	$Immm$	300	222.5	Superconductivity studied previously for this structure. Ref. [?] found ScH8 above static-lattice convex hull at 150-350 GPa, but on hull at 350-400 GPa when ZPE included. Their predicted phase behaviour is $Immm$ above 320 GPa. Ref. [?] found $Immm$ ScH8 stable above 300 GPa, with $T_c \approx 115$ K at 300 GPa. Ref. [?] found ScH8 above hull at 100, 200 and 300 GPa.
MgH12	$Pm\bar{3}$	500	381	Space group not studied elsewhere to the best of our knowledge. Ref. [?] looked at lower pressures, calculated $T_c=47-60$ K for $R\bar{3}$ MgH12 at 140 GPa. Ref. [?] found MgH12 on hull at 300 GPa.
MgH13	$P3m1$	500	272	Space group not studied elsewhere to the best of our knowledge. Ref. [?] finds MgH13 above hull at 300 GPa.
SrH10	$Fm\bar{3}m$	500	302	Space group not studied elsewhere to the best of our knowledge. Ref. [?] found a $P21/m$ structure at 50 GPa, a $P2/c$ structure at 150 GPa and transition to $R\bar{3}m$ at 300 GPa. Ref. [?] found $C2/m$ SrH10 at much lower pressures of 100 GPa.
NaH9	$P63/mmc$	500	252	Space group not studied elsewhere to the best of our knowledge. Ref. [?] found a 25-300+ GPa stability range for NaH9 (though 500 GPa seems to be outside range of study) with $Cmc21$ -NaH9 stable at 300 GPa.
MgH10	$C2/m$	500	251	Space group not studied elsewhere to the best of our knowledge. Ref. [?] found a $P63/mmc$ structure of MgH10 which was dynamically unstable at 300 GPa. Ref. [?] predicts MgH10 to be above the hull at 300 GPa.
SrH24	$R\bar{3}$	500	231.5	Stoichiometry not studied elsewhere to the best of our knowledge. Refs. [? ?] both study Sr-H structures, but don't look at hydrogen content this high.
YH18	$P\bar{1}$	500	229.5	Space group not studied elsewhere to the best of our knowledge. YH18 stoichiometry mentioned in Fig. 3b of Ref. [?].
YH20	$P\bar{1}$	500	228	Stoichiometry not studied elsewhere to the best of our knowledge. No high hydrogen content on/near hull up to 300 GPa in Ref. [?]. Higher H content YH24 on hull at 200 and 300 GPa in Ref. [?].
SrH10	$R\bar{3}m$	500	209	Superconductivity studied previously for this structure. Ref. [?] found a $P21/m$ structure at 50 GPa, a $P2/c$ structure at 150 GPa and transition to $R\bar{3}m$ at 300 GPa. Ref. [?] calculated $T_c=259$ K for $R\bar{3}m$ at 300 GPa.
CaH10	$R\bar{3}m$	500	202	Superconductivity studied previously for this structure. Ref. [?] found $R\bar{3}m$ -CaH10 metastable at 400 GPa with $T_c=157-175$ K. They find CaH10 lies above the hull at 50-400 GPa, but gets closer with increasing pressure.

TABLE II. Dynamically stable superconductors with $T_c > 200$ K found in this work, along with their converged (average) Eliashberg T_c values and notes on findings for these systems in previous work.

Stoichiometry	Space group	P(GPa)	T_c (K)	Comments
Na2H11	$Cmmm$	100	147.5	Stoichiometry not studied elsewhere to the best of our knowledge.
KH10	$C2/m$	100	145.5	Space group not studied elsewhere to the best of our knowledge. Ref. [?] finds KH10 not on hull at 50 GPa, but $Immm$ -KH10 stable at 150 GPa with an Allen-Dynes T_c of 148K.
NaH8	$I4/mmm$	200	163.5	Space group not studied elsewhere to the best of our knowledge. Ref. [?] finds $P1$ structure below 180 GPa, and $Cmcm$ above.
AcH6	$Fmmm$	200	186.5	Space group not studied elsewhere to the best of our knowledge. Ref. [?] finds this stoichiometry is not on hull at 150 or 250 GPa.
Na2H11	$Cmmm$	200	145.5	Stoichiometry not studied elsewhere to the best of our knowledge.
MgH14	$P\bar{1}$	200	123	Stoichiometry not studied elsewhere to the best of our knowledge. Ref. [?] did not find MgH14 on the hull at 300 GPa.
LaH7	$C2/m$	200	119.5	Superconductivity studied previously for this structure. Ref. [?] found LaH7 not on hull at 200 GPa. They report metastable $C2/m$ LaH7 (17meV/atom above the hull at 150 GPa) with Allen-Dynes $T_c=158-185$ K at 180 GPa.
LiH2	$P6/mmm$	300	192	Space group not studied elsewhere to the best of our knowledge. Ref. [?] predicted 130-300+ GPa stability range for LiH2, with lowest energy structure having $P4/mbm$ symmetry. Ref. [?] found that LiH2 does not exhibit superconductivity at 150 GPa. Ref. [?] looked at lower pressures, found LiH2 to be stable at 130-200 GPa and also looked at $P4/mbm$.
NaH7	$C2/m$	300	182.5	Superconductivity not previously studied to the best of our knowledge. Stability range of NaH7 from Ref. [?] is 25-100 GPa; they study a Cc structure at low pressures and predict a transition to $C2/m$ at 245 GPa.
Sch12	$P\bar{1}$	300	151	Space group not studied elsewhere to the best of our knowledge. Ref. [?] found $Immm$ -Sch12 stable above 320 GPa with $T_c=141-194$ K at 350 GPa. They found the Sch12 stoichiometry to be on the static-lattice hull at 350 GPa and above, close at 300 GPa. Ref. [?] found Sch12 on the hull at 300 GPa, identifying a $C2/c$ structure at this pressure.
LiH6	$R\bar{3}m$	300	145.5	Superconductivity studied previously for this structure. Ref. [?] found a 140-300+ GPa region of stability for LiH6 and found $R\bar{3}m$. Ref. [?] calculated $T_c=82$ K at 300 GPa for $R\bar{3}m$ LiH6. Ref. [?] also studied the $R\bar{3}m$ structure.
Sch6	$Im\bar{3}m$	300	148	Superconductivity studied previously for this structure. Ref. [?] predicted $Im\bar{3}m$ Sch6 stable above 265 GPa with $T_c=130$ K at 285 GPa. Ref. [?] found Sch6 on hull at 300 GPa and identified the $Im\bar{3}m$ structure. Ref. [?] predicted a region of stability for $Im\bar{3}m$ Sch6 above 350 GPa.
NaH5	$P4/mmm$	300	151	Space group not studied elsewhere to the best of our knowledge. Ref. [?] studied lower pressures region, finding a structure with $P-1$ symmetry.
LiH6	$C2/m$	300	146.5	Space group not studied elsewhere to the best of our knowledge. See entry for $R\bar{3}m$ LiH6, $C2/m$ structure of LiH6 not mentioned in these references.
LiH3	$Cmcm$	300	126	Space group not studied elsewhere to the best of our knowledge. LiH3 found to be off-hull in Ref. [?] but no structure given, same as in Ref. [?].
Sch14	$P\bar{1}$	300	103	Stoichiometry not studied elsewhere to the best of our knowledge. Refs. [?], [?] and [?] do not study hydrogen content this high.
Na2H11	$Cmmm$	500	160.5	Stoichiometry not studied elsewhere to the best of our knowledge.
CaH15	$P\bar{6}2m$	500	150.5	Superconductivity not previously studied to the best of our knowledge. Structure found at 200 GPa in Ref. [?], but superconductivity not studied.
SrH15	$P\bar{6}2m$	500	124.5	Stoichiometry not studied elsewhere to the best of our knowledge. Refs. [? ? ? ?] do not study hydrogen content this high.
MgH8	$C2/m$	500	106	Space group not studied elsewhere to the best of our knowledge. MgH8 found to lie off of the convex hull at the lower pressures of 100/200 GPa in Ref. [?].

TABLE III. Dynamically stable superconductors with T_c between 100 and 200 K found in this work, along with their converged (average) Eliashberg T_c values and notes on findings for these systems in previous work.

IV. CONVEX HULLS

On the following pages, we include the static-lattice convex hulls used to assess the stability of structures in the results stage of this work. These are produced from our focused searches as described in Section IV of the main text. To the right of each hull is a list of the on-hull stoichiometries and the space groups of the corresponding on-hull structures. The four columns in this list are stoichiometry, number of formula units in the cell, space group and composition label (x), respectively.

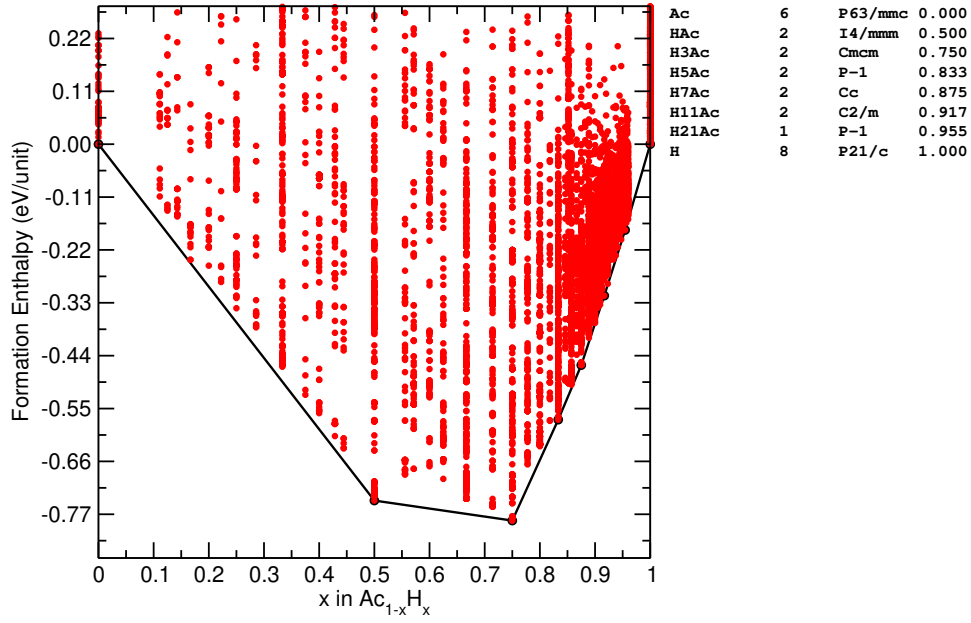


FIG. 1. The convex hull of Ac-H at 100 GPa.

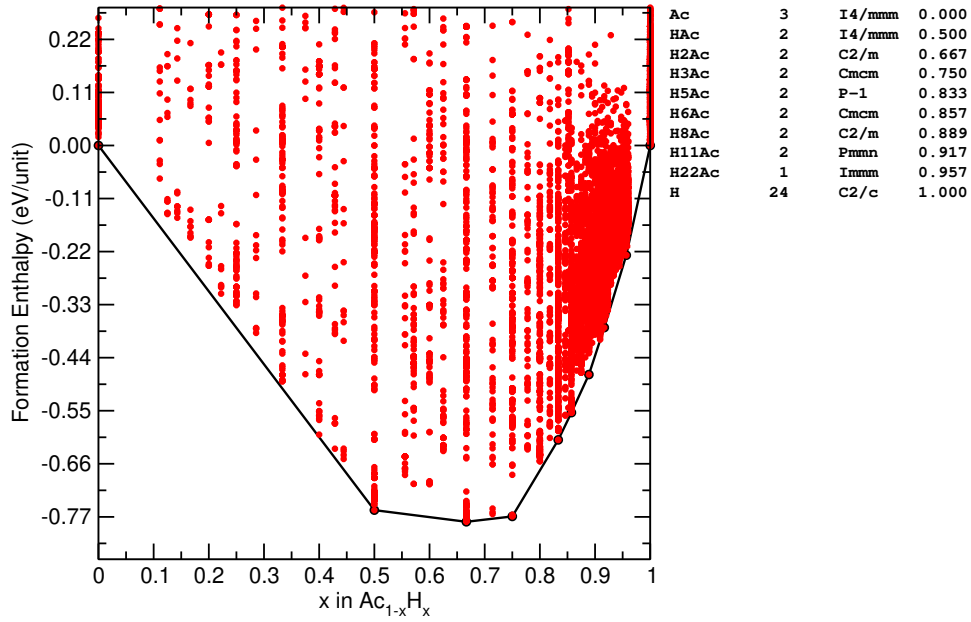


FIG. 2. The convex hull of Ac-H at 200 GPa.

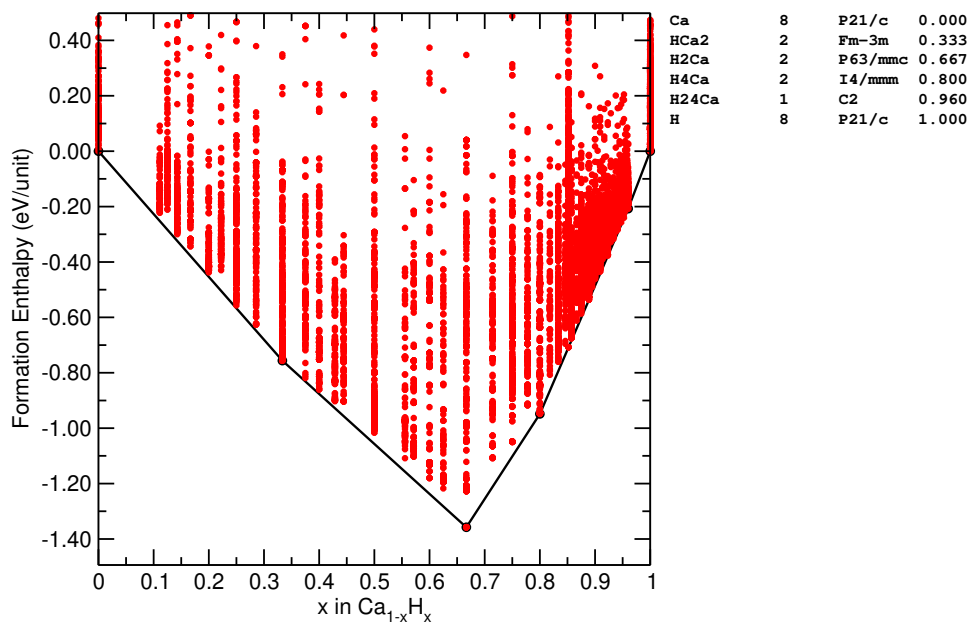


FIG. 3. The convex hull of Ca-H at 100 GPa.

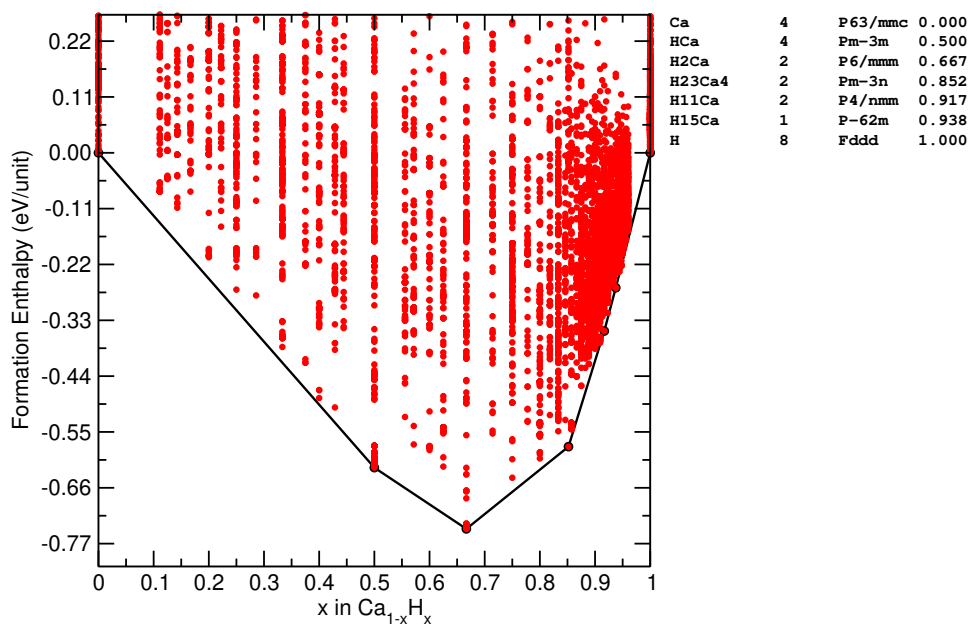


FIG. 4. The convex hull of Ca-H at 500 GPa.

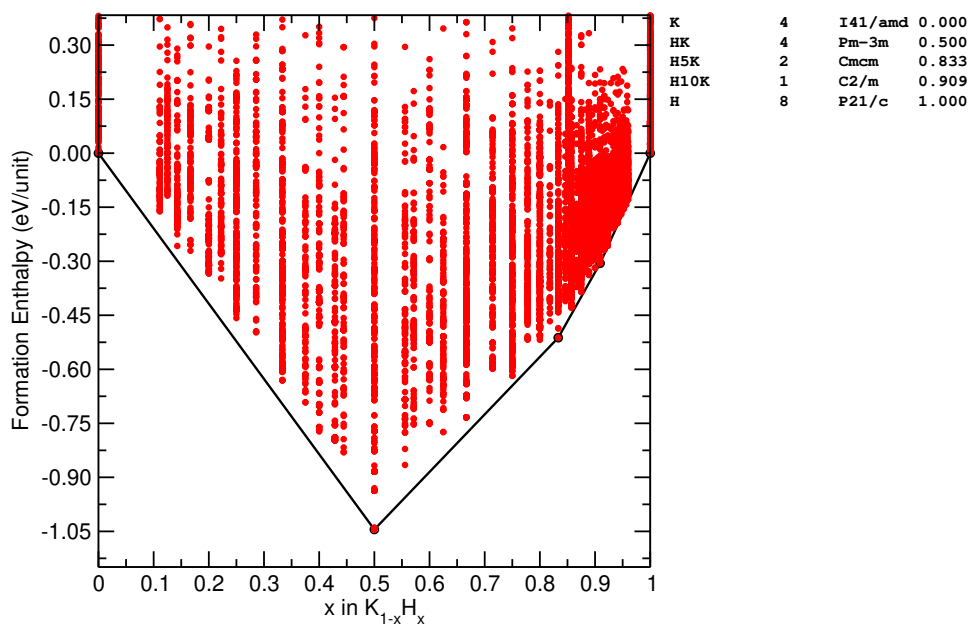


FIG. 5. The convex hull of K-H at 100 GPa.

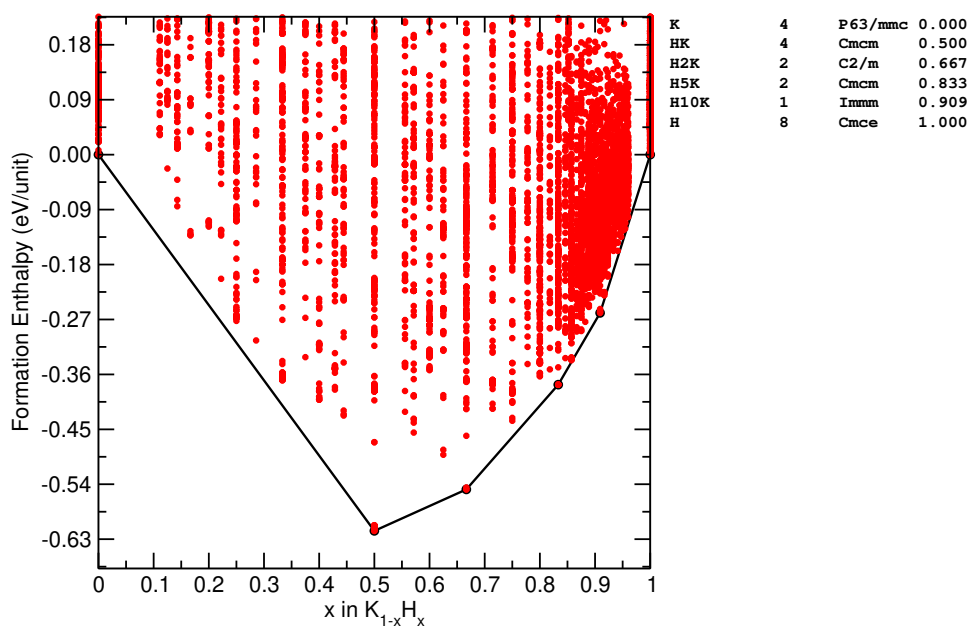


FIG. 6. The convex hull of K-H at 300 GPa.

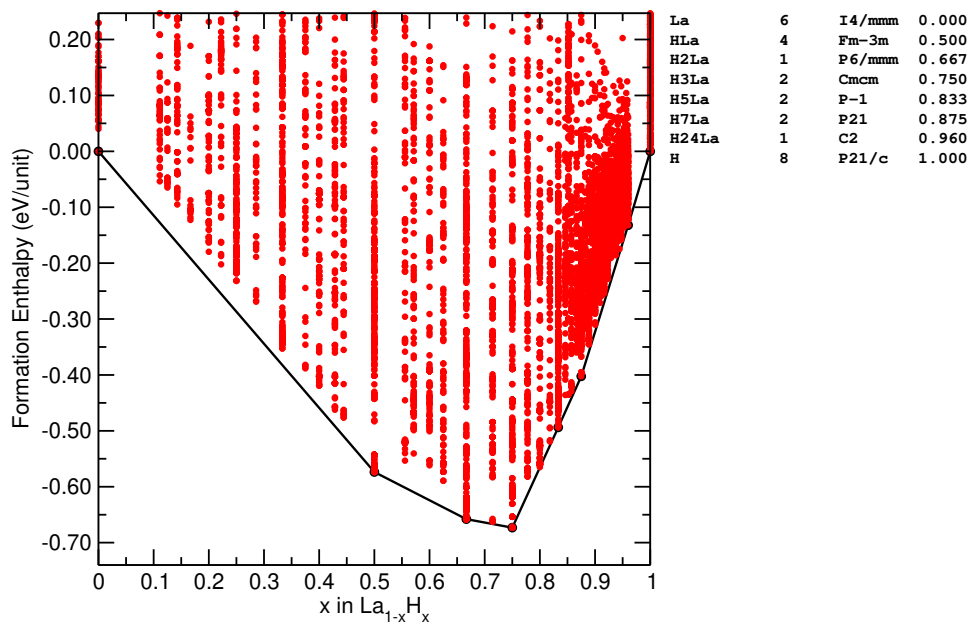


FIG. 7. The convex hull of La-H at 100 GPa.

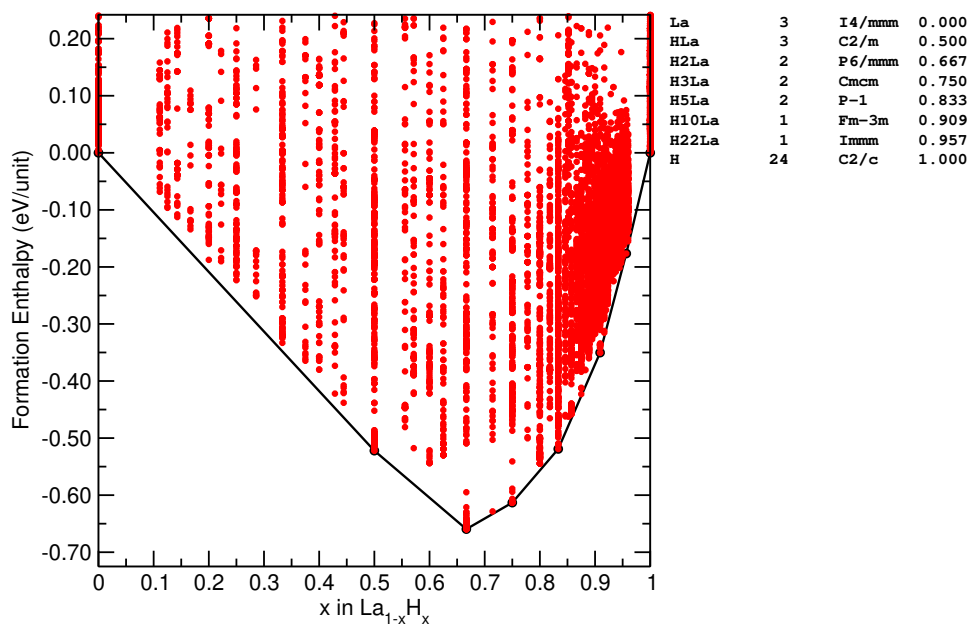


FIG. 8. The convex hull of La-H at 200 GPa.

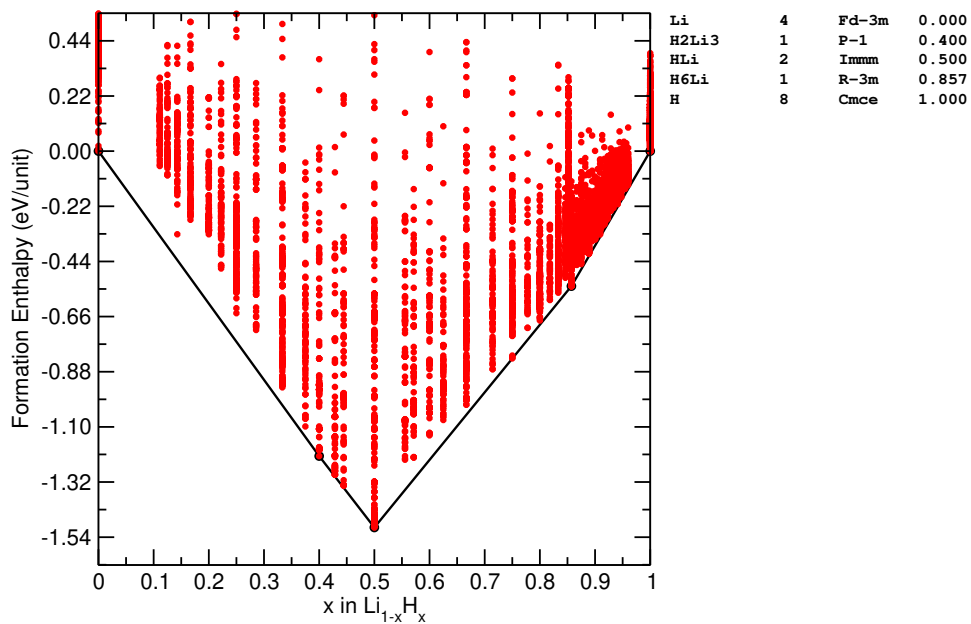


FIG. 9. The convex hull of Li-H at 300 GPa.

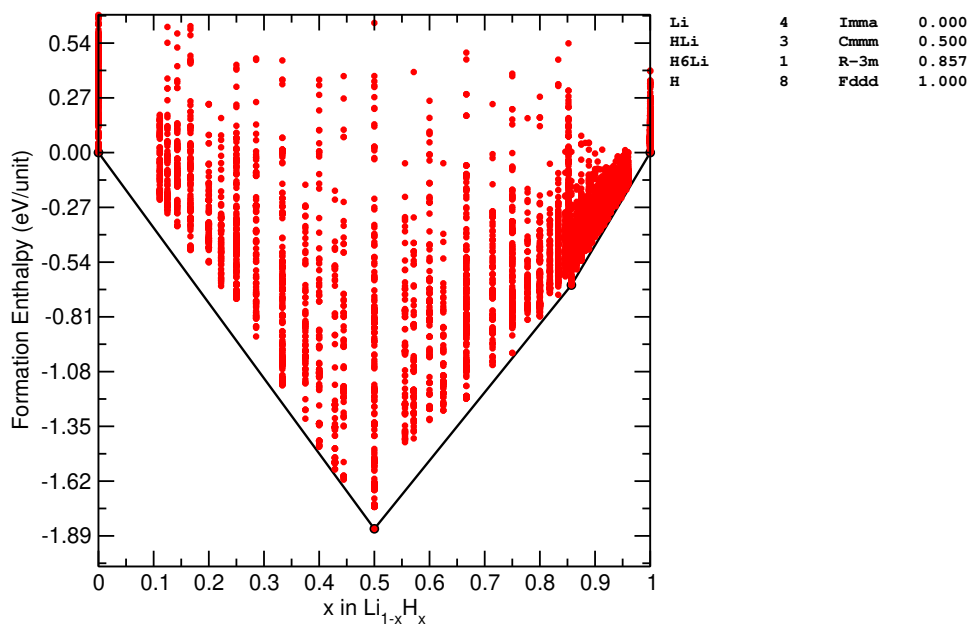


FIG. 10. The convex hull of Li-H at 500 GPa.

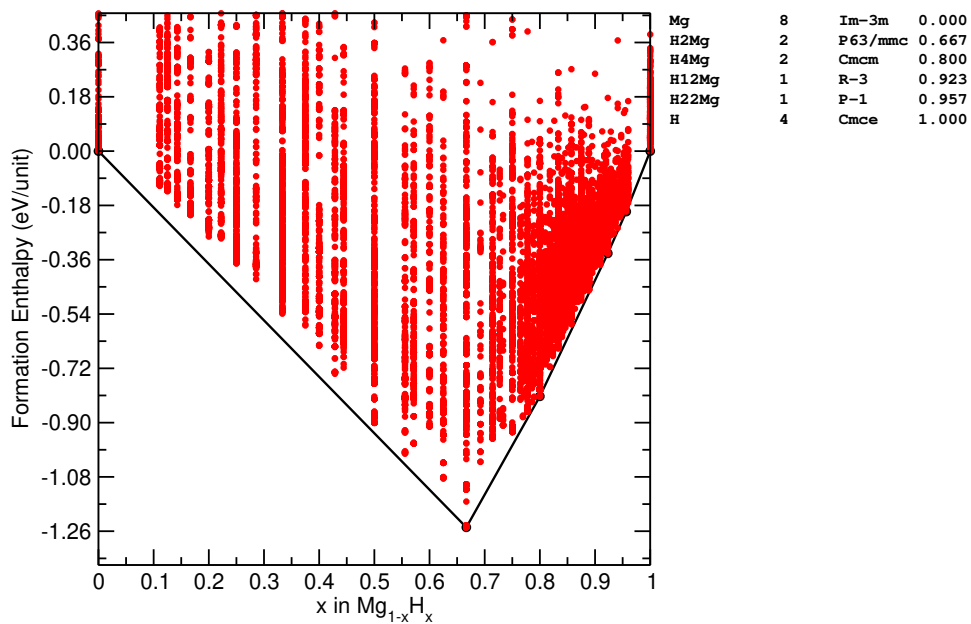


FIG. 11. The convex hull of Mg-H at 200 GPa.

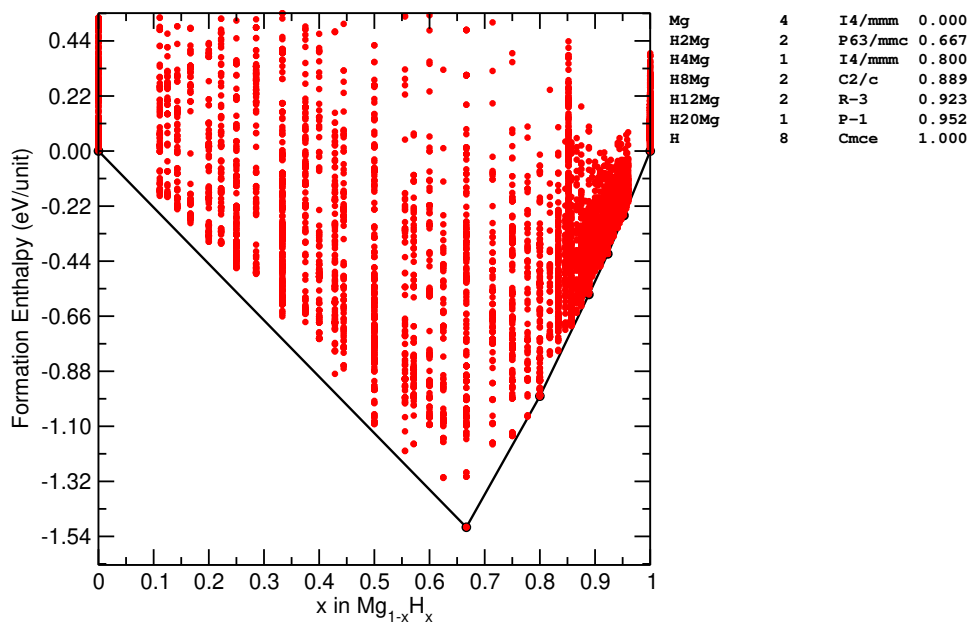


FIG. 12. The convex hull of Mg-H at 300 GPa.

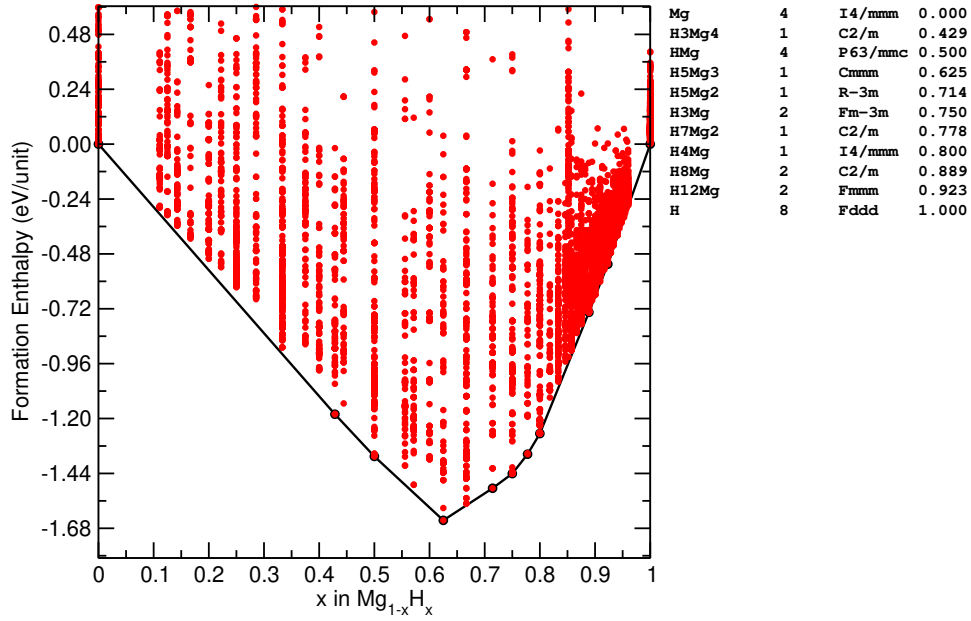


FIG. 13. The convex hull of Mg-H at 500 GPa.

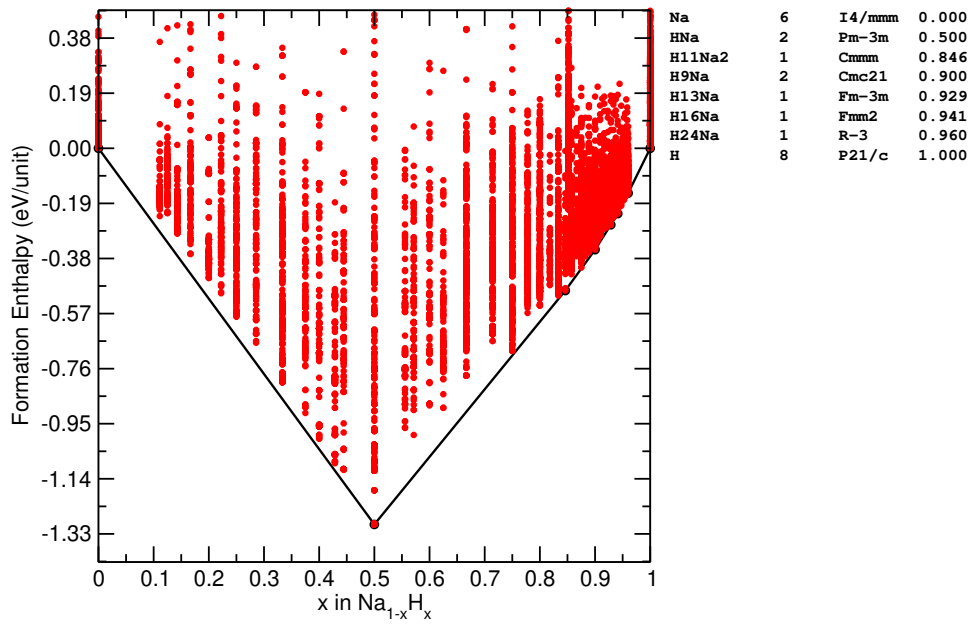


FIG. 14. The convex hull of Na-H at 100 GPa.

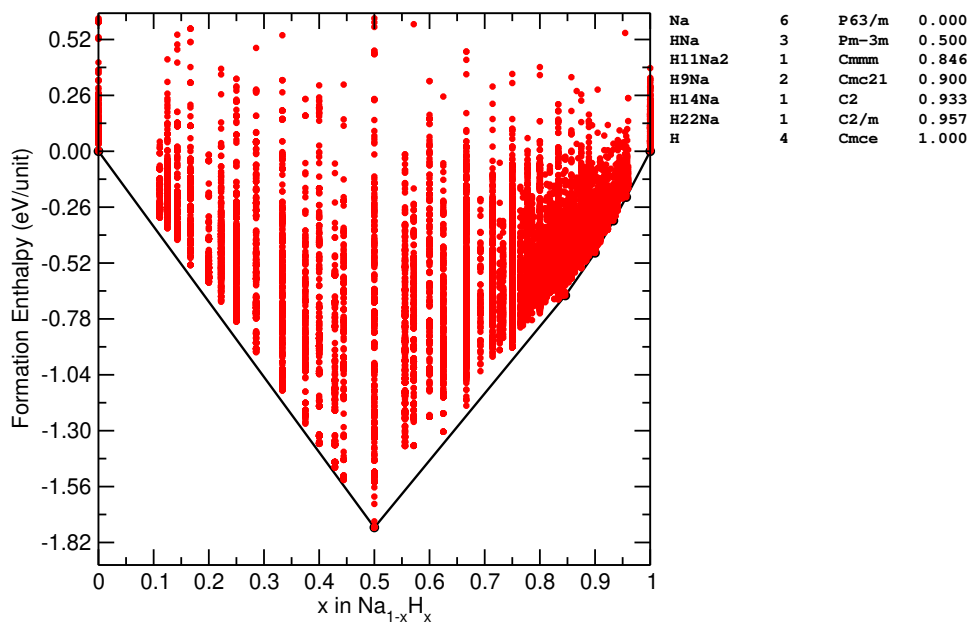


FIG. 15. The convex hull of Na-H at 200 GPa.

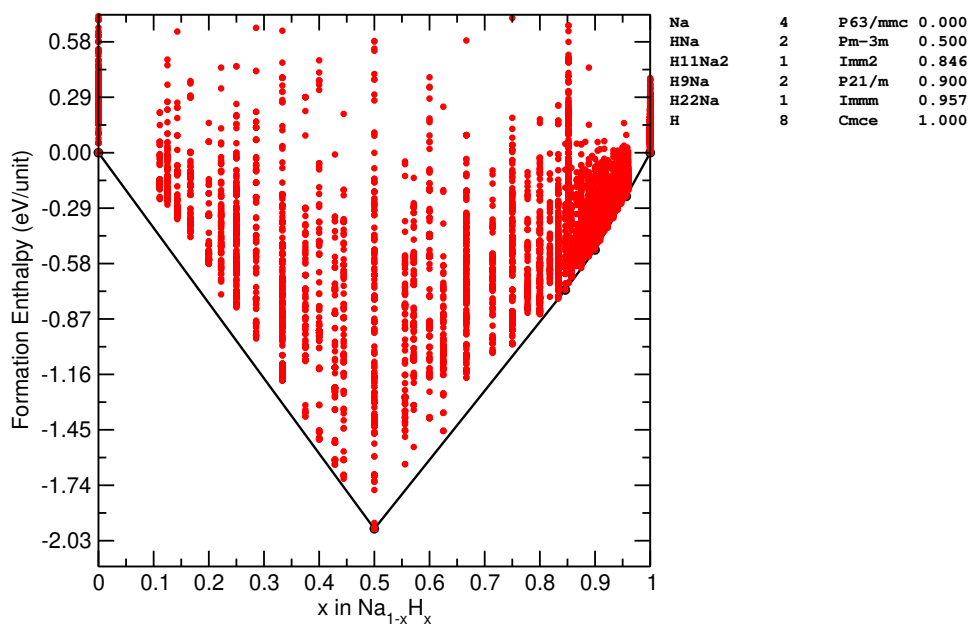


FIG. 16. The convex hull of Na-H at 300 GPa.

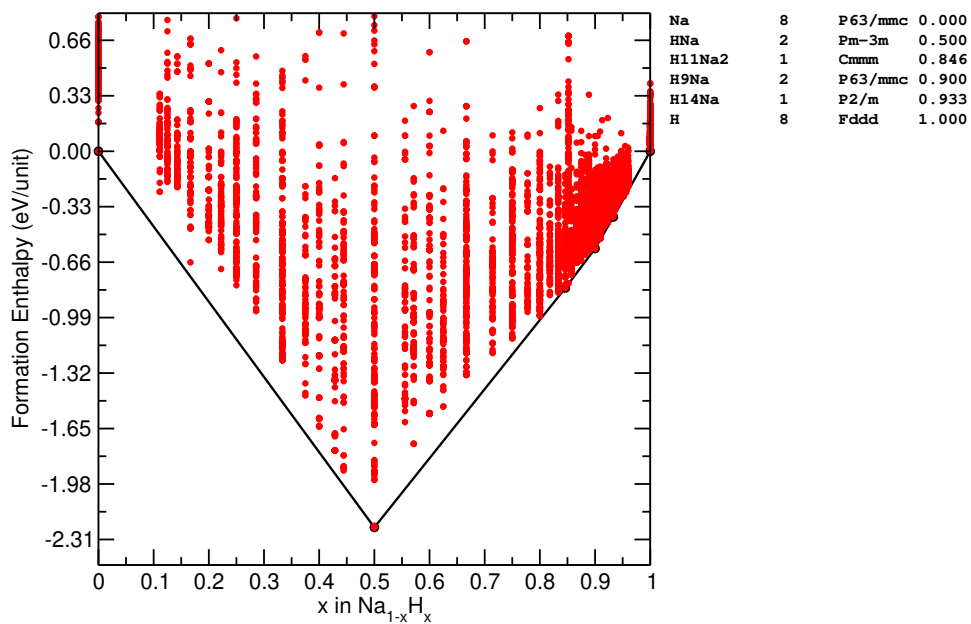


FIG. 17. The convex hull of Na-H at 500 GPa.

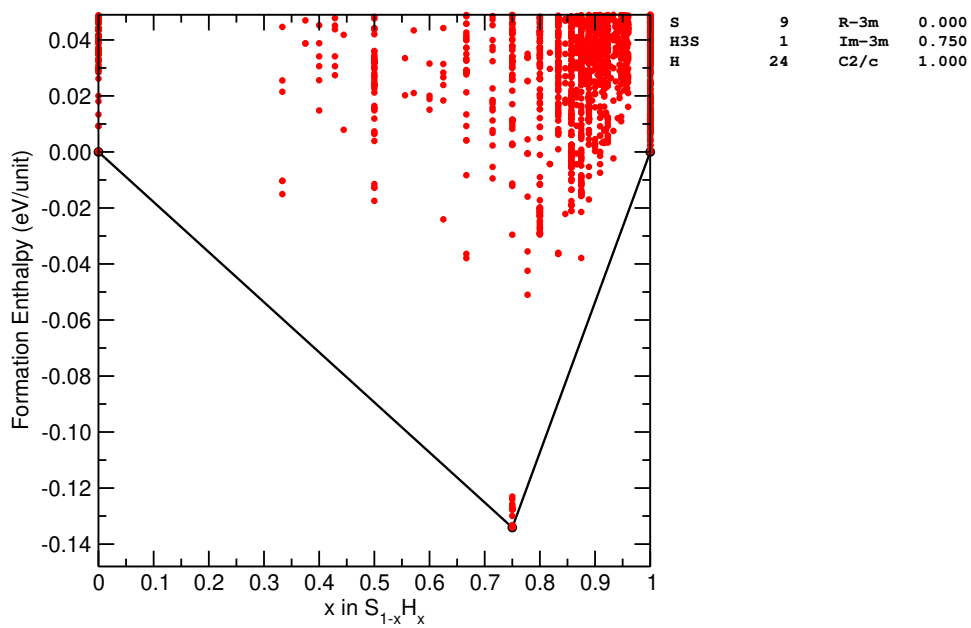


FIG. 18. The convex hull of S-H at 200 GPa.

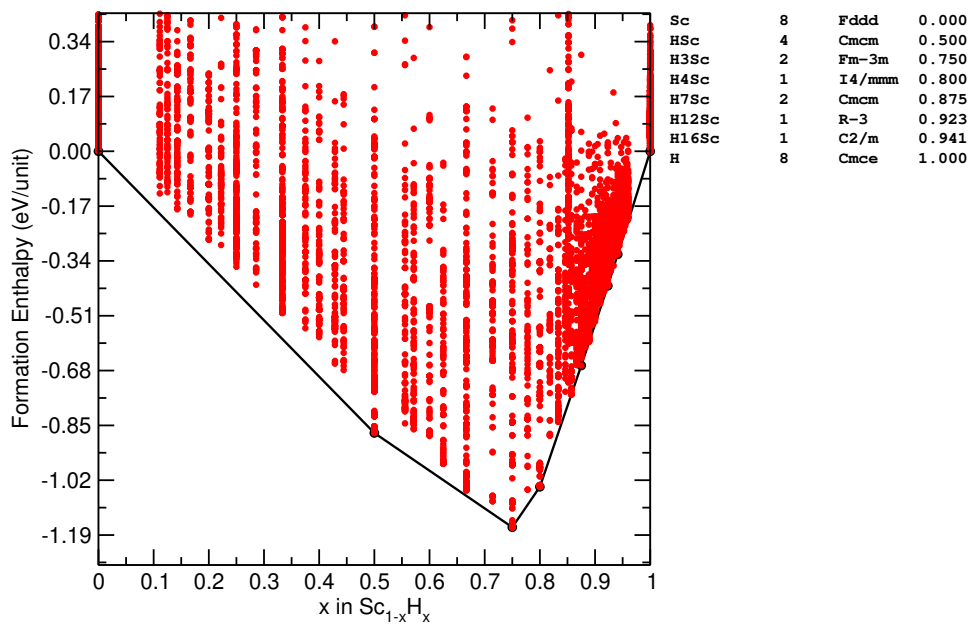


FIG. 19. The convex hull of Sc-H at 300 GPa.

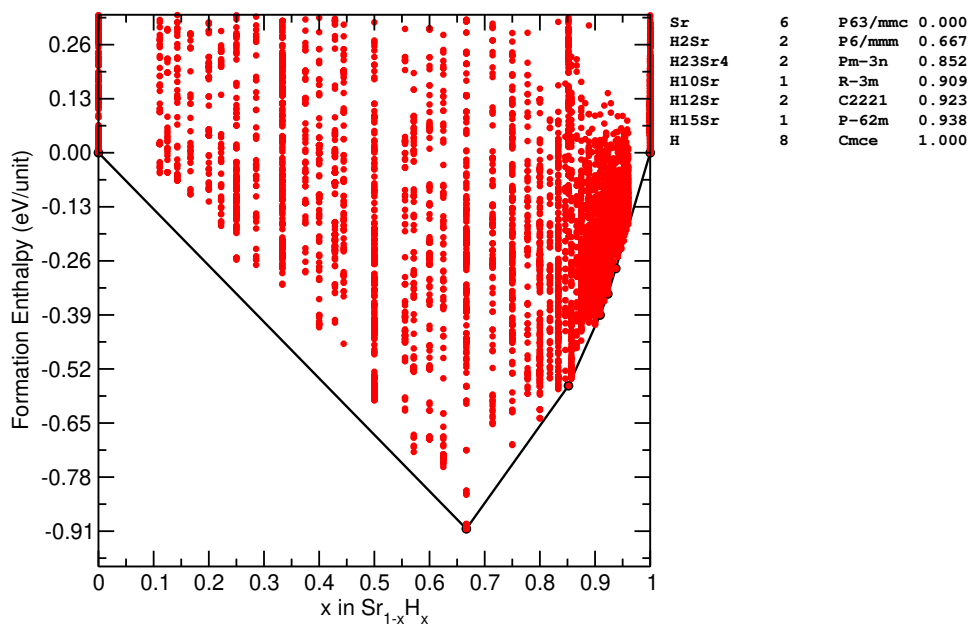


FIG. 20. The convex hull of Sr-H at 300 GPa.

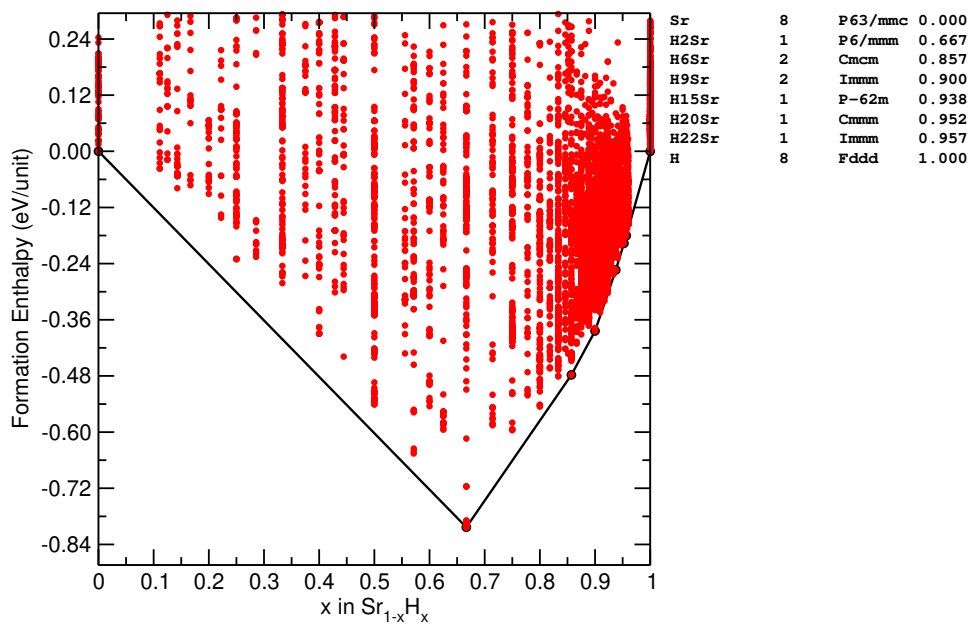


FIG. 21. The convex hull of Sr-H at 500 GPa.

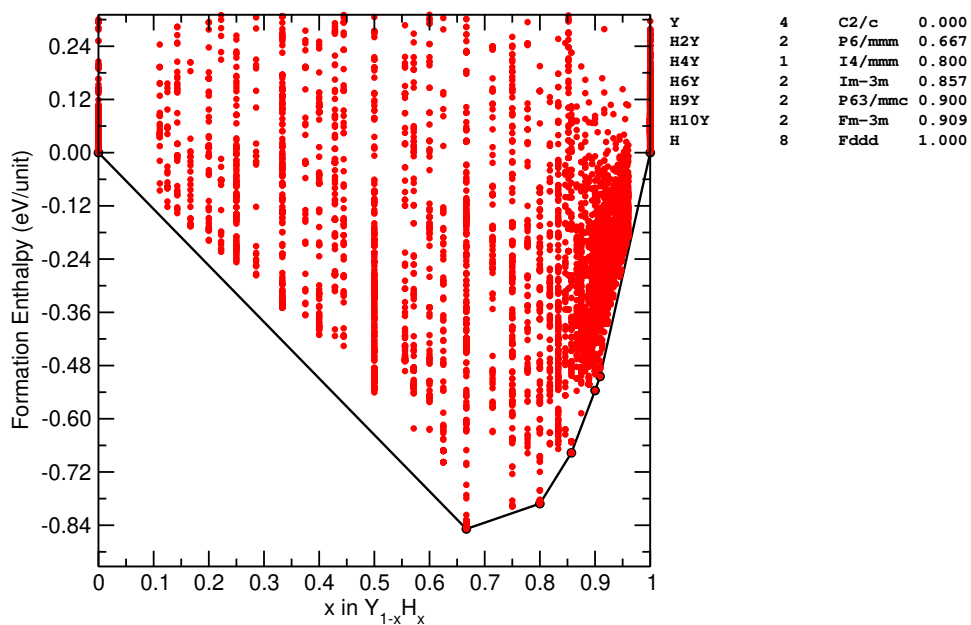


FIG. 22. The convex hull of Y-H at 500 GPa.

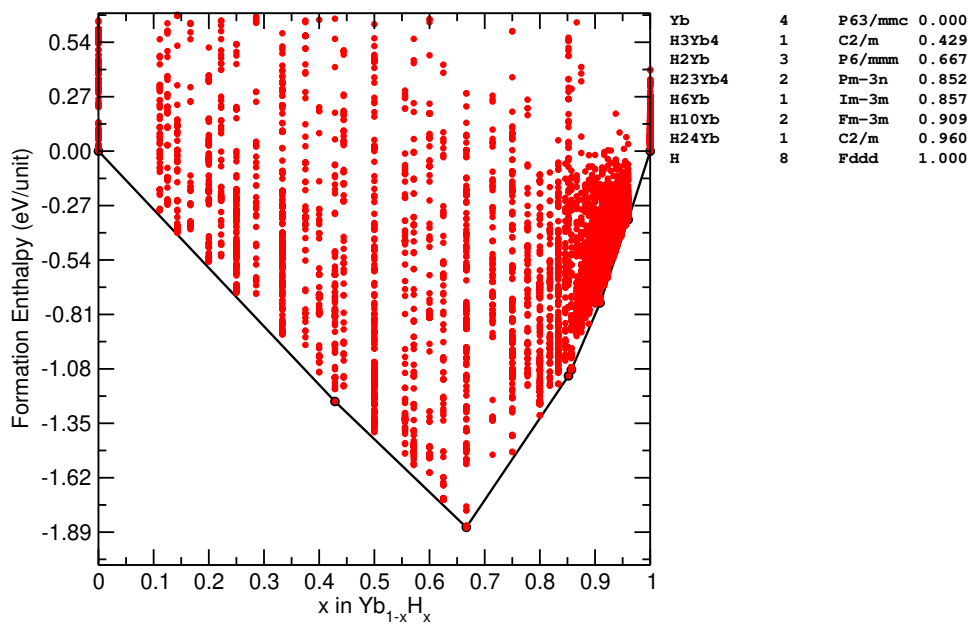


FIG. 23. The convex hull of Yb-H at 500 GPa.